# FUSION OF SENSOR INFORMATION TO MEASURE THE TOTAL ENERGY OF AN AIRCRAFT AND PROVIDE INFORMATION ABOUT FLIGHT PERFORMANCE AND LOCAL MICROCLIMATE.

*by*

Bruce Johnson

A dissertation submitted to the Department of Electrical Engineering, University of Cape Town, in fulfilment of the requirements for the degree of Master of Science in Engineering.

Supervisors
Robyn Verrinder and Samuel Ginsberg



# Declaration

I declare that this project is my own work; all sources that I have used have been referenced and are listed in the Bibliography. This work has not been submitted before for any other degree or examination in any other university.

Signature of Author: .....

Cape Town

February 2013

# ACKNOWLEDGEMENTS

I wish to thank my supervisors Robyn Verrinder and Samuel Ginsberg for all of your help, your dedication and knowledge has been amazing.

I would also like to thank my parents for their support and guidance throughout this project.

## EBE Faculty: Assessment of Ethics in Research Projects

Any person planning to undertake research in the Faculty of Engineering and the Built Environment at the University of Cape Town is required to complete this form before collecting or analysing data. When completed it should be submitted to the supervisor (where applicable) and from there to the Head of Department. If any of the questions below have been answered YES, and the applicant is NOT a fourth year student, the Head should forward this form for approval by the Faculty EIR committee: submit to Ms Zulpha Geyer (Zulpha.Geyer@uct.ac.za; Chem Eng Building, Ph 021 650 4791). Students must include a copy of the completed form with the thesis when it is submitted for examination.

---

Name of Principal Researcher/Student: Bruce Edward Johnson  Department: Electrical Engineering

If a Student:  Degree: MSc( Electrical Engineering)  Supervisor: Robyn Verrinder

If a Research Contract indicate source of funding/sponsorship: N/A

Research Project Title: FUSION OF SENSOR INFORMATION TO MEASURE THE TOTAL ENERGY OF AN AIRCRAFT AND PROVIDE INFORMATION ABOUT FLIGHT PERFORMANCE AND LOCAL MICROCLIMATE.

**Overview of ethics issues in your research project:**

| | | |
|---|---|---|
| **Question 1: Is there a possibility that your research could cause harm to a third party (i.e. a person not involved in your project)?** | YES | (NO) |
| **Question 2: Is your research making use of human subjects as sources of data?** If your answer is YES, please complete Addendum 2. | YES | (NO) |
| **Question 3: Does your research involve the participation of or provision of services to communities?** If your answer is YES, please complete Addendum 3. | YES | (NO) |
| **Question 4: If your research is sponsored, is there any potential for conflicts of interest?** If your answer is YES, please complete Addendum 4. | YES | (NO) |

If you have answered YES to any of the above questions, please append a copy of your research proposal, as well as any interview schedules or questionnaires (Addendum 1) and please complete further addenda as appropriate.

**I hereby undertake to carry out my research in such a way that**

- there is no apparent legal objection to the nature or the method of research; and
- the research will not compromise staff or students or the other responsibilities of the University;
- the stated objective will be achieved, and the findings will have a high degree of validity;
- limitations and alternative interpretations will be considered;
- the findings could be subject to peer review and publicly available; and
- I will comply with the conventions of copyright and avoid any practice that would constitute plagiarism.

Signed by:

| | Full name and signature | Date |
|---|---|---|
| Principal Researcher/Student: | | 21/05/2012 |

This application is approved by:

| | | |
|---|---|---|
| Supervisor (if applicable): | | 21/05/2012 |
| HOD (or delegated nominee): Final authority for all assessments with NO to all questions and for all undergraduate research. | | 21/05/2012 |
| Chair : Faculty EIR Committee For applicants other than undergraduate students who have answered YES to any of the above questions. | | |

Janine Buxey
Department Administrator
Authorised Signatory for the
HoD, Electrical Engineering, UCT

# ABSTRACT

The application of using Unmanned Aerial Vehicles (UAVs) to locate thermal updraft currents is a relatively new topic. It was first proposed in 1998 by John Wharington, and, subsequently, several researchers have developed algorithms to search and exploit thermals. However, few people have physically implemented a system and performed field testing.

The aim of this project was to develop a low cost system to be carried on a glider to detect thermals effectively. A system was developed from the ground up and consisted of custom hardware and software that was developed specifically for aircraft. Data fusion was performed to estimate the attitude of the aircraft; this was done using a direction cosine (DCM) based method. Altitude and airspeed data were fused by estimating potential and kinetic energy respectively; thus determining the aircraft's total energy. This data was then interpreted to locate thermal activity.

The system comprised an Inertial Measurement Unit (IMU), airspeed sensor, barometric altitude sensor, Global Positioning System (GPS), temperature sensor, SD card and a realtime telemetry link. These features allowed the system to determine aircraft position, height, airspeed and air temperature in realtime.

A custom-designed radio controlled (RC) glider was constructed from composite materials in addition to a second 3.6 m production glider that was used during flight testing. Sensor calibration was done using a wind tunnel with custom designed apparatus that allowed a complete wing with its pitot tube to be tested in one operation. Flight testing was conducted in the field at several different locations over the course of six months. A total of 25 recorded flights were made during this period. Both thermal soaring and ridge soaring were performed to test the system under varying weather conditions. A telemetry link was developed to transfer data in realtime from the aircraft to a custom ground station. The recorded results were post-processed using Matlab and showed that the system was able to detect thermal updrafts. The sensors used in the system were shown to provide acceptable performance once some calibration had been performed. Sensor noise proved to be problematic, and time was spent alleviating its effects.

Results showed that the system was able to measure airspeed to within $\pm$ 1 km/h. The standard deviation of the altitude estimate was determined to be 0.94 m. This was deemed to be satisfactory.

The system was highly reliable and no faults occurred during operation.

In conclusion, the project showed that inexpensive sensors and low power microcontrollers could be used very effectively for the application of detecting thermals.

# CONTENTS

# LIST OF FIGURES

# LIST OF TABLES

# NOMENCLATURE

| | | |
|---|---|---|
| DCM | - | Direction Cosine Matrix |
| IAS | - | Indicated Airspeed |
| TAS | - | True Airspeed |
| IMU | - | Inertial Measurement Unit |
| GPS | - | Global positioning system |
| MEMS | - | Micro Electro-Mechanical System |
| DOF | - | Degrees of freedom |
| UAV | - | Unmanned Aerial Vehicle |
| RC | - | Radio Controlled |
| RTK | - | Real Time Kinematics |
| AHRS | - | Attitude and Heading Reference System |
| PCB | - | Printed Circuit Board |
| ADC | - | Analog to Digital Convertor |
| RF | - | Radio Frequency |
| CRC | - | Cyclic Redundancy Check |
| SNR | - | Signal to Noise Ratio |

| | | |
|---|---|---|
| $p$ | - | X axis angular velocity |
| $q$ | - | Y axis angular velocity |
| $r$ | - | Z axis angular velocity |
| $\rho$ | - | Pitch angle |
| $\phi$ | - | Roll angle |
| $\theta$ | - | Yaw angle |
| $A_x$ | - | Acceleration in the x axis |
| $A_y$ | - | Acceleration in the y axis |
| $A_z$ | - | Acceleration in the z axis |
| $H_{x_b}$ | - | Magnetic field in the x axis of the body |
| $H_{y_b}$ | - | Magnetic field in the y axis of the body |
| $H_{z_b}$ | - | Magnetic field in the z axis of the body |
| $H_{x_e}$ | - | Magnetic field in the x axis of the Earth plane |
| $H_{y_e}$ | - | Magnetic field in the y axis of the Earth plane |

CHAPTER 1

# THE INTRODUCTION

## 1.1 BACKGROUND

Throughout the history of aircraft, pilots and designers have wanted to improve the performance of these machines. These performance improvements might be to go faster, fly higher or in modern times, reduce operating costs by maximising the energy efficiency of their aircraft.

There are various types of aircraft, such as a conventional powered aircraft that would have one or more engines. This type of aircraft takes off and lands using its own power. As a result, the flight endurance is dictated by the amount of fuel it can carry. A glider however is very different to a conventional powered aircraft in that they generally do not have an engine; instead a pure glider either relies on a powered tow aircraft to tug the glider up to a given altitude, or utilises a ground based winch to pull it to altitude. Some gliders use a small engine to allow them to take off under their own power; this engine is then stopped and the flight continues without engine power. The engines used in this application are either built into the nose of the glider, like a conventional powered aircraft; or are placed above the wing and are retracted back into the fuselage after use.

Unmanned Aerial Vehicles (UAVs) have become more widespread over the last few years as technology has advanced. UAVs rely on computer based flight control and navigation systems; this means that sophisticated control problems have to be implemented in order to maintain stable and most importantly, safe flight. The reduction in size and power required by the flight control systems in conjunction with an increase in computational power, has allowed ever smaller UAVs to be developed. This has allowed UAVs to be developed that previously were either not feasible or practical.

Many different types of UAVs have been developed over the years. These range from defence type UAVs which can be used for reconnaissance or as weapons. Other types of UAVs are used for scientific purposes; these include land survey, meteorological survey or even payload transport to name but a few.

A glider utilises thermal updraft energy in order to increase flight duration. Thermals develop as a result of convective heating of the Earth's surface, this heating causes air currents to develop. On a hot day, one can often see Cumulonimbus clouds forming, these form as a result of rising

air currents. A thermal relies on the same principle.

As thermal energy is essentially free and renewable, the cost to the environment is insignificant. This makes thermal soaring an environmentally responsible method of flight.

Thermal soaring allows the aircraft to increase flight duration and therefore range. As a power plant or engine is not required (or in the case of a motor glider which might use an engine occasionally), fuel consumption is reduced drastically or completely. This makes the use of gliders an attractive alternative as compared to powered aircraft when one considers the running costs involved. If one is particularly skilled at locating and exploiting thermals, an aircraft can stay airborne for most of the day.

A full size glider would rely on a pilot to locate and exploit thermal updraft energy. As a UAV does not have a pilot, this process needs to be implemented within the flight control system.

## 1.2 SCOPE

The detection of thermal activity is usually not done directly, rather one has to measure the effect the thermal has on the aircraft as it passes through them.

Thus, in order to sense thermal updrafts, one first has be able to accurately measure several parameters of an aircraft.

Simply knowing the vertical velocity of the aircraft is not sufficient to make decisions, one must rather know the total energy of the aircraft; this takes into account both altitude and airspeed.

A significant emphasis has been placed upon using inexpensive sensors. Commercial products and those used by defence agencies typically use high quality sensors that have very low noise levels and drift [1]. The cost of these sensors is not insignificant, and due to limited funding, were outside this project's budget. The project will therefore attempt to make the best use of the sensors available by developing and applying techniques and algorithms to help mitigate the poor performance of low cost sensors, so that an effective and accurate system can be developed that provides acceptable performance.



The goals of this project are as follows:

- Review the existing literature to determine what has and what has not been done previously,
- Review methods of integrating inexpensive sensors,
- Develop an initial set of hardware and software components,
- Test the above components to determine their suitability for the task,
- Produce a revised set of hardware components that take into account the aforementioned changes,

- Develop test apparatus so as to allow the completed system to be tested and then calibrated using a wind tunnel,
- Develop and construct a glider of suitable size that can be used for flight testing,
- Develop a realtime telemetry system and ground control station,
- Perform flight testing on the system in the field,
- Analyse the data gathered and post process the data,
- Draw conclusions on the results obtained,
- Make recommendations and discuss possible future work.

## 1.3 LIMITATIONS

Due to the nature and complexity of this project, a number of limitations had to be accepted.

Some of the limitations are:

1. The sensors typically used for inertial measurement in avionic systems are outside the budget of this project; this meant that low cost sensors had to be used;
2. Processing power on the microcontroller is limited; this means that there is a limit to the complexity and accuracy of the algorithms that could be implemented. A powerful embedded computer could be used, but this would go against the project goal to keep costs and complexity to a minimum;
3. The system will operate purely as an instrument; it will thus not perform any control functions over the aircraft;
4. The avionics package will be limited to the troposphere; this is perfectly acceptable as this project will be tested on aircraft that only operate in this region.



## 1.4 PLAN OF DEVELOPMENT

This dissertation will be organised into the following chapters.

**Chapter 1** provide an introduction to the dissertation; this chapter discusses how and why the project will undertaken.

**Chapter 2** is a literature review. This chapter investigates what others in the field have done in addition to comparing different approaches to the problem being investigated.

**Chapter 3** provides a description of the hardware and software developed.

**Chapter 4** discusses the process of calibrating the sensors used.

**Chapter 5** describes the design and construction of the gliders used.

**Chapter 6** describes the realtime telemetry and ground system developed for this project.

**Chapter 7** presents and discusses the results obtained from lab and field testing.

**Chapter 8** provides conclusions based on the results obtained.

**Chapter 9** presents future work and improvements that can be made to the system to improve its performance, and migrate the system towards use in UAV applications.

**Appendix A** contains photographs from the field testing phase.

**Appendix B** shows all of the schematic and printed circuit board designs developed for this dissertation. These designs provide all of the details needed to reproduce the system hardware used in this dissertation.

**Appendix C** contains drawings of the apparatus that was designed and fabricated for use in the wind tunnel. In addition, photographs showing the setup within the wind tunnel are presented.

**Appendix D** provides details of additional files contained on the supplied CD.

CHAPTER 2

# LITERATURE REVIEW

## 2.1 AIRCRAFT

Man has always been fascinated with flight. Many attempts were made prior to the first successful heavier than air flight by the Wright brothers in 1903 [2].

From their first flight, the technology and performance of aircraft has been steadily improving and designers and pilots alike generally look for new ways of improving the performance, cost and efficiency of their aircraft.

Gliders have, however, been around for longer than powered aircraft. Sir George Cayley (1773-1857) developed the first glider capable of carrying a human in 1849 [3].

### 2.1.1 Airspeed

As an aircraft relies on the flow of air over its wings to provide valuable lift, it stands to reason that the speed of the air flowing over the wings is a very important factor to a pilot.

A loss of airspeed will result in a loss of lift and thus a drop in altitude. This may or may not be a problem depending on where the aircraft is in relation the ground.

The airspeed of an aircraft is typically measured using a differential pressure sensor; a differential pressure sensor is comparative in nature and will compare the pressures applied on each of its two input ports to find the difference.

When measuring airspeed, one port is kept static at atmospheric pressure and the other port is connected to a Pitot tube. A Pitot tube is a single tube device that faces directly into the incoming airstream; the airstream causes a pressure to develop within the tube and this pressure is then applied to the dynamic port of the pressure sensor. The pressure difference experienced is positively related to the airspeed of the aircraft.

There are two types of airspeed references, these two are described below.

***Indicated airspeed***

Indicated airspeed (IAS) assumes that the density of the air surrounding the aircraft is constant.

Using Bernoulli's equation the indicated airspeed can then be calculated as follows.

$$V_{indicated} = \sqrt{\frac{2 \times (P_{dynamic} - P_{static})}{\rho_{STP}}} \tag{2.1}$$

Where $P_{differential}$ is in Pascals and $\rho_{STP}$ is standard air density at STP (Standard Temperature and Pressure).

***True airspeed***

When measuring true airspeed, the density of the air surrounding the aircraft needs to be calculated.

By using the ideal gas formula as described in [4].

$$PV = nRT \tag{2.2}$$

We can calculate the density of air as:

$$\rho_{actual} = \frac{P_{static}}{R \times T} \tag{2.3}$$

Where $P_{static}$ is the static air pressure in Pa, $R$ is the ideal gas constant for air and $T$ is the temperature in Kelvin.

This equations shows us that the density is related to both the static pressure surrounding the aircraft and the temperature of the air surrounding it. As these two parameters change dramatically depending on the altitude at which the aircraft is flying and its geographical location, the density of air cannot always be ignored.

Since the density can now be adjusted for changes in static pressure and temperature, we can now calculate the true airspeed.

$$\begin{aligned} V_{true} &= \sqrt{\frac{2 \times (P_{dynamic} - P_{static})}{\rho_{actual}}} \\ &= \sqrt{\frac{2 \times (P_{dynamic} - P_{static})}{\frac{P_{static}}{R \times T}}} \end{aligned} \tag{2.4}$$

## 2.2 INERTIAL MEASUREMENT

### 2.2.1 Conventions

The following conventions will be used in this dissertation.

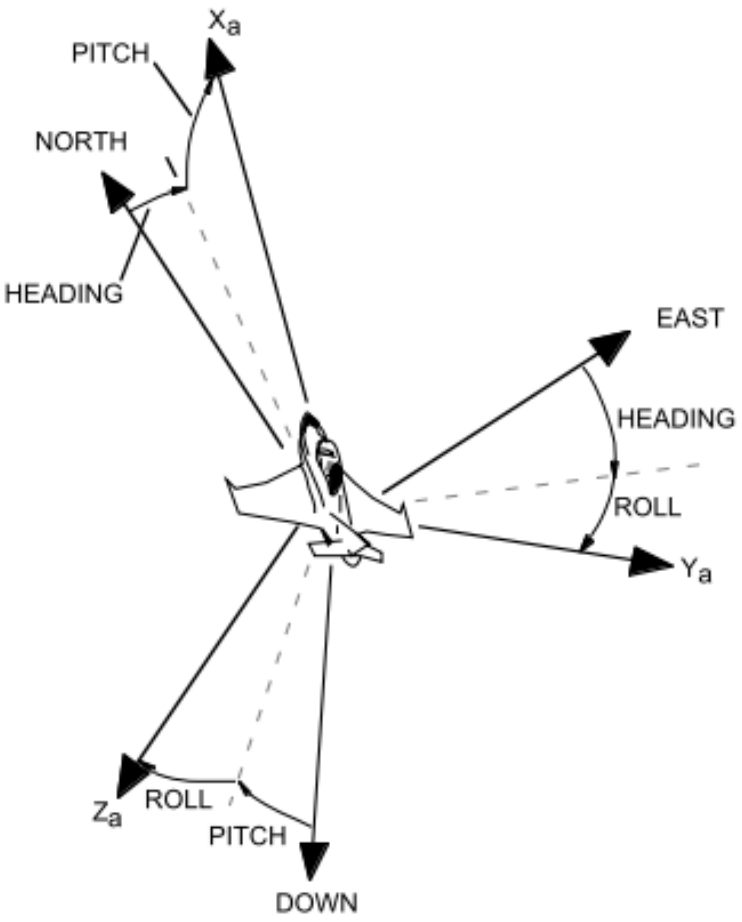


Figure 2.1: Figure defining the aircraft axes used (Figure taken from [5]).

Where North, East and Down represent the Earth's frame of reference, and Xa, Ya and Za represent the aircraft's frame of reference.

### 2.2.2 **Accelerometers**

Accelerometers by virtue of their name measure acceleration. This means that an accelerometer can be used to measure gravity. Since gravity exerts a force on an object in a set direction, one can measure pitch and roll using an accelerometer by measuring the magnitude and direction of gravity.

Unfortunately this only applies when the accelerometer is static; as any dynamic acceleration will either add or subtract from the reading gained from the gravitational acceleration depending on the axis in which the dynamic acceleration is acting.

The general formula of a linear accelerometer, as described in [6] is:

$$A = \frac{V_{out} - V_{off}}{S} \tag{2.5}$$

Where $A$ is the acceleration in g, $V_{out}$ is the voltage output of the accelerometer, $V_{off}$ is the offset voltage and $S$ is the sensitivity of the accelerometer.

***Offset calibration methods***

In order to measure acceleration accurately, one has to be able to reference the measured value with some known reference. This requires that each accelerometer is calibrated in order to determine the 0 G offset voltage. Unfortunately this offset is not constant even between devices of the same type from the same manufacturer; this means that each device needs to be calibrated individually to determine this offset [7].

Since the IMU sensing package used contains a three axis accelerometer, each of these axes will need to be calibrated.

As described in [7], the following two methods are available.

**Flat table method**

This method involves placing the device on a table that is assumed to be flat and taking the offset measurements directly.

This method is flawed in that it assumes that the table is flat and that the surface on which the table sits (i.e. the floor and the rest of the building) is flat and level.

There is no guarantee that this is the case and therefore this method is not acceptable.

**Rotation method**

This method involves rotating the device about each of its axes in order to determine the minimum and maximum range of the sensor's output.

During rotation, the sensor will experience a g force range of between -1 g and +1 g. The beginning and end sensor output value is unimportant as long as a complete rotation is completed.

The minimum sensor output will correspond with the offset required; this offset can then be subtracted from the uncorrected reading in order to determine the actual acceleration.

This method is advantageous when compared with the flat table method as it does not require specialised hardware to level the device.

It does, however, require someone to carefully rotate the device which, in a production environment, would be very time-consuming.

***Tilt sensing***

Gravity can be used to measure the pitch $\phi$ and roll $\theta$ of the aircraft.

Given that gravity will be measured, it stands to reason that the output of an accelerometer will be bounded between +1 g and -1 g, this assumes that the device is static.

As described in [6], the basic attitude of the aircraft can be determined from the acceleration in the x,y and z axes using the following three formulae.

$$\rho = \frac{A_x}{\sqrt{A_y^2 - A_z^2}} \tag{2.6}$$

$$\phi = \frac{A_y}{\sqrt{A_x^2 - A_z^2}} \tag{2.7}$$

$$\theta = \frac{\sqrt{A_x^2 - A_y^2}}{A_z} \tag{2.8}$$

Where $A_x$, $A_y$ and $A_z$ are the measured acceleration values in the $x$,$y$, and $z$ axis respectively.

### 2.2.3 **Gyroscopes**

A gyroscope is a device that measures the angular velocity of a body in motion; this allows the pitch $\rho$, roll $\phi$ and yaw $\theta$ rate of an aircraft to be measured.

There are several different types of gyroscopes available today; however, for the purposes of this project, Micro Electro-Mechanical System (MEMS) sensors will only be considered because one of the aims of this project is to use low cost MEMS sensors. Therefore other sensor types such as laser ring gyroscopes have not been evaluated or considered.

MEMS technology is different to conventional gyroscopes and accelerometers in that the mechanical construction of the device is small when compared to conventional mechanically rotated gyroscopes and accelerometers.

The small size means that a device can be incorporated into different consumer electronic devices that previously would have been too small or unable to justify the extra weight penalty of a large sensor device.

MEMS technology is mechanical in its design; this means that reliability can be a problem due to material stress during normal use and ageing during the product's life cycle [8].

### 2.2.4 **Magnetometers**

A magnetometer is a device that measures the relative strength of a magnetic field. For the purposes of this project a 3 DOF magnetometer will be used to measure the strength of the Earth's magnetic field; this will allow a magnetic heading to be calculated.

#### *Magnetic heading*

An important parameter when flying an aircraft is the direction in which the glider is travelling; this is known as the heading of the aircraft.

A magnetic compass is typically used for this purpose as the aircraft's heading is normally referenced to magnetic north.

In order to measure the direction of the Earth's magnetic field, a magnetometer can be used.

Following the method as described in [9], the heading or yaw of an aircraft can be corrected for changing pitch and roll attitudes using the rotation equations.

$$H_{x_e} = H_{x_b} \times cos(\phi) + H_{y_b} \times cos(\theta)sin(\phi) - H_{z_b} \times cos(\theta)sin(\phi) \quad (2.9)$$

$$H_{y_e} = H_{y_b} \times cos(\theta) + H_{z_b} \times sin(\theta) \quad (2.10)$$

Where: $H_{x_b}$, $H_{y_b}$ and $H_{z_b}$ refer to the measured magnetic field strength values in the $x$,$y$, and $z$ axis of the body frame respectively. $H_{x_e}$ and $H_{y_e}$ refer to the computed magnetic field strength in the $x$ and $y$ axis of the Earth frame respectively.

The relationship of the axis can be seen in figure 2.1.

These equations rotate the reference frame from the body of the aircraft to that of the Earth; this allows magnetic north to be determined as follows.

$$Yaw = arctan(\frac{H_{y_e}}{H_{x_e}}) \quad (2.11)$$

**Magnetic declination correction**

Magnetic declination refers to the correction angle between true north and magnetic north. Magnetic declination is not constant throughout the world and thus needs to be re-computed if one is moving over large distances.

For the purposes of this project it will be assumed to be constant given that the distances travelled will be small enough to ignore changes in declination.

Another approach that would allow more flexibility would be to allow the user to manually enter the declination of the area in which he/she intends to operate; this would have the advantage because declination is not a static variable for a particular area and thus would require periodic update.

## 2.3 DATA FUSION

The attitude of an aircraft refers to the pitch, roll and yaw of an aircraft with respect to a fixed reference frame. In the case of an aircraft, the fixed reference frame is the earth or inertial frame of reference.

In order to determine the attitude of an aircraft, a number of sensor outputs need to be combined to create an overall picture of the attitude of the aircraft. Some of these sensors are accelerometers, gyroscopes and magnetometers.

Data fusion needs to be employed to correct for the non-ideal properties of these sensors so that reliable attitude measurement can be accomplished.

Additional sensors such as barometric pressure sensors and GPS can also be fused so as to achieve a more accurate estimation of the vehicles states. This will be discussed below.

### 2.3.1 Direction cosine matrix method

The direction cosine matrix (DCM) **D** is a rotation matrix that rotates the earth reference frame to the body reference frame.

The DCM as described in [10] **D** is given by:

$$\mathbf{D} = \begin{bmatrix} cos\,\theta\,cos\,\psi & cos\,\theta\,sin\,\psi & -sin\,\theta \\ sin\,\phi\,sin\,\theta\,cos\,\psi & sin\,\phi\,sin\,\theta\,sin\,\psi & sin\,\phi\,cos\,\theta \\ -cos\,\phi\,sin\,\psi & +cos\,\phi\,cos\,\psi & \\ cos\,\phi\,sin\,\theta\,cos\,\psi & cos\,\phi\,sin\,\theta\,sin\,\psi & cos\,\phi\,cos\,\theta \\ +sin\,\phi\,sin\,\psi & -sin\,\phi\,cos\,\psi & \end{bmatrix} \tag{2.12}$$

The matrix **D** represents a ordered rotation through the angles $\phi$ followed by $\theta$ and then lastly $\psi$ [10]. Since matrix multiplication is not commutative, the order in which the rotations are done is important.

### 2.3.2 Non-linear Complementary filter

Many methods are available when one wishes to perform data fusion; according to [11], the two most common filters used are the Kalman filter and the complementary filter

Many systems that perform attitude estimation use a Kalman filter of some sort; however, many have found that they can be difficult to implement, computationally intensive and not sufficiently robust [11], [12], [1]. This is often because inexpensive sensors were used which have far more non-Gaussian noise and drift when compared to aerospace grade IMU's; this in turn caused the Kalman filter or Extended Kalman filter to perform poorly [1].

This implies that the Kalman filter is better suited to high-end aerospace IMU/INS systems where sufficient processing power and high grade IMU's are available.

The complementary filter is a comparatively simpler filter both in terms of its implementation and computational requirements and is thus better suited to applications where limited hardware resources are available.

A basic overview of the filter design can be seen in figure 2.2 [13].

Gyroscope data is sampled at high frequency and then integrated using a numerical integrator. Ideally integrating the output from the gyro's would result in the exact angle travelled through being known; however, gyro's are far from ideal as they suffer from bias and drift errors that vary with time. This means that the data fusion algorithm needs to counteract these non-ideal

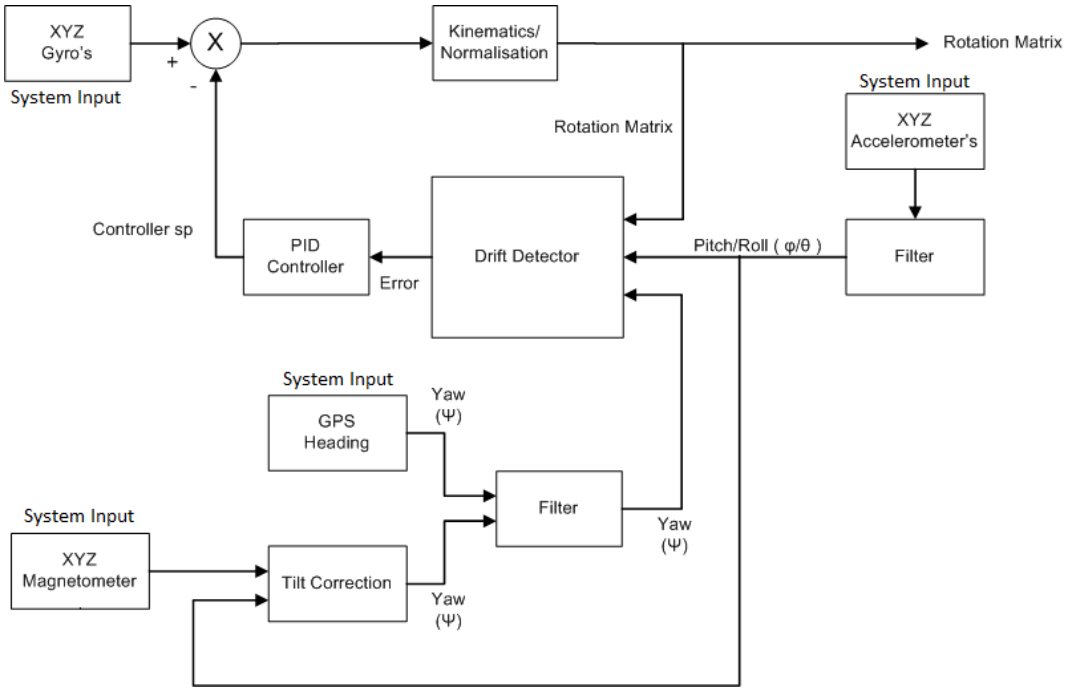


Figure 2.2: Non-linear complementary filter block diagram (Adapted from [13]).

quantities.

The integrated gyro data $d\theta$ is then fed into the DCM **D** using the method described in [13].

$$\mathbf{D} + dt = [\mathbf{D}] \begin{bmatrix} 1 & -d\theta_z & d\theta_y \\ d\theta_z & 1 & -d\theta_x \\ -d\theta_y & d\theta_x & 1 \end{bmatrix} \tag{2.13}$$

Accelerometers are used to determine the gravitational vector in the aircraft or body frame $g^b$. However, an aircraft does not always fly straight and level but rather rolls and pitches; this causes additional acceleration in addition to gravity.

Euston [11] describes a method to compensate for the centripetal acceleration caused by a bank or turn. Their method is to assume that the turn is of constant radius and zero side slip. Following [11], the acceleration is approximated by the following formula.

$$\hat{a} = \Omega \times V_{air} \tag{2.14}$$

Where $\Omega$ is the angular velocity of the aircraft, and $V_{air}$ is calculated as follows.

$$V_{air} = |v_{air}| \begin{pmatrix} cos(\alpha) \\ 0 \\ sin(\alpha) \end{pmatrix} \tag{2.15}$$

Where $\alpha$ is the angle of attack of the aircraft.

What is of particular interest is that Euston et al [11], notes that the error performance improved by 85% for pitch and 99% for roll once this compensation was added. In addition the same performance as a full Kalman filtered INS system was achieved by [11] using a complementary filter with angle of attack compensation. The aircraft used during these tests is not known at this stage.

This is a very important finding as it shows that significant improvements can be made just by including this small compensation algorithm.

***Euler angles***

The pitch, roll and yaw angles of the aircraft can be calculated from the DCM **D** using the following formulae.

$$pitch = -arcsin(\mathbf{D}_{32}) \tag{2.16}$$

$$roll = arctan(\frac{\mathbf{D}_{32}}{\mathbf{D}_{33}}) \tag{2.17}$$

$$yaw = arctan(\frac{\mathbf{D}_{21}}{\mathbf{D}_{11}}) \tag{2.18}$$

### 2.3.3 Additional Sensors

Much work has been done to include additional sensors into the system so as to improve the accuracy to which the system measures position, attitude, and altitude.

Barometric sensors, as used to measure altitude, rely on pressure measurements of the surrounding air to compute altitude. As the day to day air pressure of a particular region changes depending on the weather conditions, one has to adjust for these changes in pressure. As a result, altitude sensors are only accurate (in an absolute sense) over short periods of time [14]. Absolute accuracy is however less important than relative accuracy for this project as we are more concerned with a change in altitude.

One approach to determining altitude is simply to use the altitude measurement of the GPS as discussed in [15], however, GPS altitude accuracy is poor at the best of times [16] and is certainly not good enough for energy estimation.

Real time kinematics (RTK) GPS allows the performance of a GPS to be significantly improved. RTK-GPS is widely used in the land survey industry as it is highly accurate. Tang et al [14] compared the performance of RTK-GPS to that of a barometric pressure sensor and found that there altitude estimates closely resembled each other. RTK-GPS is also implemented on the Piccolo II flight controller to improve positioning accuracy [17].

A common method of improving the altitude measurement accuracy is to fuse GPS altitude and barometric altitude using a Kalman filter. Additionally, vertical acceleration can be integrated

and included in the aforementioned Kalman filter [18]. A good description of a Kalman filter that performs this type of sensor fusion can be found by reading Kim and Sukkarieh [16].

## 2.4 Energy Harvesting from the Environment

Energy harvesting from the surrounding environment allows the endurance of an aircraft to be increased almost indefinitely under the right conditions.

According to Ariff and Go [19], there a number of natural phenomena that can be exploited to add to the total energy of an aircraft. Some of these methods are described below

- thermal soaring
- dynamic soaring
- ridge soaring
- gust soaring
- wave soaring

The following figure describes and compares each of the flight methods.

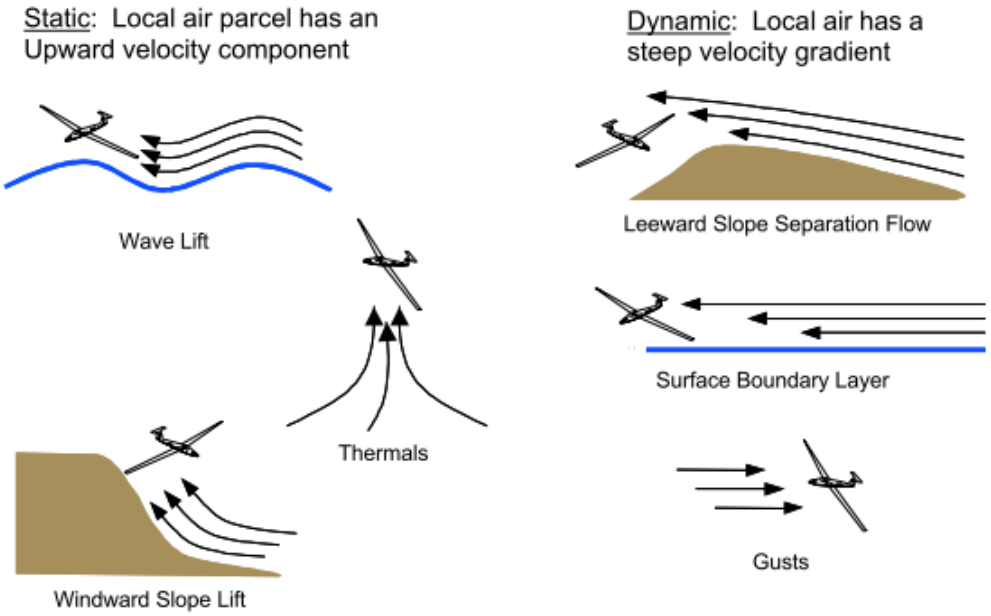


Figure 2.3: Figure illustrating thermal, dynamic, ridge, gust, and wave soaring (Taken from [20]).

Thermal soaring relies on convection heating of the land to generate rising air and therefore lift. The air rises in columns which vary greatly in diameter but increase in diameter with increasing

altitude. Thermals are not limited to areas of high temperatures but rather rely on a difference in air temperature to create lift. However, stronger thermals can usually be found in areas that are hotter than areas that are colder.

Dynamic soaring takes advantage of wind field gradients to provide energy to a glider. In order to take advantage of these wind gradients, the aircraft or UAV must fly back and forth along the wind gradient. Ariff and Go [19], notes that dynamic soaring is often more versatile for long range UAVs as the method allows an aircraft to travel over the ocean and during the night when thermal activity would be at its lowest; this has the obvious advantage in that an aircraft could, under the right circumstances, be able to fly almost anywhere and at any time. As noted by Grenestedt et al [21], long endurance flight is limited by the control systems/sensors and/or payload power requirements of the UAV and thus as these components are becoming smaller, the power required is less of a concern [19]. Grenestedt et al [21] proposes that a ram air turbine might be more effective as it could operate day and night; this is an interesting proposal provided that the drag induced during operation does not significantly reduce the performance of the aircraft. Air turbines have been used for many years on powered and un-powered full-size aircraft to generate electricity and to power fertiliser pumps for crop dusting aircraft. According to Allen [22], solar panels produce more power than ram air turbines at a small UAV size scale, but ram air turbines may be easier and cheaper to implement. One would have to conclude that the choice between a ram air turbine or solar panel depends heavily on the airframe used, and the payload that needs to be carried. What may be optimal in one situation might not be optimal in another.

Grenestedt et al [21] proposes that a UAV might be able to operate indefinitely while flying in the jet stream. Their proposal relies on the idea that the jet stream is comprised of continual wind gradients. These wind gradients would allow sufficient energy to be extracted to allow perpetual flight.

Grenestedt et al [23] also proposed a method of utilising dynamic soaring in hurricanes for storm monitoring for a prolonged period. Grenestedt noted that it could be possible under the right wind gradient condition, however they did not prove the theory in practise. The stresses imposed on an airframe while soaring in a hurricane would be significant. In addition, due to the high winds and turbulence within a hurricane, control of a small UAV could be a significant challenge.

Furthermore, gust soaring has also been proposed; however, to the author's knowledge, no practical use has been made of this type of energy extraction process.

Ridge or slope soaring, as it is often termed, is the practice of utilising lift that is generated when air that flowing across the land or sea, encounters a mountain and is forced up the slope. This causes the air to have a velocity component in the vertical direction, thus generating lift. Ridge soaring is limited to areas where the wind strikes a mountain or hill at a particular angle causing the required lift; this means that an aircraft is limited in its range based on the geography of the region of operation. In some circumstances this may be acceptable but for the most part, it is a limiting constraint. Simulation work has been done by Langelaan [24], who simulated a flight over a distance of 60 km along a uniform ridge, Langelaan [24] developed a method of determining the optimal flight path of the UAV so as to maximise the total energy of the aircraft

in a ridge soaring environment.

Wave soaring or wave lift occurs when air strikes a mountain and spills over the top, under the right geographical conditions, this can cause standing waves to occur on the leeward side of the mountain. The lift (and sink) generated under these conditions can be very strong and is commonly used by full size glider pilots. The current world altitude record for gliders was set by Steve Fossett while flying in wave lift to an altitude of 15,453 m [25].

The idea of UAVs using natural air currents to improve their endurance was first proposed in 1998 by Wharington and Herszberg [26], their idea was to develop a method of exploiting thermal air currents to increase the flight duration of UAVs by finding and positioning the UAV around the centre of the thermal, to then extract energy from the thermal.

Wharington and Herszberg noted that a significant problem during soaring was sensor uncertainty.

Their method included the use of re-enforcement learning algorithms; this was done to avoid the use of a system model which might be difficult to determine in practice [26].

Wharington and Herszberg's goal was to develop reinforcement learning methods of centering and maintaining a flight path around the thermal centre without commanding excessive bank angles; high bank angles cause the aircraft to sink and thus result in less overall energy gain.

The sensors used during Wharington and Herszberg's simulation were a set of GPS's and a total energy compensated (or TEK) variometer. The TEK variometer was used to determine the energy rate of the aircraft, and thus removed the need to calculate the total energy of the aircraft based on its speed and altitude. Their simulation results were never verified in the field, because at the time, their system did not converge on a solution sufficiently quickly so as to allow realtime operation.



### 2.4.1 Thermal Localisation Methods

In order to extract energy from a thermal, a few steps need to be taken, namely:

- one first has to know where to look,
- detect the thermal,
- exploit the thermal to extract as much energy as possible,
- track the thermal along its drift path,
- decide whether to stay in the current thermal or move on to another.

Each of the steps above will be discussed in more detail below.

### *Where to look for thermals*

As mentioned previously, a thermal occurs when energy from the sun is absorbed by the land causing convective heating; this causes a temperature difference to occur thus causing the flow of air from one place to another. The vertical velocity of a thermal varies greatly from thermal to thermal but often is between 1-10 m/s [27].

The size and shape of a thermal is also highly dependant on altitude, Ákos et al [27] note that updraft strength is generally stronger at medium altitudes when compared to low and high altitudes, while at the same time, growing in diameter with increasing altitude. Allen [28] notes that the vertical velocity distribution is highly time dependant and thus one can surmise that predicting a thermals velocity distribution would be very difficult in practice. For this reason Edwards [29] decided to forgo simulations and rather performed field testing as he reasoned that simulations would not account for the unpredictable nature of thermals.

Both Wharington and Herszberg [26] and Edwards [29] used a Gaussian distribution to describe vertical velocity across the cross-section of a thermal. This model is however somewhat simplistic in that is does not address the sinking air surrounding a thermal [30], although it does simplify calculations [30].

The Gaussian velocity as used by Edwards [29] can be seen in figure 2.4.

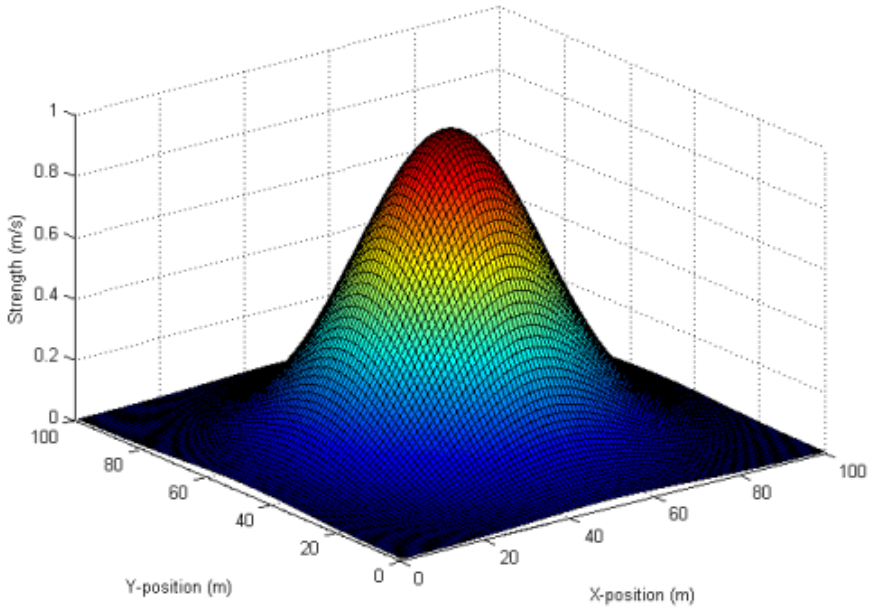


Figure 2.4: Figure showing the thermal updraft velocity distribution as used by Edwards (Taken from [29]).

Allen [28], developed an updraft model of a thermal using recorded data from weather balloons. This data allowed him to develop a more accurate velocity distribution model for thermals. From his work a more accurate model was developed. Sinking air (sink) that often occurs around a strong thermal [28] was introduced; however, the model did not make provision for this [30, 28].

Following the work of Allen [28], Clarke and Chen [30] developed a more accurate model that took note of sink.

An example of the model proposed by Clarke and Chen [30] can be seen in figure 2.5.

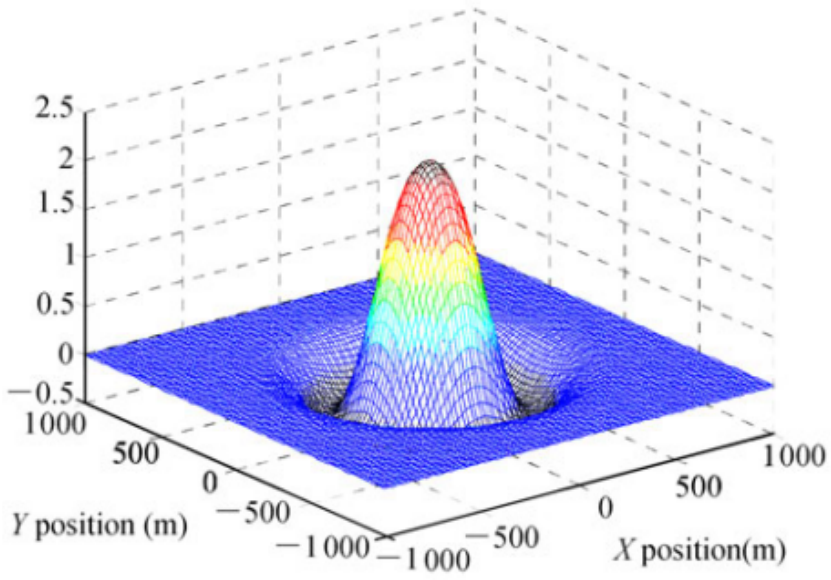


Figure 2.5: Figure showing an improved thermal updraft velocity distribution as used by Clarke and Chen (Taken from [30]).

Clarke and Chen [30] note that the effect of sink is more pronounced in weaker thermals and thus should be accounted for if one wants to improve their thermal exploitation success rate. The numerical difference in the success rate between accounting for sink and excluding it, is not known at this stage.

Allen [22] and Edwards [31], [29], have had good success by simply using a Gaussian (or sightly modified version thereof) vertical velocity distribution without accounting for sink, Antal et al [15] used Allen's [28] model in their simulations although they did not account for thermal drift. As a result, one can conclude that while it may not be optimal, it is still acceptable as seen during flight testing. In future a more complete model will probably be used, but at this stage, a Gaussian model is a fair approximation.

***Localisation of Thermals***

The total energy allows a pilot or computer to determine whether or not they are in lift. A net rise in energy indicates that energy is being added to the system (in this context, the glider), as this energy has to be coming from somewhere, and, given that a propulsion system is not present, one can deduce that the energy must be coming from the environment.

Therefore, it stands to reason that the accurate measurement of the total energy of the glider is of paramount importance. An inaccurate or poor-performing total energy estimation system would directly influence any process that takes input from it.

**Total energy estimation**

Total energy estimation refers to an estimate of the total amount of energy contained within a system.

The total energy $E_{Total}$ refers to the sum of the kinetic energy, $E_{Kinetic}$, which is determined by the airspeed of the aircraft, and the potential energy $E_{Potential}$, which is determined by the altitude.

According to Allen [32], the total energy contained within a aircraft can be estimated using the following method.

$$\begin{aligned} E_{Total} &= E_{Potential} + E_{Kinetic} \\ &= mgh + \frac{1}{2}mV^2 \\ &= h + \frac{1}{2g}V^2 \end{aligned} \tag{2.19}$$

By normalising the total energy equation to unit mass, we can remove the effect of a changing aircraft mass that may occur as a result of different pilot's weight, varying levels of ballast and different payloads in the case of a UAV.

The total energy rate $\dot{E}_{Total}$ is the first differential of the total energy $E_{Total}$.

Through experimental testing, Edwards [33] determined the sink polar for his aircraft; this allowed the natural sink of the aircraft to be removed from the system thus resulting in a measurement that better reflects the air condition around the aircraft.

Thus the corrected total energy rate $\dot{E}_{Total}$ can be corrected for glider sink by performing the following calculation.

$$\dot{E}_{Actual} = \dot{E}_{Total} - \dot{E}_{Glider} \tag{2.20}$$

(Equation adapted from [29].)

Unfortunately, the sink polar for the glider that will be used for this dissertation is not known and thus a more correct estimate of $\dot{E}_{Actual}$ is not available.

A TEK variometer is a type of total energy compensated variometer that performs these calculations mechanically using a specialised type of Pitot tube. This Pitot tube mechanically fuses airspeed and altitude to determine total energy.

An advantage of TEK variometer is that the calculations to determine the total energy do not have to be performed by the PC/microcontroller; however, having separate airspeed and altitude sensors allows more specialised digital filtering to be done and is thus considered more optimal

for this application. Edwards [33] used a TEK variometer as a reference during his testing phase, although the output of the TEK variometer did not interface into the control system of the aircraft.

**Airspeed and Altitude Filtering**

Noise filtering of the sampled altitude and airspeed sensor values is critical to overall system performance.

A simple solution might be to simply average the sampled readings to determine an average altitude or airspeed reading; however, this might not be an optimal solution given the time constraints experienced by the system.

Any phase difference or lag in the total energy estimation system would cause the GPS and energy estimates to be out of sync [29]; this would therefore affect any further calculations. Allen [32] developed a series of digital filters to deal with the noise experienced by the system. However Edwards [29] noted that this causes a lag of approximately two seconds, his solution was to use a filter with no phase delay; this was reported to significantly improve thermal location performance. This appears to be a sound solution to the problem.

Wharington and Herszberg [26] determined that the TEK variometer he used had a standard deviation of 0.3 m/s, additionally he chose to ignore readings below 0.1 m/s. As each variometer will be sightly different, experimental testing will be required to determine the sensor noise floor and thus what threshold to set in order to reduce the effects of noise.

**Interesting Applications**

Several interesting applications have been proposed for soaring UAVs in the literature. The application of soaring UAVs is not limited to just an academic exercise, but rather allows new opportunities to be explored that might not been feasible given the power constraints of small UAVs.

From a defence point of view, the application of soaring UAVs allows small UAVs that can be carried by the average person to increase their operational range and reduce their power requirements [34]. These UAVs would typically be used to provide reconnaissance over short distances.

Lee and Andersson [35] developed a UAV to act as a communication bridge to improve the range of a radio network by adding soaring capability to utilise thermals, so as to increase the range and duration of the UAV.

Lee and Andersson [35] used Allen's [32] work as a starting point, but added additional path planning criteria. These additional criteria introduced the Signal to Noise Ratio (SNR) of the wireless bridge into the control system. The idea is that the UAV needed to both maximise thermal exploitation and the SNR of the wireless bridge [35]. Although Lee and Andersson [35] did perform flight testing, only simulations were done when the SNR of the wireless bridge was added, Lee and Andersson [35] found that they could extend the flight endurance from the original two hours to six hours or more. Whether this is feasible is not known by the author as

it is a significant improvement. Given the unpredictable nature of thermals, the bounded flight region imposed by the range of the wireless bridge and local weather conditions, this endurance improvement could be highly variable and time of day dependant. Allen [22] notes that the success rate of finding thermals depends heavily on the season and time of launch.

Multiple UAV soaring has also been proposed and simulated by Antal et al [15]. The idea is that a group of UAVs could fly in a particular area, each one would search for thermals and communicate their findings within the group; this application is particularly interesting given Lee and Andersson's [35] work mentioned previously. This would allow greater range and increased bandwidth to be available due to the increased number of aircraft.

Kagabo [36] developed an interesting system. He positioned a thermal camera on a UAV to look forward so that the UAV could potentially identify areas on the ground that were warmer than the surrounding terrain, for example, a tar road or concrete structure, or, on the other hand, areas to avoid, such as a lake or dam. This would allow the UAV to follow a more effective flight path as compared to other methods that might involve flying in a grid pattern, which could cause the UAV to fly over areas with very little or no thermal activity.

**Hardware and Sensors Used**

The hardware used in most projects will make or break a project; this is certainly true in the case of UAV instrumentation. A good set of sensors will often make implementing algorithms easier as one does not have to deal with noise to the same extent as compared to low-cost sensors.

Much of the work done in autonomous soaring is simulation based. This means that less information is available about aircraft platforms and sensor payloads as compared to, say, a conventional powered UAV.

Allen [22], [32] and Edwards [29], [31] appear to have done the most practical work that the author is aware of. Their work has been a foundation onto which others have added.

Allen, Edwards, Hazard [37] and Lee and Andersson [35] used a SBXC built by RnR Products, this glider has a wingspan of 4.32 m and is typically used for long distance thermal endurance flights [38]. One of the main advantages of this airframe is its size. Firstly, this makes it easier to see from a distance and, secondly, it allows more space for a payload; this means that significant space limitations are not imposed on the avionics.

One common decision that has been made in the literature, is that a third party controller was used for inner loop control of the aircraft. For the most part, a Piccolo Plus or Piccolo II from Cloud Cap Technologies was used.

The use of an external flight controller is beneficial in this context, and is encouraged by Edwards [31] as it allows more time to be spent on soaring specific algorithms and processes.

This flight controller is a commercial product and performs all of the inertial sensing, GPS, airspeed and altitude data sampling and control functions needed for a UAV. Unfortunately, an item like the Piccolo II is well above the budget of this project and thus will not be considered.

Allen [32] used the Piccolo II to perform his soaring calculation onboard, whereas Edwards [31] used a separate computer connected to the ground station of his Piccolo II system to perform the soaring calculation needed. Edwards' approach is probably simpler to implement as it does not require integration with embedded hardware, which can be troublesome at times. It also allows more complex calculations to be made in realtime due to the increased computational ability of a PC. Allen's system is, however, more independent as it does not rely on a ground station to operate and thus is probably a more complete solution.

CHAPTER 3

# SYSTEM DESIGN

The design of the hardware and software can be broken down into a number of separate yet equally important sections. Two hardware versions were implemented: the first was a proof of concept design to determine what components would be suitable. The second prototype was a condensed version of the first where certain components were added and removed in order to reduce the physical size and complexity of the overall design. An global overview of the complete system can be seen in figure 3.1.

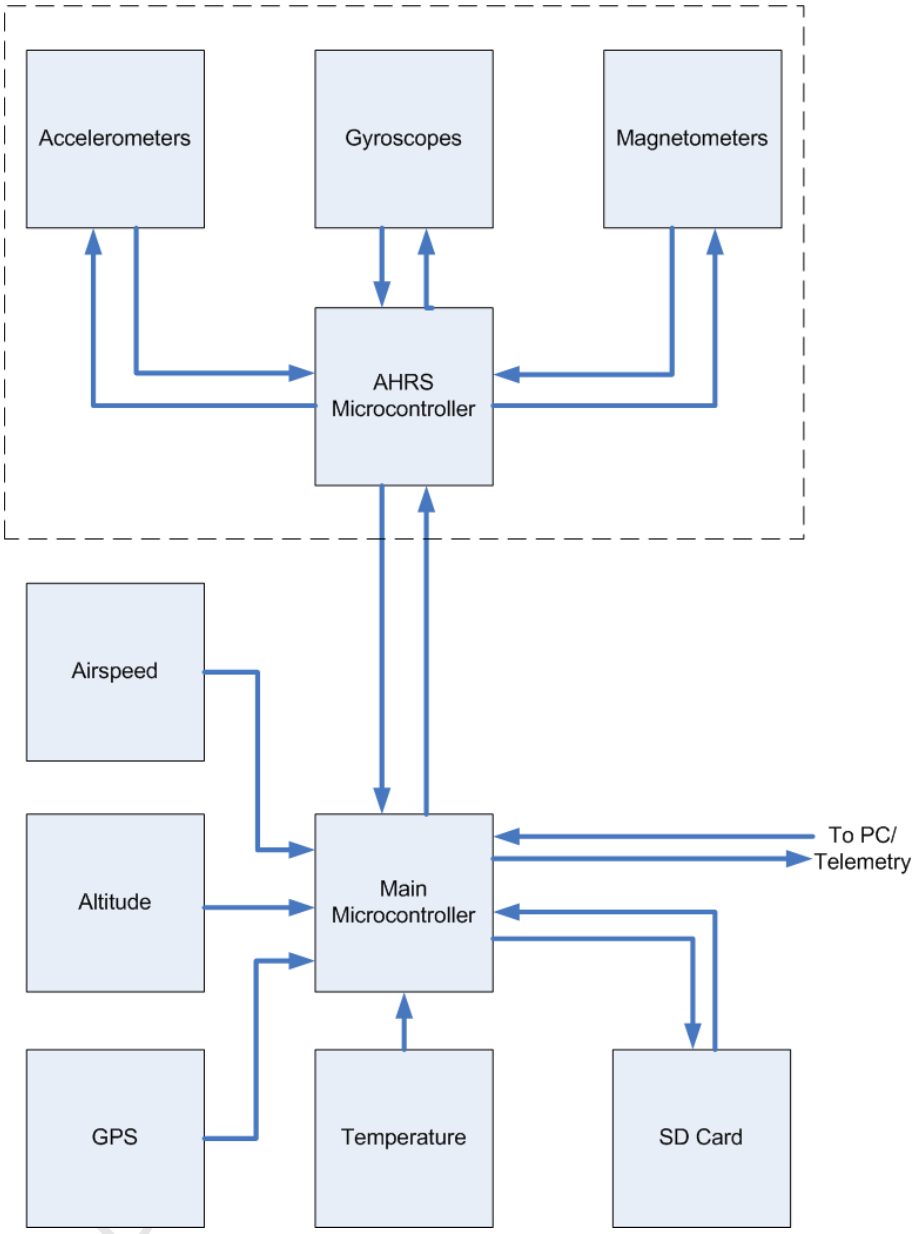


Figure 3.1: Figure showing the overall system; this figure also illustrates the data flow paths within the system. The attitude and heading reference system (AHRS) is contained within the dotted line. This dotted line also differentiates between the two primary system boards within the final design.

The basic overview in figure 3.1 above is the same for both the initial and final designs.

## 3.1 Initial Design

An initial proof of concept was built to determine sensor requirements and identify any potential pitfalls that might arise. The printed circuit boards (PCB's) that were designed for this initial prototype were designed in such a way that components could be changed so as to allow flexibility during the early stages of the design.

This was done as follows:

- the printed circuit boards were designed to be larger than they would typically be for a finalised design; this allows easier access to components,
- larger 0805 resistors and capacitors were used,
- The main microcontroller was of through-hole mounting technology; this allows a damaged microcontroller to be easily replaced,
- serial ports for the AHRS and GPS were simple pin headers; this allows different GPS modules to be used,
- the analog sensor power supply and ADC are placed on a separate printed circuit board; this allows only a single part of the design to be re-designed or replaced as required.

### 3.1.1 **Analog Hardware Design**

All of the analog hardware was designed on a single board. The design of this board is such that it fulfils the following functions:

- accepts an unregulated power source in the range of 7 V to 12 V,
- effectively regulates the power supply to 5 V,
- contains an absolute pressure sensor capable of measuring barometric pressure; this allows the altitude to be calculated. The precision of this sensor should equate to approximately 1m of altitude resolution,
- contains a differential pressure sensor, this sensor will be used in conjunction with a pitot tube to determine the airspeed of the aircraft. The differential pressure sensor should be capable of measuring differential pressures equivalent to approximately 200 km/h,
- contains a temperature sensor with an accuracy of $\pm 2^{\circ}C$, this allows the density of the surrounding air to be calculated thus allowing the indicated airspeed to be corrected to determine true airspeed,
- contains an analog to digital convertor with sufficient resolution to effectively measure the analog sensors.

The basic sensor requirements were decided upon by reviewing the performance of commercial autopilots such as the CloudCap Piccolo Plus and open source projects such as the Ardu-Pilot project. The performance of these devices was deemed to be a good starting point for the sensor specification.

***Airspeed***

As discussed in the literature review, airspeed is determined by measuring the differential pressure between the orifice of a pitot tube and static air pressure. A conventional differential pressure sensor was used to perform this task.

The sensor used was a Freescale MPXV5004DP [39]. This sensor was used because of its ready availability, acceptable performance and cost-effective price.

This sensor has an operational pressure range of 3.92 kPa [39].

At 3.92 kPa, airspeed is as follows:

$$\begin{aligned} V_{air} &= \sqrt{\frac{2 \times (P_{dynamic} - P_{static})}{\rho}} \\ &= \sqrt{\frac{2 \times (3920)}{1225}} \\ &= 80\ m/s\ or\ 288\ km/h \end{aligned} \tag{3.1}$$

As 288 km/h is well above the normal operating speed of the glider used for testing, the operational range is more than sufficient for the task.

For the purposes of the this project, airspeed is assumed to be indicated airspeed and not true airspeed.

The sensor calibration procedure and the results obtained can be found in chapter 4. The results obtained from calibration indicated that the sensor was not truly linear and had an offset. These discrepancies were corrected for however during the calibration process.

***Altitude***

Altitude is a critically important variable in the context of this design. The process of determining glider energy relies heavily on the performance of the altitude sensor as potential energy is determined using the present height of the glider.

The sensor used was a Freescale MPXA6115 [40].

Performance characteristics can be found in the following table.

Table 3.1: Performance characteristics for the Freescale MPXA6115 absolute pressure sensor. The values quoted in this table are taken from [40]

| Parameter | Value |
|---|---|
| Range | 15 - 115 kPa |
| Sensitivity | 45.9 mV/kPa (typ) |
| Accuracy | 1.5 % (max) |

The pressure range of 15 to 115 kPa allows barometric pressure to be measured with ease.

***Temperature***

Temperature was measured using a ADT7301 [41] digital temperature sensor, Analog Devices claim that this sensor has an accuracy of $\pm 1^{\circ}$C; this accuracy is more than sufficient for basic airspeed air density compensation.

***Power Supply***

The pressure sensors used to measure airspeed and altitude are both ratiometric, thus a stable and accurate power supply is needed in order to achieve and maintain accurate air pressure readings.

The specification was that the power supply output should be both accurate in terms of the voltage supplied, but, more importantly, it should be consistent in its performance. It is highly important that the power supply voltage does not drift over time and temperature as the calibration of both the airspeed and altitude sensors would be affected; this would obviously be detrimental to the overall system performance.

A simple voltage regulator was constructed to provide an accurate and stable 5 V supply to the sensors.

The voltage regulator consisted of a linear emitter follower in negative feedback. An ADR02 [42] precision voltage reference manufactured by Analog Devices was used to provide the required set point for the operational amplifier.

The operational amplifier used was a Analog Devices AD8675 [43] low input offset model; this product was selected so that the voltage reference provided by the voltage reference would be accurately reproduced on the output of the power supply.

A general purpose MJD31C [44] transistor was used, this part was selected based on its current handling capacity and gain performance. As the components that required a stable 5 V supply draw very little current, the pass transistor showed no appreciable rise in temperature. Maximum current tests were not performed as it was deemed not necessary. The risk of damaging components out-weighed the benefits of knowing the regulators power and current limits.

The circuit can be seen in the following schematic diagram.

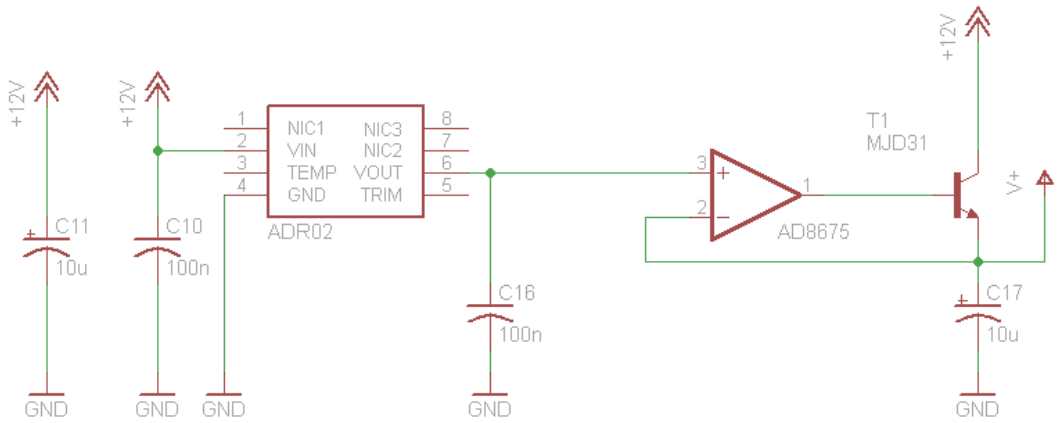


Figure 3.2: Figure showing a schematic drawing of the precision power supply stage.

Specifications of the regulator's components can be seen in the following tables.

Table 3.2: Specifications for the Analog Devices ADR02AR precision voltage reference. These values were taken from [42]

| Parameter | Maximum Value |
|---|---|
| Voltage Output | 5 V |
| Maximum Voltage Deviation | 5 mV |
| Temperature Coefficient | 10 ppm/$\circ$C |

Table 3.3: Specifications for the Analog Devices AD8675 precision operation amplifier used in the precision voltage regulator. These specifications were taken from [43].

| Parameter | Maximum Value |
|---|---|
| Offset Voltage | 75 $\mu$V |
| Offset Voltage Drift With Temperature | 0.6 $\mu$V/$\circ$C |

Photographs of both the initial digital and analog system boards can be seen in figures 3.3 and 3.4.

Figure 3.3: Figure showing the initial digital system board used.

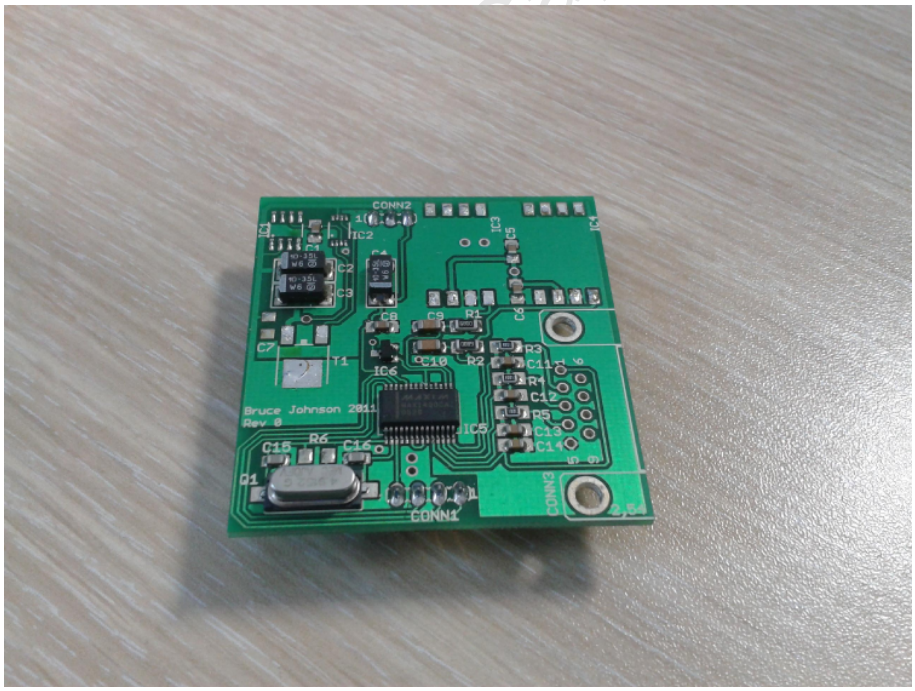


Figure 3.4: Figure showing the initial analog board; the sensors had been removed when this photograph was taken.

The schematics for this design can be found in Appendix B.

### 3.1.2 Digital Hardware Design

The digital hardware used in the initial design was contained on its own board. The following design criteria were deemed necessary:

- Contain one or more microcontroller(s),
- the device should be self-contained and operate without the assistance of a computer,
- be flexible in terms of its design so that hardware can be added without a complete re-design of the system,
- have a user serial debug interface.

## 3.2 Final Design

The second and final design that was developed, incorporated all of the lessons learnt during the testing and evaluation of the initial design. This design was more integrated compared to the initial design, and as a result, it was smaller in size.

The final design can be seen in figures 3.5 and 3.6 below.

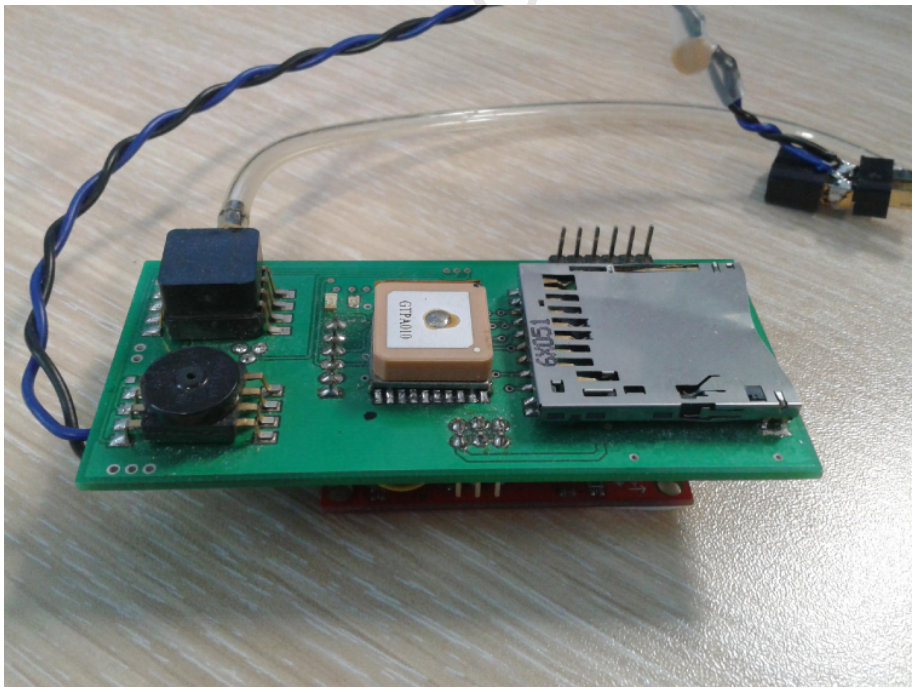

Figure 3.5: Figure showing a top view of the final system board. The red IMU board can be seen below the main board. The square component in the centre of the board is the GPS module.

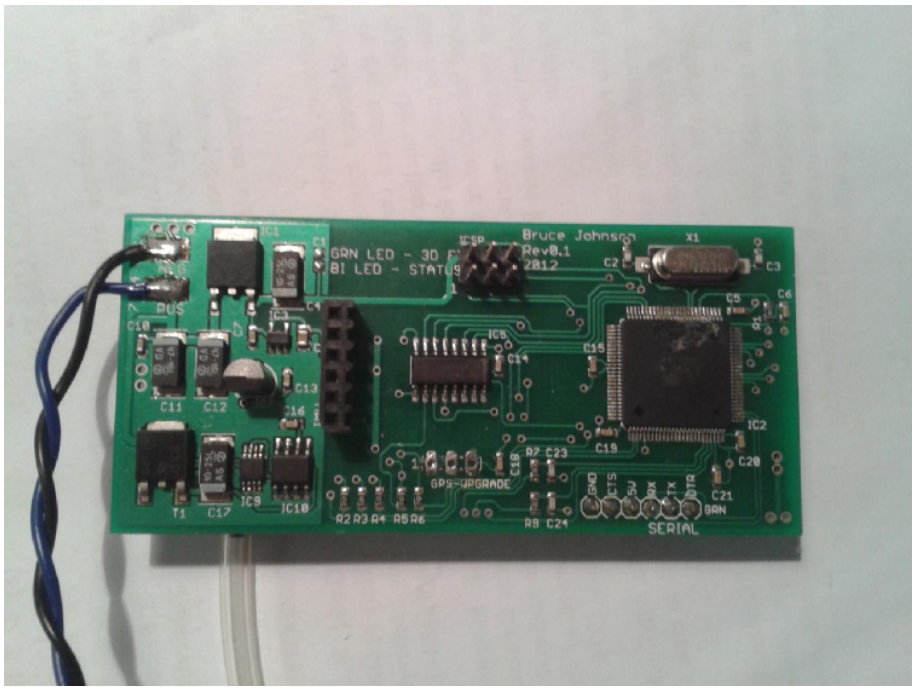


Figure 3.6: Figure showing a bottom view of the final system board. The power supply section can be seen on the left hand side of the board.



The schematic for this design can be found in Appendix B.

The system used an Atmel ATMega1280 microcontroller and was programmed using the Arduino development environment (version 0022). This code can be found on the CD provided.

### 3.2.1 **Temperature**

Temperature is not required when determining the airspeed and altitude of an aircraft, however it does improve the accuracy of the airspeed and altitude by allowing the measured pressures to be adjusted for air density. This allows airspeed (indicated airspeed) to be converted to true airspeed.

***Oversampling***

A goal set early on in the project was to be able to measure the height of the glider with a resolution of at least 1.5 m. This goal required the use of either a high performance ADC or another method of increasing the on-board ADC resolution.

Initially an external 18-bit ADC was used to measure the output voltages from both the airspeed and altitude sensors; this was done so that the required resolution could be attained. However the second iteration eliminated this device and rather used the on-board ADC in combination with oversampling techniques to improve the resolution of the samples. This approach reduced the size and complexity of the overall design.

However, during testing it became evident that in order to attain sufficient resolution, a great

number of samples would be required; this caused extra latency and additional processing overhead to be placed on the system. For this reason, a different barometric sensor was chosen.

A Bosch BMP085 [45] digital pressure sensor was used to replace the Freescale MPXA6115, as discussed in the testing chapter, this sensor proved to perform far better than the original sensor.

The specifications of the BMP085 can be seen in the table below:

Table 3.4: Specifications for the Bosch BMP085 barometric pressure sensor. These specifications were taken from [45]

| Sensor Type | Interface | Range | Resolution | Additional Features |
|---|---|---|---|---|
| Barometric | Digital $I^2C$ | 300 - 1100 hPa | 0.25m | Temperature Sensor |

## 3.3 DATALOGGING

In order to perform post-processing and analysis of the data acquired during flight, a method of storing the data is required so that it might be retrieved at a later stage. Several options are available in this regard. Only one, however, stood out as the most acceptable method.

A comparison of the various methods can be found in table 3.5.

Table 3.5: Comparison of the various technologies available to store the flight data.

| Technology | RAM | SD Card | EEPROM | RF link |
|---|---|---|---|---|
| Storage Capacity | KB | GB | MB | Zero |
| Data Retention | Power On | Years | Years | Zero |
| Ease of use | Easy | Moderate | Easy | Moderate |

The average data throughput assuming a storage frequency of 10 Hz is approximately 1 200 bytes per second. Assuming a one hour flight, the storage requirements should allow at least 4.3 MB.

Following on with the above calculation, the only viable options are either to use an SD card or to transmit the data to a receiving station. An RF link would require more hardware, software and firmware in order to realise a reliable data storage system.

An SD card was thus used as it is a reliable, inexpensive method of achieving a high capacity storage system, using an SD card also almost ensures that no data is lost (assuming no file corruption occurs); this is an important consideration as a loss of even a few seconds of data would hamper algorithm development and data analysis post-flight.

A Sandisk 1GB SD card was selected.

The diagram below shows the setup and operational procedure for the SD card.

When the system is first powered up, an attempt is made to initialise the SD card. If the card is not present or is incompatible, the initialisation operation will fail. System power needs to be

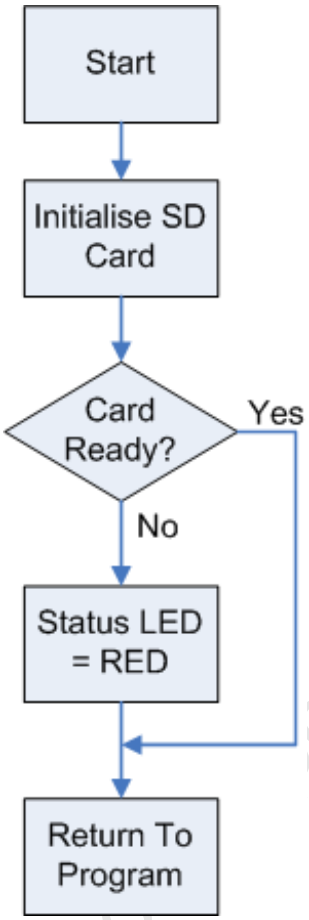


Figure 3.7: Flow diagram illustrating how the SD card is initialised.

cycled in order to retry the initialisation procedure. A method was implemented to detect the SD card automatically and to re-initialise the card; this would allow the operator to remove the card during operation and re-insert it without having to cycle power, however the method was not used in the final version of the firmware as it was deemed unnecessary.

During the testing procedure, a number of successive flights were performed before the SD card was removed and the contents downloaded. This was done because if the system is powered down, the GPS will have to perform a cold start, thus taking more time than necessary. A cold start was required for each GPS start as backup power was not provided. Re-initialisation of the SD card was essentially redundant as the card would not be removed during operation under normal operating conditions.

The filename used during the logging operation is automatically generated by a random number algorithm in the range of one to one million. The seed for this operation is generated using a spare ADC port that is left floating; this allows noise from the environment to govern the voltage sampled by the ADC thus allowing a good seed to be gathered. This seed was then passed onto the random number generating algorithm which then created the filename. The likelihood of having two filenames that are the same over the course of a half dozen flight is very remote. Even if such an event would to occur, the data would simply be appended to the end of the last

flight that carried the same filename.

The use of a random variable is acceptable for the purposes of this project as the time and date are extracted post-flight from the saved GPS data; this means that the actual filename plays a minimal role in the overall context of the datalogging system. GPS time and date information could have been used for the filename, however, the logging process starts before this time and date information is available due to the logging of the other sensors present in the system. Renaming of the file would have been possible but would have added additional complexity.

The following figure shows the procedure for creating and writing to a file.

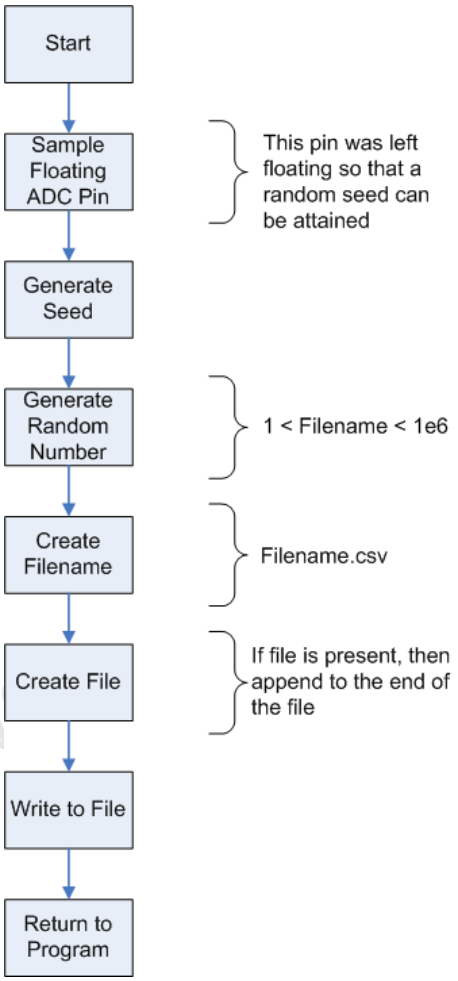


Figure 3.8: Flow diagram describing how a filename is generated and then used during the datalogging process.

## 3.4 Inertial Measurement Unit

An inertial measurement unit was used as an attitude and heading reference system (AHRS); this system provides real time pitch, roll and yaw information to the system.

An aviation grade inertial measurement unit was outside the budget of this project; this neces-

sitated the use of a cheaper and less accurate IMU.

The IMU used in this system is a nine degree of freedom Razor IMU developed by Sparkfun Electronics [46]. The unit features an ADXL345 triple axis accelerometer, LPR530AL dual axis gyroscope, LY530AL single axis gyroscope, HMC5843 triple axis magnetometer.

Other IMU's were considered, but due to a limited budget, and the ease with which this component could be integrated into the system, this device was chosen.

Individual sensors could have been sourced, and a breakout board designed; however a choice was made to rather spend time on other aspects of the project.

The IMU board can be seen in figure 3.9 below. The second smaller board is the Bosch BMP085 pressure sensor.

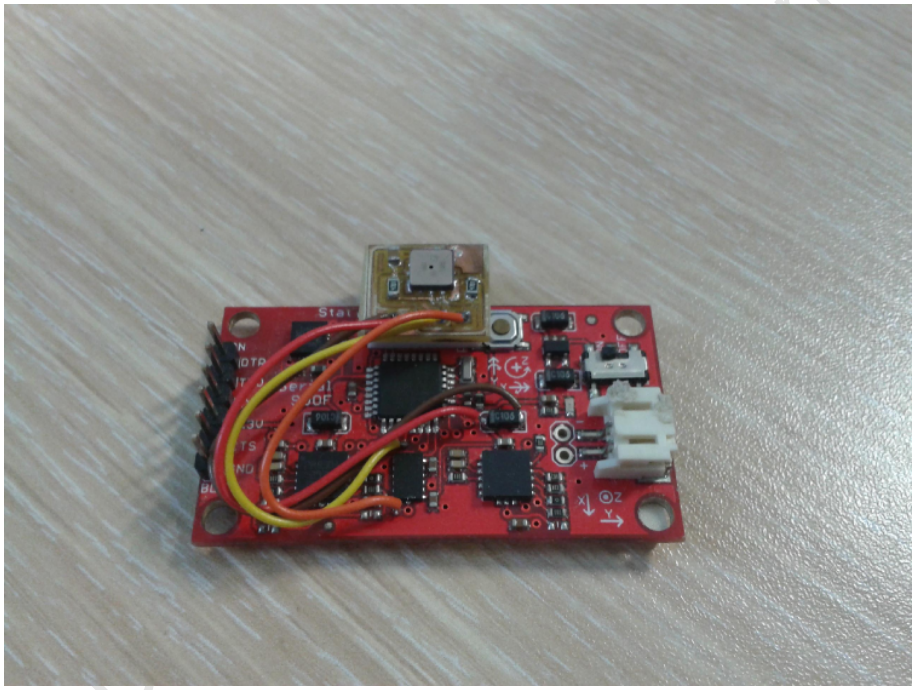

Figure 3.9: Figure showing the IMU used, the Bosch BMP085 can be seen on the second smaller board.

Sensor performance figures can be found in table 3.6.

Table 3.6: Table of characteristics and performance figures for each of the sensors found in the inertial measurement unit.Specifications for each of the above sensors taken from their respective datasheets [47, 48, 49, 50]

| Sensor model | Sensor type | Electrical interface | Measurement Range | Sensitivity |
|---|---|---|---|---|
| ADXL345 | triple axis accelerometer | $I^2C$ | $\pm$2g, $\pm$4g, $\pm$8g, $\pm$16g | 3.9mg/LSB |
| LPR530AL | dual axis gyroscope | Analog | 300°/s | 3.33mV/°/s |
| LY530AL | single axis gyroscope | Analog | 300°/s | 3.3mV/°/s |
| HMC5843 | triple axis magnetometer | $I^2C$ | $\pm$4G | 7mG |

The sensor accuracy and linearity was assumed to be what the manufacturer claimed. This was done because facilities were not available to verify the performance of the these sensors.

The unit also includes a small Atmel ATMega328 8-bit microcontroller to perform sensor sampling and data post-processing.

The onboard microcontroller was used to both sample each of the sensors, filter the data gained, and implement an attitude and heading reference system (AHRS). As described in the literature review, this system performs data fusion algorithms to process the data from the sensors so as to estimate the pitch, roll and yaw of the glider. The software used for the IMU was adapted from existing software provided by Sparkfun Electronics, see [46, 51] for additional details.

Once the system had finished processing each of the aforementioned variables, the data was passed to the main microcontroller via a full duplex serial link.

The method used to transfer the data to and from the AHRS micro-controller was accomplished using a packetised system.

Each of the packets are made up in the following way.

Table 3.7: AHRS to main micro-controller Packet layout.

| | | | | | | | | | | | |
|---|---|---|---|---|---|---|---|---|---|---|---|
| \$ | $\rho$ | $\phi$ | $\theta$ | $A_x$ | $A_y$ | $A_z$ | $p$ | $q$ | $r$ | $Heading_{Magnetic}$ | * |

Table 3.8: Main micro-controller to AHRS Packet layout

| | | | |
|---|---|---|---|
| \$ | TAS | GPS Heading | * |

Where the dollar symbol (\$) signifies the first byte to be transmitted in both cases, each of the variables transmitted are of float type, however TAS and GPS Heading are of byte type.

A start and end byte may seem redundant, but the use of these two bytes simplifies the parsing of the arriving packet significantly. A cyclic redundancy check (CRC) byte was not used as the system proved to be sufficiently reliable in its current form.

In future versions of the system, all nine direction cosine matrix (DCM) elements should be transmitted. However, a lack of serial buffer space limited the overall packet size and thus forced the author to only transmit the bare essential variables to the main microcontroller.

As float data types were used for most of the variables, the use of a higher serial bus speed of 38 400 bps was necessary.

## 3.5 GLOBAL POSITIONING SYSTEM

A GlobalTop GMS-U1LP GPS [52] was used to provide position, heading, ground speed, time, date and approximate altitude to the system. This GPS module has an integrated antenna and thus makes the unit very compact. The unit simply requires a 3.3 V supply voltage and the required serial communication data lines; this makes the unit ideally suited for the small confined spaces within a model aircraft fuselage.

The GPS system operates at a serial bus speed of 9 600 bps. This speed was the default speed of the GPS and proved to be sufficient so it was not changed.

A status LED was added to the system to provide an easy to read indication of whether the system had acquired a 3D fix. This LED flashes at 1 Hz until such time as the system has a 3D fix, at which point the LED remains on. This proved useful during the pre-flight phase of each testing session as the pilot then knows that the system is ready for operation without having to connect the computer to the system.

## 3.6 GENERAL SYSTEM

A bi-colour LED was added to the system. This LED remains red continuously when there is a problem with the SD card; this can occur when the SD card is not present or is not compatible with the system.

The system requires a FAT file system.

During logging operations, the LED will flash green while the SD card is being written to. After file writing is completed, the LED remains off.

## 3.7 ALGORITHM DEVELOPMENT

Post flight analysis of the logged data was accomplished in an offline manner using Matlab. This method was chosen as it allows several different algorithms and methods to be implemented in a higher level language than used on the embedded system; this allows algorithms to be modified and implemented faster than an equivalent implementation in the C language.

The algorithms and design decisions will be discussed in the following sections.

## 3.8 DATA CAPTURE

The data acquired during flight testing is logged to an SD card in the form of a *.csv file, a method of directly reading out this data, parsing it and loading it into the Matlab (version r2007b, The Mathworks, Natick, Massachusetts 01760 USA) workspace was developed. The Matlab code used may be found on the CD provided.

## 3.9 PRE-FILTERING

Pre-filtering was done only once the data has been captured by Matlab, no filtering was performed within the embedded system as this would have restricted the ability to experiment with different filtering algorithms at a later stage; this would have meant that any changes to the filtering methods used would require additional flight testing, obviously this would be very inconvenient and impractical.

The data is first trimmed to remove data generated from before the GPS has acquired a 3D fix and after landing; this data has no particular value and thus can be removed.

An average altitude is determined by averaging the logged altitude from before the GPS has acquired a 3D fix; this averaged altitude is then assumed to be the altitude offset for the day. The altitude offset needs to be considered to account for changing atmospheric air pressure conditions. All further altitude measurements are corrected using the altitude offset.

CHAPTER 4

# SENSOR CALIBRATION

In order to gain the best performance from a sensor, it should be calibrated with respect to a known reference.

The sensors used for airspeed and altitude measurement were calibrated using the procedures described in the following sections.

## 4.1 WIND TUNNEL TESTING

The Freescale MPXV5004DP airspeed sensor used in this project was calibrated in a wind tunnel. This was done to determine the linearity of the sensor in addition to any offsets that might be present in the sensors output.

### 4.1.1 Method

Calibration of this sensor was done as follows: beginning at 0 km/h, the airspeed within the wind tunnel was increased to a maximum of 105 km/h in intervals of 5 km/h. At each step, the wind speed was measured three times using the device under test and a calibrated instrument; both readings were recorded. A steady state speed was also measured; this was done at the following speeds:

- 0 km/h
- 25 km/h
- 50 km/h
- 75 km/h
- 100 km/h

Ten readings were made at ten second intervals; each reading was an average of three samples.

The following variables were recorded at the specified interval.

- Sensor voltage [V]
- Calculated pressure [KPa]
- Actual pressure [KPa]
- Calculated Airspeed [Km/h]
- Temperature [°C]

### 4.1.2 Wind Tunnel Apparatus

In order to operate a wind tunnel safely, all devices under test need to be securely and accurately fixed so that the force of the wind does not cause an accident.

For this reason, a dedicated stand was constructed to securely hold the wing housing the pitot tube that required calibration. The pitot tube was located on the underside of the wing, approximately one third of the span outboard of the fuselage. This location is approximately the same for both the wind tunnel test phase and the field testing phase.

The design and fabrication of this stand will now be discussed.

***Wing stand Design and fabrication***

The stand was designed using Solidworks 2010. Materials used were 30x30x2mm mild steel square tubing for the main structure, and medium density fibreboard (MDF) for the wing spar clamp; MDF was used so as no to crush and therefore damage the carbon fibre wing spar joiner, MDF is relatively soft and will thus conform to the shape of the wing spar more than a metal clamp.

### 4.1.3 Calibration Results

Calibration results can be seen in the following figures.

From the data recorded, a look-up table was generated using the following method.

Table 4.1: Look-up table generation method

| Airspeed Range [km/h] | Look-up table generation formula |
|---|---|
| 0-50 | -2E-08x4 + 3E-05x3 - 0.006x2 + 0.590x - 22.10 |
| 50-200 | 1.058x - 8.121 |

Where:

$$\begin{aligned} V_{indcorrect} &= V_{induncorrected} + Look - upTable\left(V_{induncorrected}\right) \\ & V_{indcorrect}, V_{induncorrected} \in \mathbb{Z} \end{aligned} \tag{4.1}$$

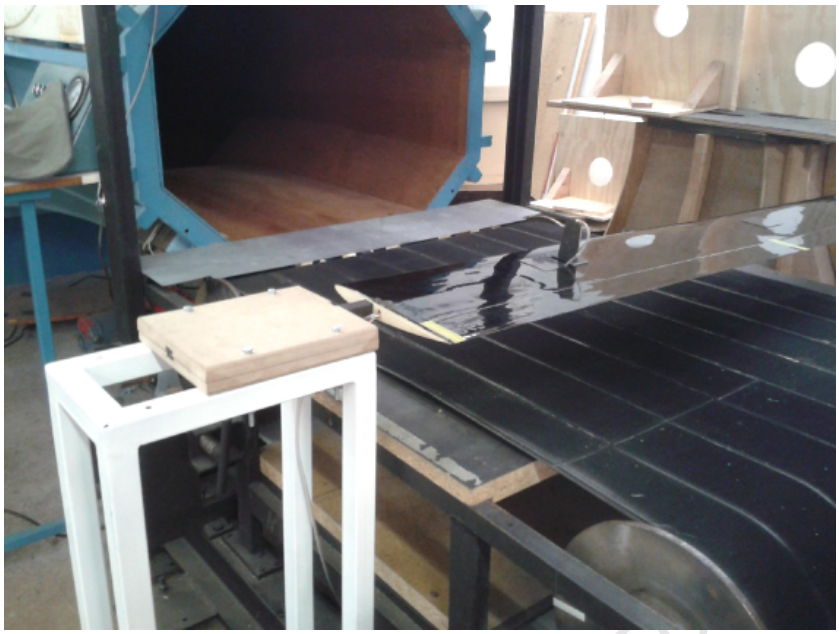

Figure 4.1: Photograph showing placement of the pitot tube on the wing. The photograph also show how the apparatus is positioned within the wind tunnel.

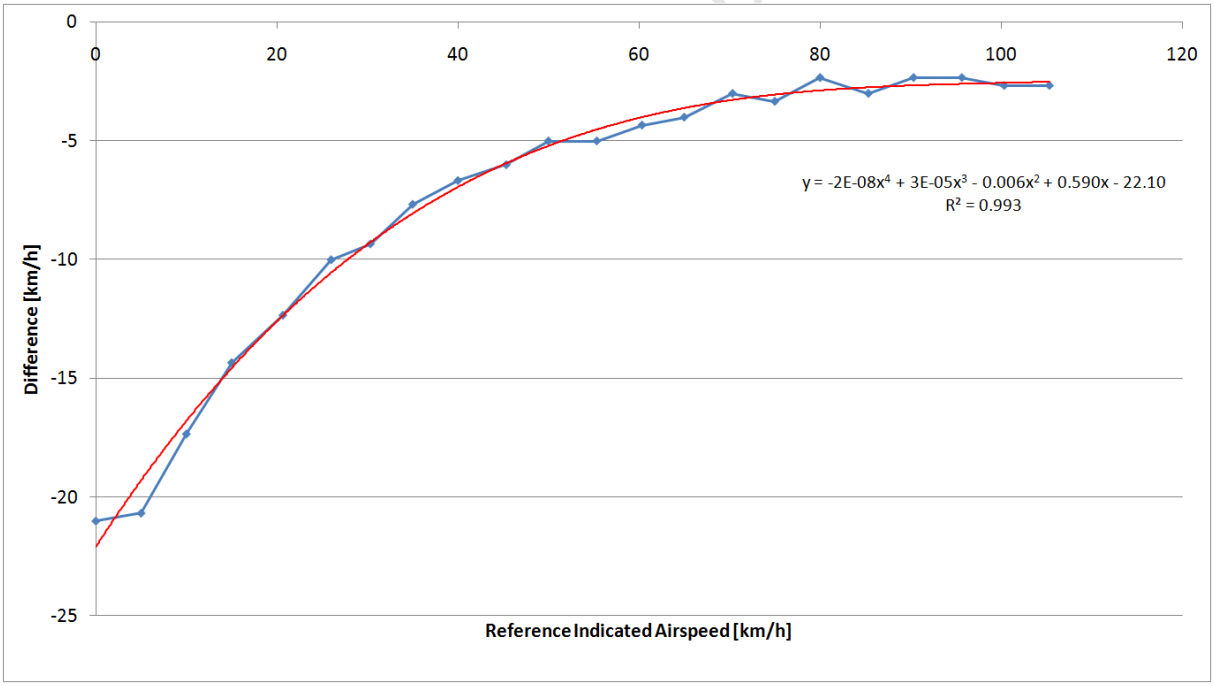


Figure 4.2: Graph of reference indicated airspeed manometer and recorded indicated airspeed from the device prior to calibration; data in blue, trendline in red

The look-up table generation operation was broken up into two ranges to improve the trend-line fit. Once the look-up table was generated, the table was loaded onto the device and the entire experiment was repeated.

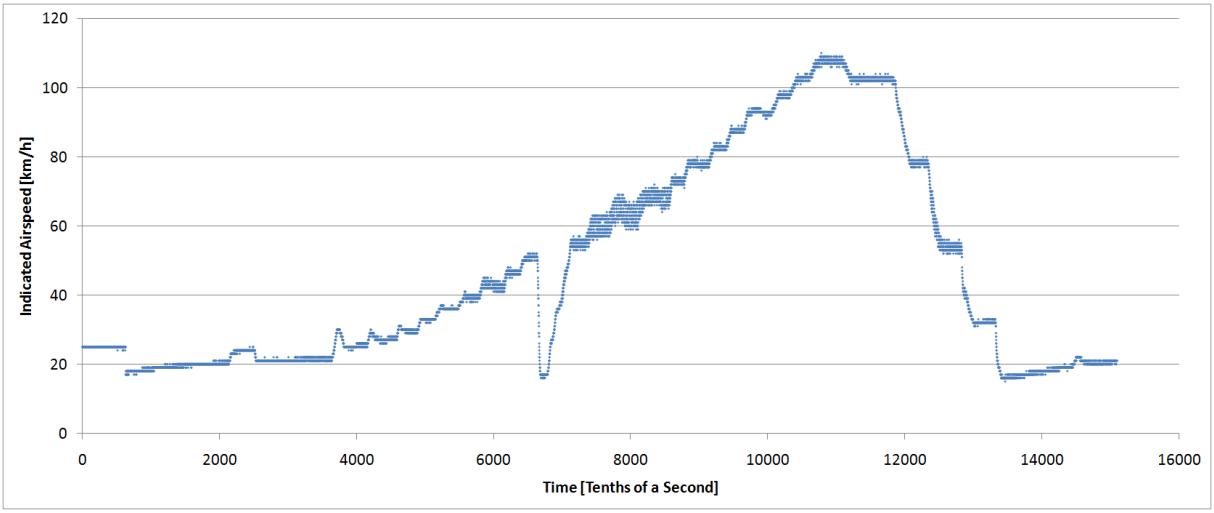


Figure 4.3: Recorded indicated airspeed from the device prior to calibration. The sudden drop in airspeed at around 6500 on the time scale represents the transition from low speed to high speed mode of the wind tunnel. This transition period is a characteristic of the wind tunnel.

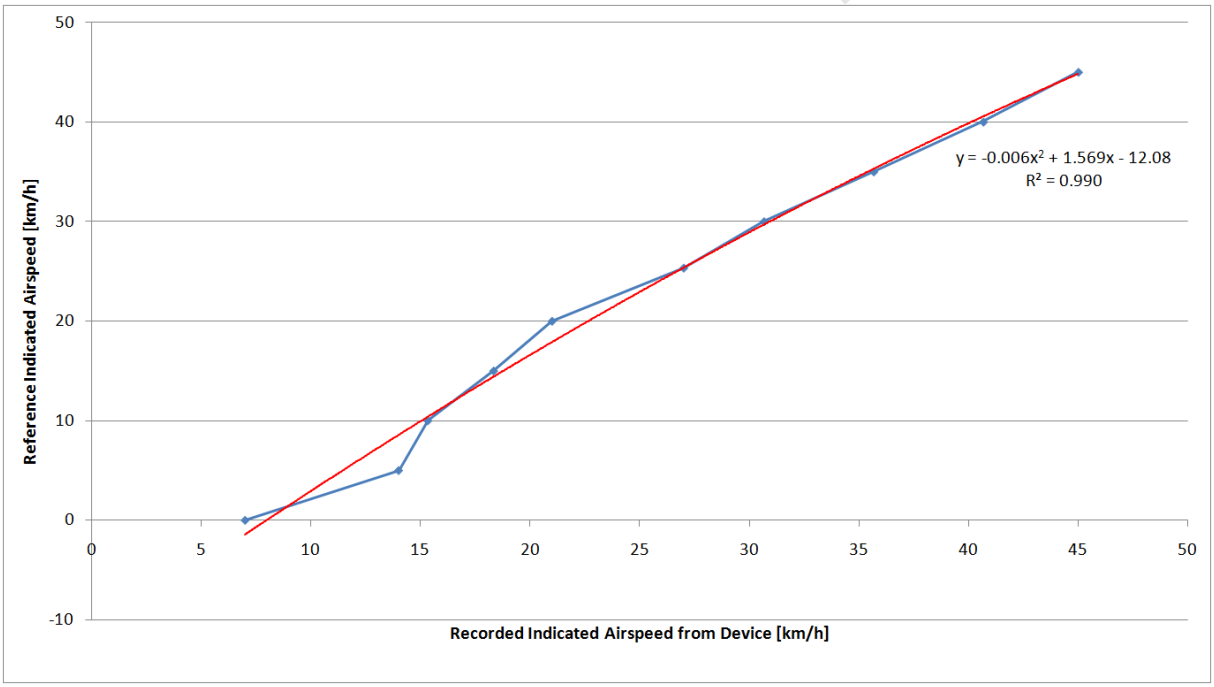


Figure 4.4: Graph of reference indicated airspeed manometer and recorded indicated airspeed from the device post calibration; data in blue, trendline in red

### 4.1.4 **Observations**

Certain observations were made during and after the experiment. The most notable are discussed below.

Pitot tube performance was not accurate at low speeds of 20 km/h or less; this was determined to be a non-issue as the glider used for flight testing operates at significantly higher speeds.

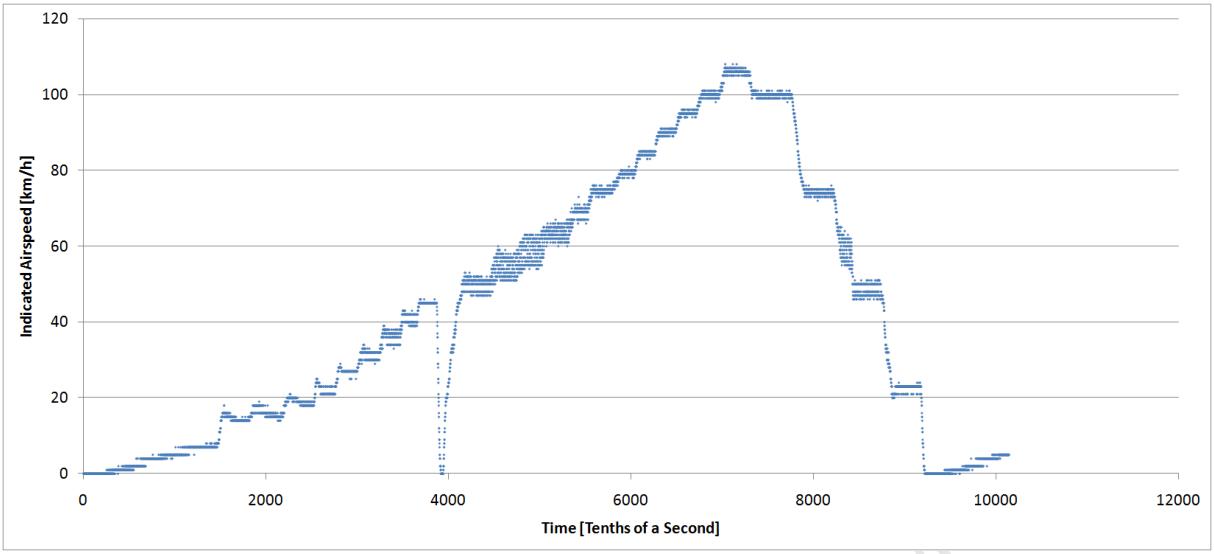


Figure 4.5: Recorded indicated airspeed from the device post calibration

Hysteresis was noted at low speeds; again, this is not a problem due to the glider's speed range.

The pitot tube operated well at higher speeds: a linear relationship can clearly be seen between the airspeed reference and the device under test. The look up table generated makes the assumption that this relationship holds up to 200 km/h.

Noticeable turbulence in the 50 - 80 km/h range was present; this turbulence caused the wing holding the pitot tube to oscillate. The turbulence experienced in this speed range manifested as noise in the airspeed measurements.

The turbulence and resulting vibration experienced reduced in magnitude as airspeed increased beyond 80 km/h. The source of the turbulence is speculated to have resulted from the wind tunnel. However, conclusive evidence is not available to support this speculation.

## 4.2 Altitude Calibration

Calibration of an altimeter requires that the sensor be placed in a chamber; the air pressure within the chamber is then either evacuated (to simulate rising altitude) or pressurised (to simulate decreasing altitude). As no facility was available to test the sensor, the accuracy of the sensor has been assumed to be what the manufacturer claims it to be.

## 4.3 Attitude Calibration

Accelerometers and gyroscopes both require regular offset calibration, this was done at every system start up by placing the system on level ground and taking a number of samples to calculate an average. This method proved to be acceptable for the application.

CHAPTER 5

# GLIDER DESIGN

Initially a dedicated and specialised glider was constructed for this project. This glider was designed specifically for thermal gliding applications. However, this initial design proved to be problematic, and, due to time constraints, another glider was sourced so that experiments could be conducted within the specified time frame.

The initial glider design was inspired by the designs of Mark Drela (Massachusetts Institute of Technology) and the glider was constructed over the summer of 2011/2012. This design encompassed several composite construction methods that had to be learnt by the author prior to the construction of the glider, namely, working with carbon fibre, Aramid and vacuum bagging of wings and tail-planes. These methods proved to be highly successful and a very strong and lightweight glider was constructed.

Unfortunately, design revisions to the device meant that space within the glider's fuselage was insufficient to accommodate all of the radio control parts, the instrumentation electronics and sufficient lead to correct the centre of gravity of the glider.

The specifications of the first glider that was built are as follows:

Table 5.1: Glider specifications for the first glider built.

| | | |
|---|---|---|
| Wingspan | - | 3.7m |
| Fuselage length | - | 1.72m |
| Glider weight | - | 2.3kg |
| Aspect ratio | - | 14.5 |

Isoboard foam was used for the wing and tail cores; this material was used as it has a significantly higher compressive strength (160-310 KPa) than conventional polystyrene [53]

The glider used the following layup schedule for the wings.

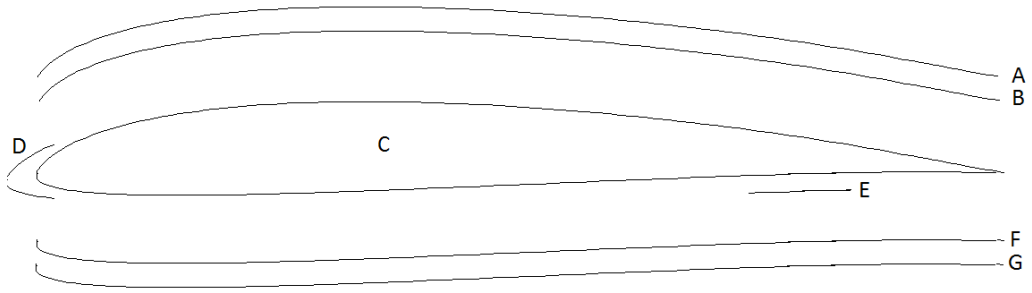


Figure 5.1: Figure showing a cross sectional profile of the wing. This figure illustrates how the various wing skin components are arranged within the wing.

Where:

A - 49 g/m$^2$ Glass cloth at 90 °

B - 150 g/m$^2$ Uni-directional carbon fibre at 90 °

C - Isoboard foam core

D - 60 g/m$^2$ Aramid and 45 g/m$^2$ glass cloth composite at a 45° bias cut leading edge

E - 60 g/m$^2$ Aramid live control surface hinge

F - 150 g/m$^2$ Uni-directional carbon fibre at 90 °

G - 49 g/m$^2$ Glass cloth at 90 °

Live hinges were used for all of the control surfaces as they provide a very strong and robust hinge that will not wear out under normal operating conditions. Aramid material, 40mm wide and on a 45° bias, was used for the hinges.

The following layup schedule was used for the tailplane.

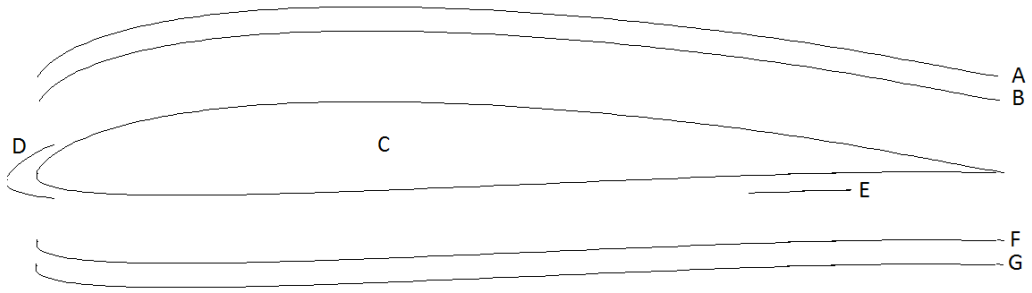


Figure 5.2: Figure showing a cross-sectional profile of the wing. This figure illustrates how the various wing skin components are arranged within the wing.

Where:

A - 49 g/m$^2$ Glass cloth at 90 °

B - 60 g/m$^2$ Aramid cloth at 45 ° bias

C - Isoboard foam core

D - 60 g/m$^2$ Aramid and 45 g/m$^2$ glass cloth composite at a 45° bias cut leading edge

E - 60 g/m$^2$ Aramid live control surface hinge

F - 60 g/m$^2$ Aramid cloth at 45 ° bias

G - 49 g/m$^2$ Glass cloth at 90 °



Note that the horizontal stabiliser/elevator does not have component E as it is full flying surface. This means that the entire stabiliser moves to control pitch instead of just an elevator.

To obtain more torsional strength, the glass cloth could have been placed at 45 °; this is the angle of the weave of the glass cloth with respect to the span of the wing; however, from past experience, applying the glass at 90 ° has proven to be sufficiently strong, and also reduces the quantity of glass used as there is less wastage when using the 90 ° configuration.

The leading edges were constructed by laminating a layer of 60g/m$^2$ Aramid on a 45° bias together with a layer of 49g/m$^2$ glass on also on a 4 ° bias. These cloths were laminated using Airtac 2E from Airtech Advanced Materials Group; this allows a temporary bond to be made without compromising the performance of the main epoxy structure.

All of the flying surfaces were molded using a Mylar film as the molding surface. Mylar has the advantage in that one can paint all of the flying surfaces prior to laying up the wing. As

the paint is applied onto the Mylar molding surface prior to layup, the resulting paint finish is exceptional and also light-weight.

Vacuum bag technology was used during the layup process to compress all of the wing and tailplane components while the epoxy (Epolam 2022) cures.

The fuselage was constructed again using Isoboard foam; this was done using a lost foam technique whereby the fuselage is cut using a hot wire and then manually sanded to shape. Once this was done, fibreglass cloth using epoxy (Ampreg 21) was applied and then wrapped tightly using plastic tape. By wrapping the fuselage with tape, the fibreglass is compressed and the resulting structure is both stronger and free from voids that might arise had the structure not been compressed. A vacuum bag could have also been used, however imperfections would have been introduced as a result of vacuum bag pleating.

Once the structure had cured, foam was removed from areas in the fuselage that would contain the electronic components. The rest of the foam within the fuselage was left in position as it adds significant strength to the structure.

Carbon fibre was not used within the fuselage of the glider as a 2.4 GHz radio control system was used: the risk of interference and signal loss was deemed more important than saving a small amount of weight.

Some photographs of the first glider built can be seen below.

Figure 5.3: Photograph showing the glider from the right hand side.

Figure 5.4: Photograph showing the glider from the left hand side.

Figure 5.5: Photograph showing the tail of the glider. Note the horizontal tail surfaces are full flying.

The second glider used was a professionally manufactured item. It was acquired second hand so that testing could resume without delay.

The model is a scale replication of a Glaser-Dirks DG-600, specifications of the second glider

that was assembled are as follows:

Table 5.2: Glider specifications for the second glider.

| | | |
|---|---|---|
| Wingspan | - | 3.6 m |
| Fuselage length | - | 1.47 m |
| Glider weight | - | 2.5 kg |
| Aspect ratio | - | 16.4 |

The glider is completely molded by means of solid molds using glass cloth and epoxy as the primary structural components.

This glider proved to be highly successful during flight tests and was able to find thermals even during the relatively cold winter months in Cape Town.

The additional space within the fuselage was particularly useful as it allowed the instrumentation electronics to be placed away from the other electronics within the fuselage.

Initially a power pod constructed from carbon fibre was used to power the glider to altitude, this system proved to be insufficient in power (despite having over 700 W available) and also added complexity to the overall system.

A tow release was fabricated from stainless steel and installed in the nose of the glider; this tow release allowed the glider to be towed to altitude using another aircraft. The advantage of this setup is that a powered propulsion system is not required; this reduces the overall weight of the glider and the associated drag from the power pod.

The tow release performed flawlessly during flight tests.

The main disadvantage with the tow release setup is that unless one finds a thermal, a forced landing is required. This meant that more flights were required to attain the same results.

CHAPTER 6

# TELEMETRY AND GROUND STATION DEVELOPMENT



During flight testing, it became evident that a real-time instrument panel on the ground would be highly beneficial. This prompted the development and implementation of a telemetry system to transmit the recorded data down from the aircraft to a ground station.

The primary design criteria were:

- Real-time data transfer,
- A range of at least 450 m,
- Small and compact hardware that can be seamlessly added to the existing system.

The XBee system from Digi International has been extensively used by the hobbyist radio control autopilot community to good effect. As a result, the author felt that the XBee system was a proven and reliable system and thus selected it as the primary telemetry link.

A packet system was devised to allow the transfer of data between the aircraft and ground station. This packet system was kept simple. A cyclic redundancy check (CRC) was not implemented, testing revealed that packet error rates were sufficiently low to justify not implementing a CRC. Error rates were tested during ground operation only, more work needs to be done to assess error rates over long distances however.

The packet layout is shown in table 6.1.

Table 6.1: Telemetry packet layout from airborne station to ground station

| Number | Item | Data Type |
|---|---|---|
| 1 | $ | Byte |
| 2 | Date | Float |
| 3 | Time | Float |
| 4 | Pitch | Integer |
| 5 | Roll | Integer |
| 6 | Yaw | Integer |
| 7 | Latitude | Float |
| 8 | Longitude | Float |
| 9 | Pressure Altitude | Integer |
| 10 | GPS Altitude | Integer |
| 11 | Ground Speed | Integer |
| 12 | IAS | Float |
| 13 | temp | Integer |
| 14 | Total Energy | Integer |
| 15 | Total Energy Rate | Integer |
| 16 | Vertical speed | Integer |
| 17 | * | Byte |



## 6.1 AIRBORNE TELEMETRY STATION

A adaptor board was designed such that the telemetry subsystem could be seamlessly added to the existing main system.

During the initial design of the main system, a spare serial port was set aside to allow debugging and firmware upgrades; this serial port was thus re-purposed within the firmware to output telemetry data on a continuous basis.

This adaptor board was designed to be as simple as possible. Its main task was to accept serial data from the main system. The main system operates at 5 V voltage levels, whereas the XBee system operates at 3.3 V levels, thus a level translation circuit was utilised. A simple resistor divider was selected as the serial data rate was low at 57 600 bps. The slew rate of a resistor divider network can be an issue at higher speeds, but this proved to not be a problem.

A linear low drop out regulator was used to regulate the 5 V supply from the main system to 3.3 V. The main system already has a 3.3 V regulator; however, there is insufficient current available to operate the XBee radio reliably.

An LM1117-3v3 was selected as it has a current output capacity of 800 mA [54].

Lastly, an LED was added to display the association status of the XBee; this provides an indication of the status of the telemetry link.

The schematics for this design may be found in Appendix B.

The completed circuit board can be seen in figure 6.1 below.

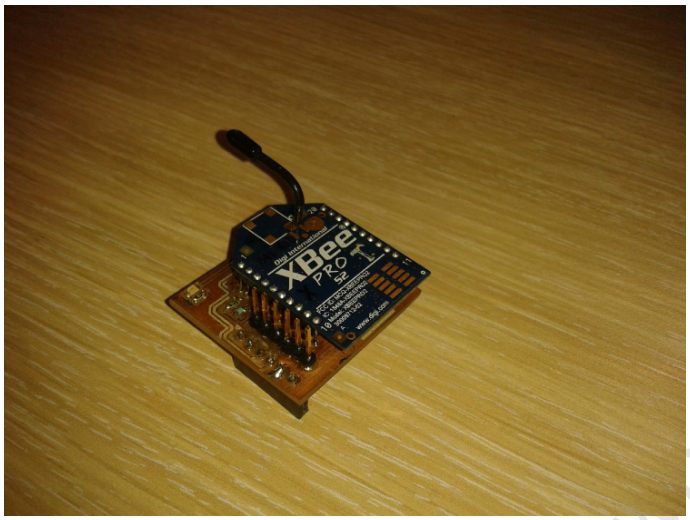


Figure 6.1: Figure showing the airborne XBee printed circuit board in conjuction with the XBee module used.

## 6.2 GROUND TELEMETRY STATION

A ”USB XBee Explorer” interface board from Sparkfun Electronics was used to connect the XBee radio to a computer [55].

This board allows bi-directional communication from the computer to the XBee radio via the USB port.

The USB XBee explorer board with the XBee module used can be seen in figure 6.2 below.

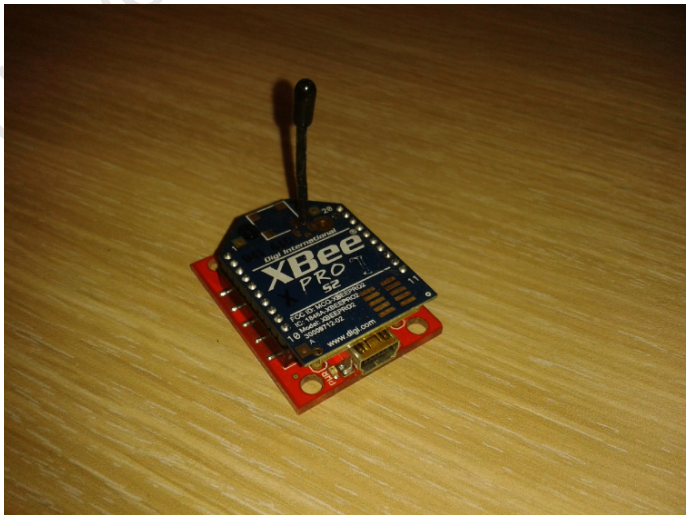


Figure 6.2: Figure showing the ground based USB XBee Explorer board in conjuction with the XBee module used.

### 6.2.1 Computer Ground Station

A ground station was developed using National Instruments LabVIEW 2011. This ground station accepted serial data originating from the aircraft, performed real-time processing of the data and then displayed it on a number of dials and gauges that were representative of instruments that might be found in full-size aircraft.

This system allowed all of the measured data from the aircraft to be viewed in real-time so that the pilot could have a better idea of what was going on on their aircraft.

Simple windowing filters were added to reduce gauge needle jitter. This proved to be required as without the filters, the gauges proved difficult to read. The filter coefficient was adjustable from the ground station user interface; the range of adjustment ranged from 0.8 to 1. From observation, this range proved to be adequate.

Screen shots of the ground station system can be seen below.

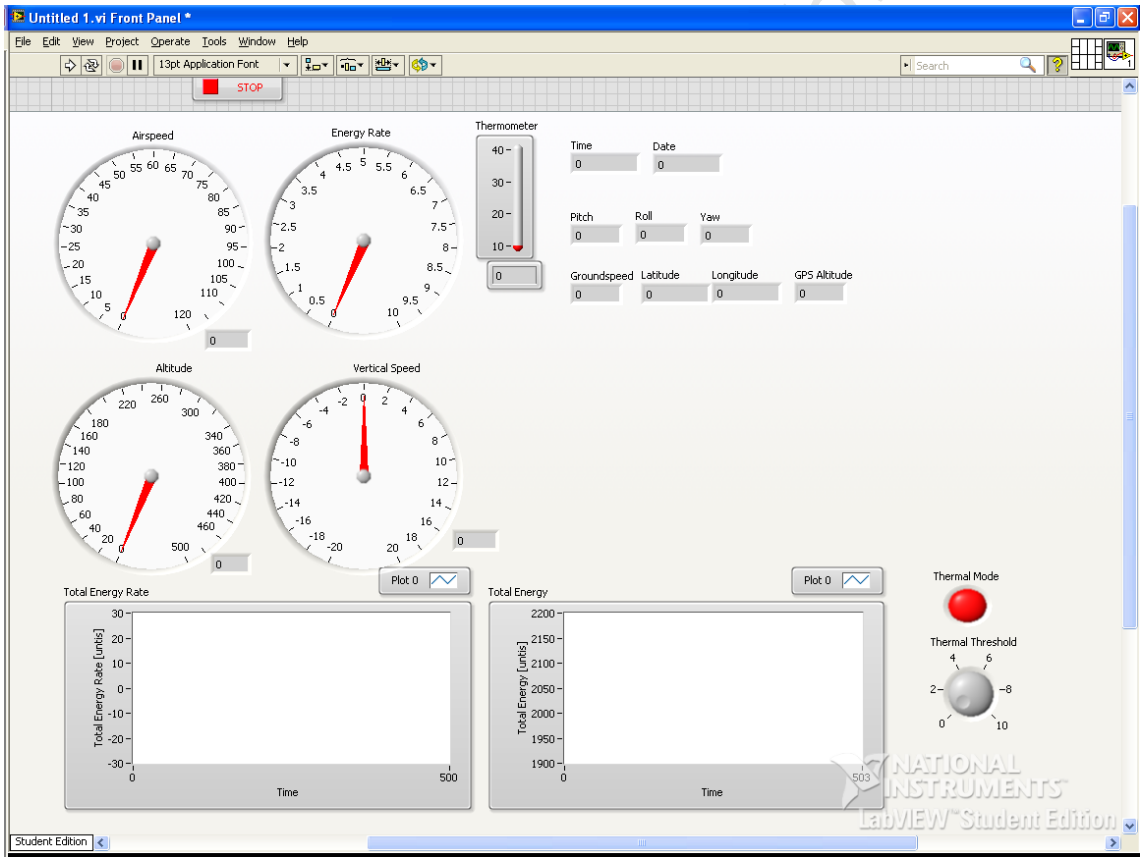


Figure 6.3: Figure showing the main ground station control panel.

In figure 6.3, one can see a screen shot of the ground system, the following variables are displayed on this screen.

- Airspeed - Top left needle gauge

- Energy rate - Top right needle gauge
- Altitude - Bottom left needle gauge
- Vertical Speed - Bottom right needle gauge
- Total Energy rate- Left hand graph
- Total Energy - Right hand graph

The other variables displayed on the right hand side are listed from left to right, and then from top to bottom.

- Thermometer
- Time
- Date
- Pitch
- Roll
- Yaw
- Groundspeed
- Latitude
- Longitude
- GPS altitude



In addition, a indicator (seen as a red oval on the bottom right) is lit when the energy rate exceeds a certain threshold; this threshold is set using the knob below the indicator. The indicator was added so that the pilot could be informed when the energy rate reached the desired set point, and thus when strong lift was detected. The indicator was experimental and was not used in practise.

The configuration control panel shown in figure 6.4 allows the user to adjust the windowing filters coefficients, thus allowing one to increase or decrease the response time as required. A more sophisticated filter design was not chosen because the simple windowing filters performed the task sufficiently well.

The user can also configure the serial port's settings from the configuration control panel, thus making the ground station easier to use.

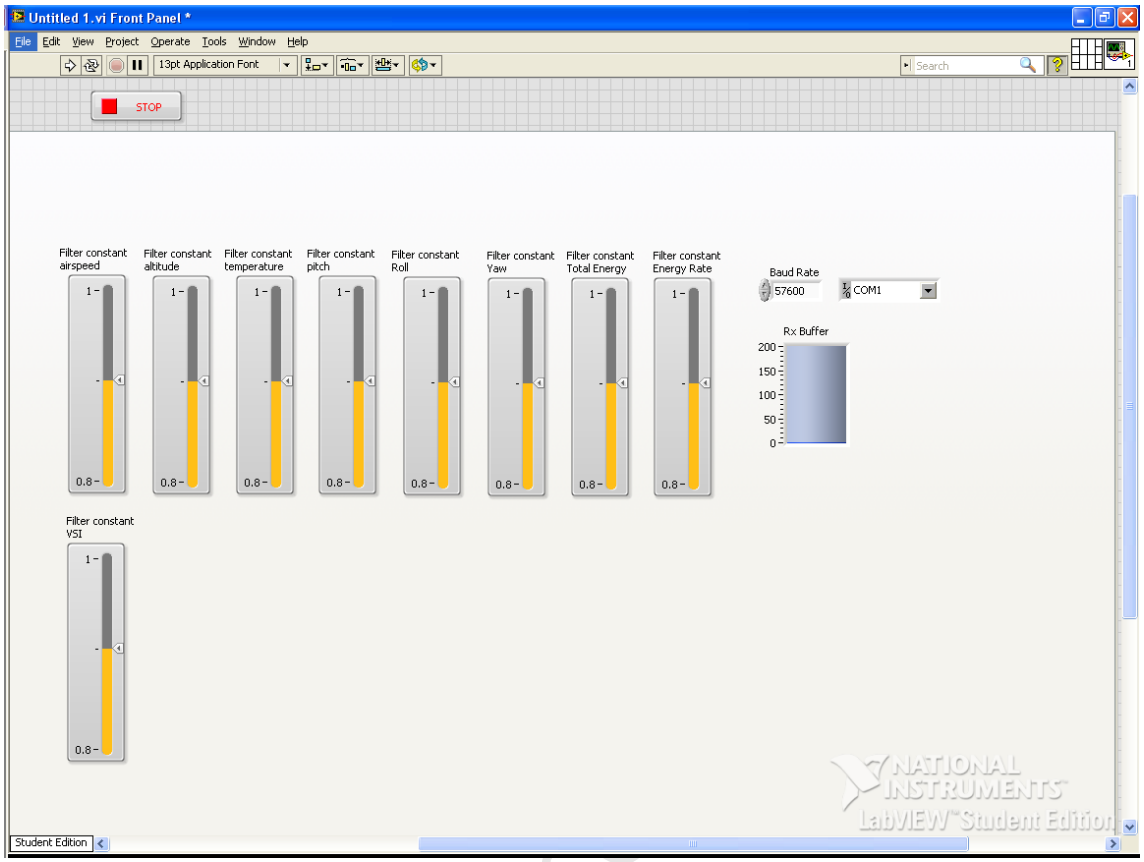


Figure 6.4: Figure showing the ground station configuration control panel.

CHAPTER 7

# RESULTS AND DISCUSSION

In this chapter, results obtained during the course of the project will be presented. These results are broken down into sections so as to maintain clarity between each of the various aspects of the projects.

## 7.1 SENSOR PERFORMANCE

Several different sensors have been used during the course of this project, some of the sensors used worked better than others; the aim of this section is to describe what worked and what did not.

### 7.1.1 Barometric Pressure

As described in the system design chapter, two different barometric pressure sensors were used during the course of this project.

From experimental testing it was found that the Freescale MPXA6115 provided a repeatable accuracy of approximately 3 m; this accuracy was not sufficient to satisfy the project goals and thus another sensor was acquired. The accuracy of the sensor could have been improved by using improved analog filtering and additional signal amplification prior to sampling. However this would have required a complete hardware re-design which was not justified given that the performance would still have not matched that of other sensors available.

The second sensor was a Bosch BMP-085, this is a digital sensor and thus removes the need for analog filtering and amplification. This sensor proved to be far superior to the Freescale MPXA6115 as it provided improved resolution and altitude accuracy to less than a metre; this was deemed sufficient.

Both sensors were left operational and thus data could be captured from both sensors during the flight testing phase. This data re-enforced the previous observation by showing far less noise and improved accuracy.

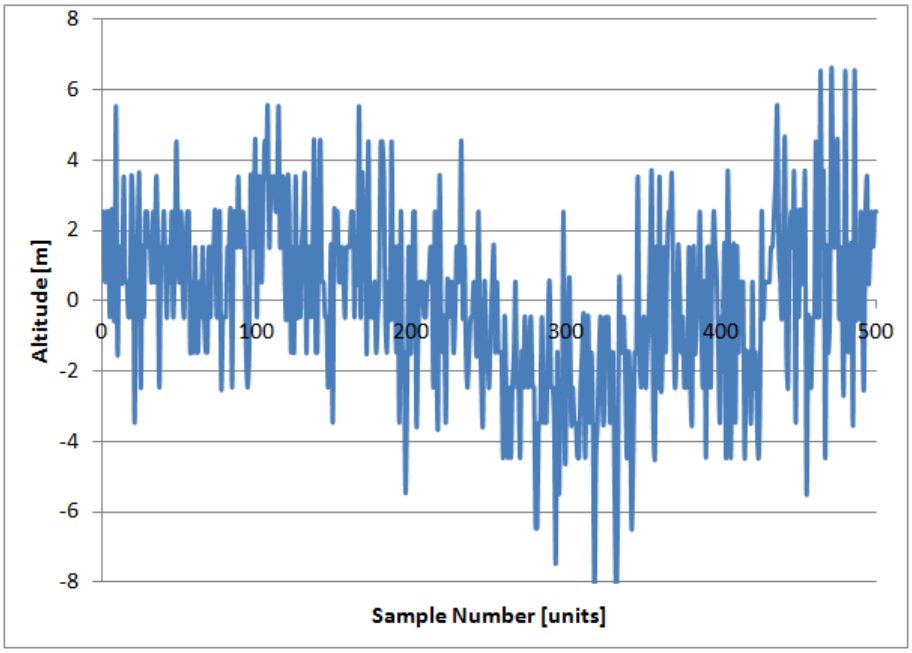


Figure 7.1: Figure showing unfiltered altitude readings from the Freescale MPXA6115A pressure sensor under steady state conditions.

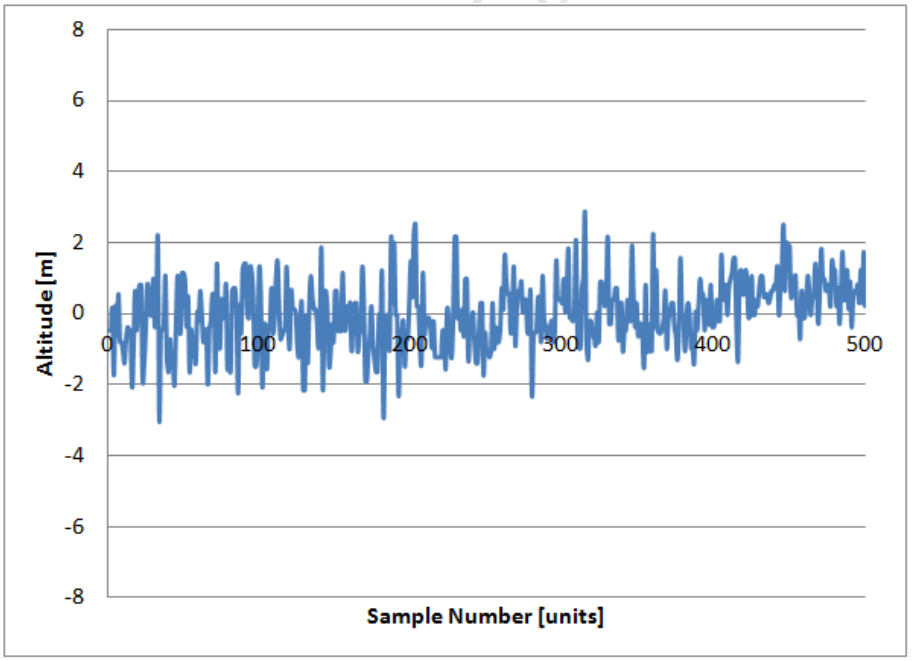


Figure 7.2: Figure showing unfiltered altitude readings from the Bosch BMP085 pressure sensor under steady state conditions.

From the above data, the standard deviation for each sensor data set was calculated; these standard deviations can be found in the following table.

Table 7.1: Table showing the standard deviation of both the Bosch BMP085 and the Freescale MPXA6115 barometric pressure sensors.

| Sensor | Standard Deviation [m] |
|---|---|
| Bosch BMP085 | 0.9457 |
| Freescale MPXV6115 | 2.5244 |

The figures in the above table agree with what was found experimentally.

### 7.1.2 **Airspeed**

The differential pressure sensor used to measure airspeed was calibrated in a wind tunnel; the experimental procedure and results of the calibration may be found in Chapter 4. Additional photographs and apparatus diagrams may be found Appendix C.

The sensor data showed some non-linearity over the range of airspeeds tested.

Low speed performance, below 25 km/h, was poor; this was expected though and did not affect the performance of the system as the glider used had a cruising airspeed of approximately 50 km/h.

More discussion regarding airspeed measurement may be found in the flight testing section.

### 7.1.3 **Attitude and Heading Reference System**

The Attitude and Heading Reference System (AHRS) was used to determine the pitch, roll and yaw of the aircraft. Although primarily the focus was the attitude, all of the parameters used to determine the attitude were logged for future reference; this allows future refinements to be added to the system without having to perform additional flight testing.

The AHRS processing was done on a secondary microcontroller in realtime due to the high computational requirements of the algorithm. This approach proved to be an effective method of offloading the processing away from the main microcontroller so as to free up some processing power.

The firmware for the AHRS was adapted from an open source implementation so as to not spend more time than necessary implementing a process that has been done many times before by other individuals.

The performance of the AHRS proved to be satisfactory given the inexpensive sensors used, however more work is required to improve the algorithms used in the AHRS system so as to improve the response time and accuracy.

Output drift proved to be an issue however the author believes that this problem will always be an obstacle when using low-cost MEMS sensors.

### 7.1.4 Other Sensors

An LM35 temperature sensor was used initially to measure ambient temperature during flight testing; this temperature sensor was later replaced with the temperature sensor built into the Bosch BMP-085. A calibration procedure was not done on this sensor as a reliable apparatus was not available to test it. The accuracy of this measurement is thus assumed to be what the manufacturers claim it to be.

This change was made because it was simpler to use the temperature sensor in the Bosch BMP085.

Temperature is not a critical measurement in the system as a whole and thus in-accuracies will not affect the performance of the overall system significantly.

## 7.2 Flight Test Results

A total of 25 flights were performed over a period of approximately six months, of these 25 flights, 15 flights provided complete data as the other 10 flights were to work out errors in the software.

In figure 7.3 below, one can see the system installed in the glider.

Figure 7.3: Photograph showing the placement of the device within the fuselage of the glider.

Additional photographs of the flight testing process can be found in Appendix A.

As it is not practical to include data from all of the flights, three of the flights have been included to illustrate the performance of the system. More data is available from these flights than is

shown but this data would not have added additional information to the discussion.

A further two flights logged while ridge soaring are also presented.

The balance of the flights performed showed similar results to that of the three flights described below.

Five flights were performed on a mountain side so as to test the system using ridge lift. The balance of the flights were done on a flat field.

The three flight tests were performed at two separate locations, flights one and two were performed at Boland Model Aircraft Club (BOMAC) in Cape Town; and flight three was performed at ArcelorMittal Saldanha Radio Control Club (AMSRCC) in Langebaan.

The weather conditions and geographic details of each of the location is shown below.

Table 7.2: Table detailing the ambient weather and geographic details for both of the flight test locations.

| Flight Number | Location | Temperature | Wind speed | Comments |
|---|---|---|---|---|
| 1 | BOMAC | 21 °C | 8 km/h | Flat field, open space |
| 2 | BOMAC | 22 °C | 10 km/h | Flat field, open space |
| 3 | AMSRCC | 20 °C | 15 km/h | Close to the sea, thermal activity is weak |

As noted in the table above, the AMSRCC is in close proximity to the sea, and therefore the location was not as good as BOMAC in terms of thermal strength. Both of these flights were made during the winter and spring of 2012, as result, thermal strength was not as good as it could have been resulting in fairly short flight times.

### 7.2.1 **Airspeed**

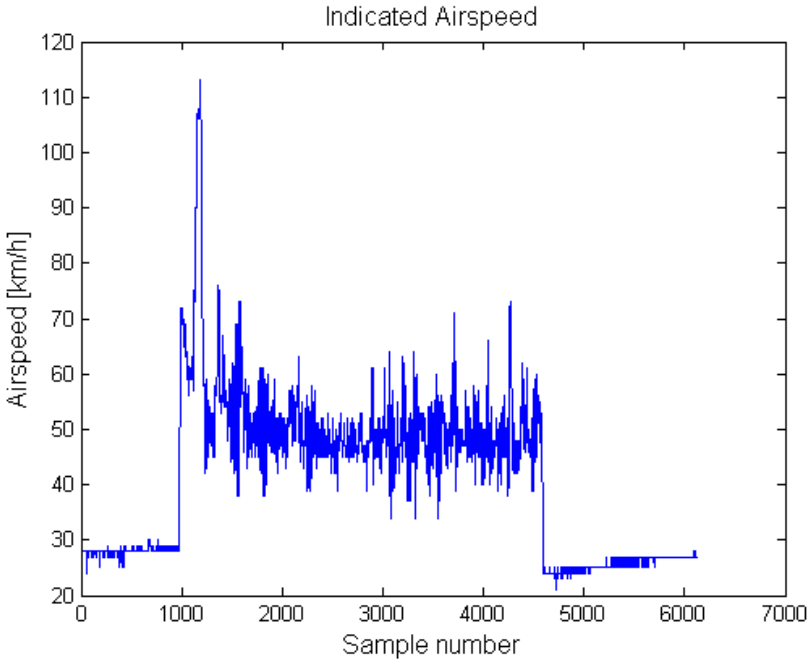


Figure 7.4: Figure showing the indicated airspeed of flight 1.

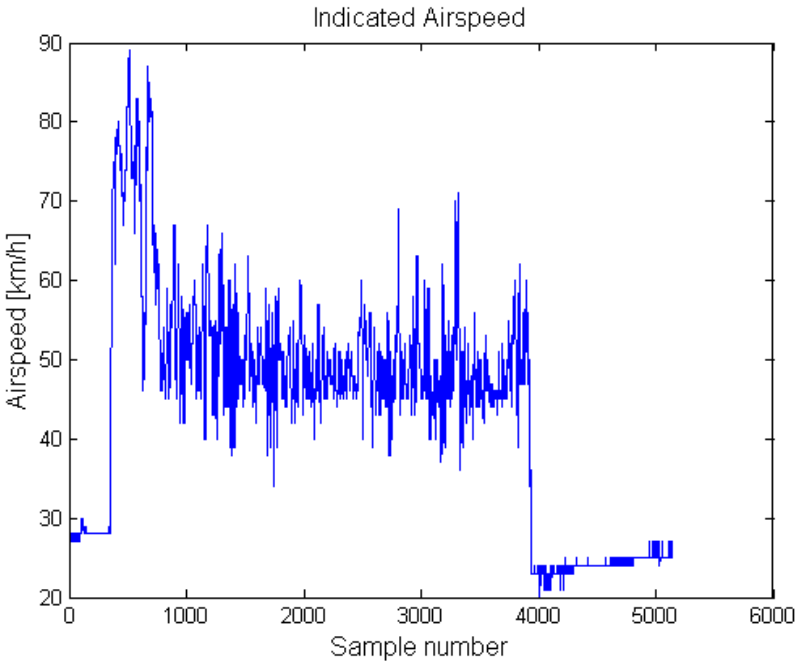


Figure 7.5: Figure showing the indicated airspeed of flight 2.

In figure 7.4 above, one can see airspeed data from flight 1. One can see that the initial climb to altitude while connected on the tow line resulted in an increased airspeed; this airspeed then

tapered off to approximately 50 km/h once the tow line was released; this speed can be assumed to be the normal cruising speed of the glider.

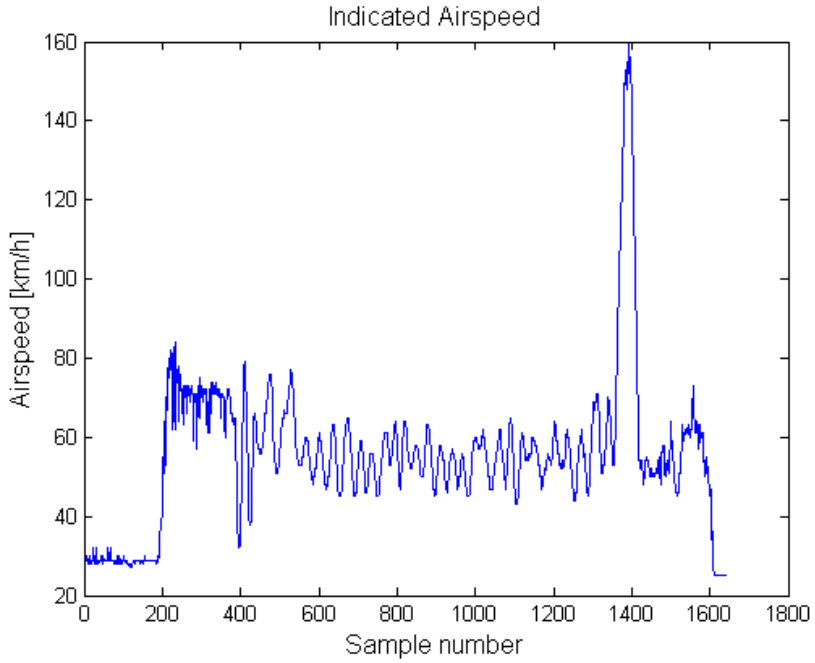


Figure 7.6: Figure showing the indicated airspeed of flight 3.

In figure 7.6 above, this flight shows a normal flight condition, the spike in airspeed at around 1400 samples represents a high speed fly by followed by a landing; this was done to test the system at higher speeds to identify any issues that might arise.

At a glance, figures 7.4 and 7.5 appear to have a higher noise content to that of figure 7.6, however this is not the case as more data is contained in figures 7.4 and 7.5 to that of figure 7.6 as they represent a longer flight.

### 7.2.2 **Altitude**

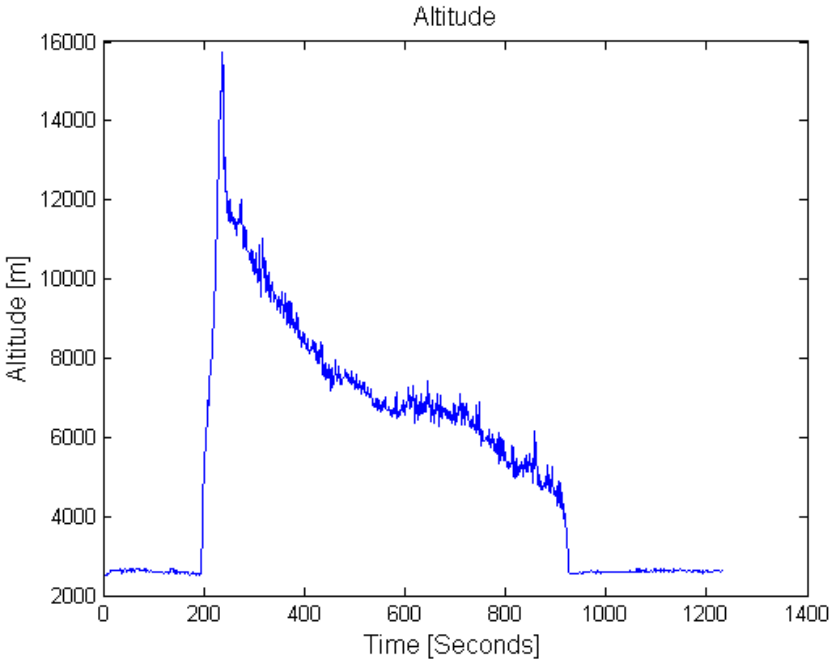


Figure 7.7: Figure showing the aircraft altitude of flight 1.

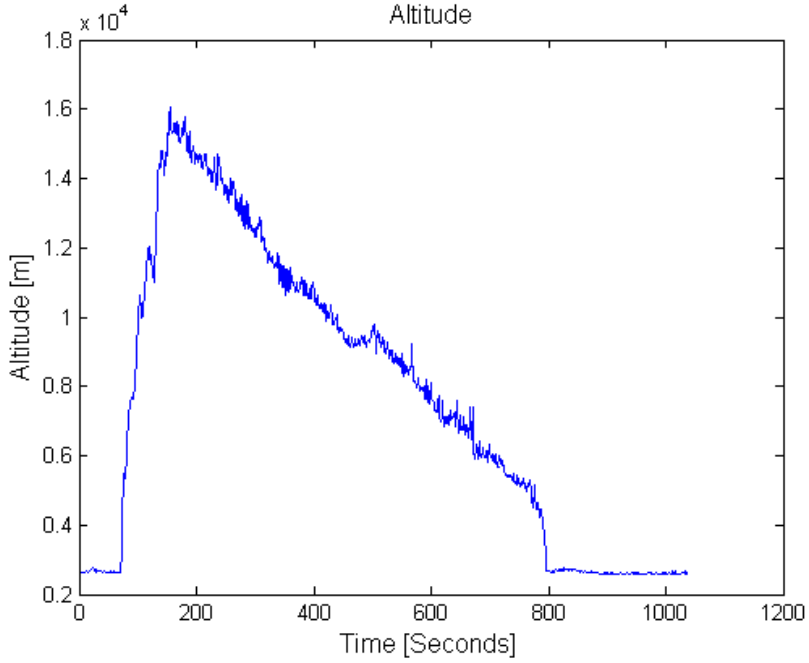


Figure 7.8: Figure showing the aircraft altitude of flight 2.

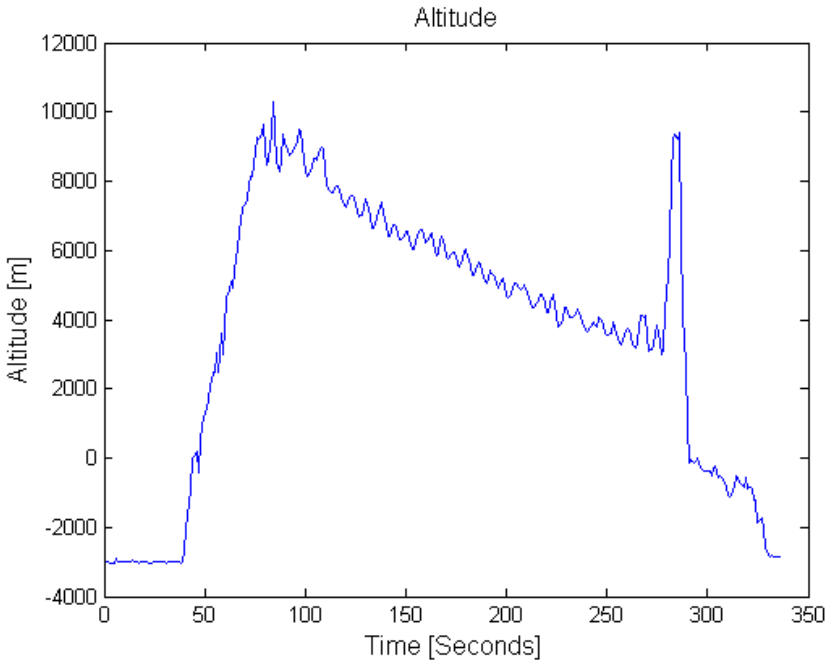


Figure 7.9: Figure showing the aircraft altitude of flight 3

The altitude spike on figure 7.9 above at around 280 seconds corresponds with the spike at around sample 1400 in figure 7.6. The static pressure port of the barometric pressure sensor was located within the fuselage, as the altitude changed with a change in airspeed, this spike was caused by a change in fuselage pressure. The change in altitude as determined by the barometer was in fact the opposite of what was happening in reality, since the system was trading altitude (potential energy) for airspeed (kinetic energy).

Three possible solutions were proposed to solve this problem, namely:

1. move the static pressure port to another location,
2. seal the fuselage of the aircraft more effectively so as to reduce open orifices that might cause sudden pressure changes,
3. employ better mechanical air filtering on the system; for example, house the system in a sealed enclosure that has a port of known size open to static pressure.

A combination of all of the above was decided to be the best compromise however additional flight testing has not been undertaken to test the solutions above as a result of time constraints.

### 7.2.3 **Total Energy Estimation**

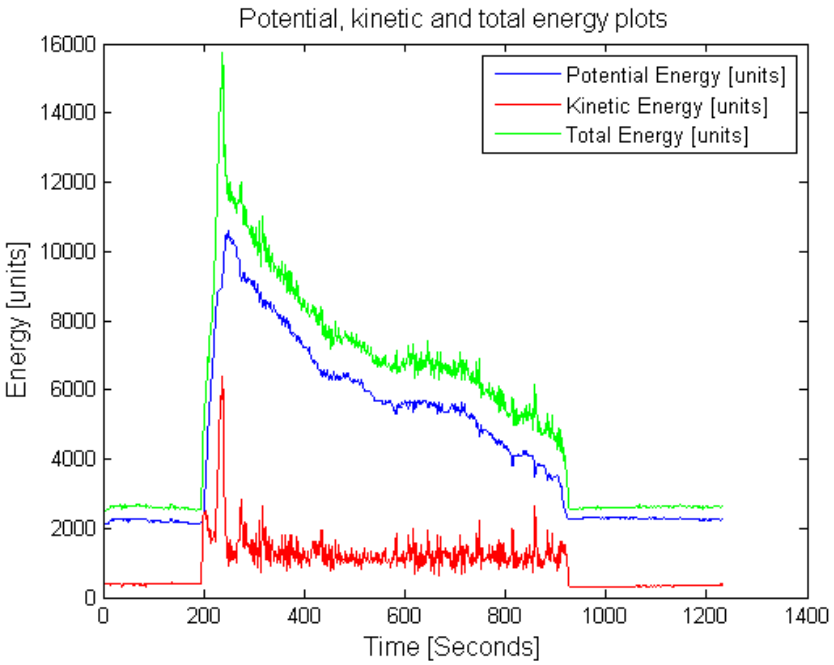


Figure 7.10: Figure showing the potential energy, kinetic energy and total energy of the aircraft for flight 1.

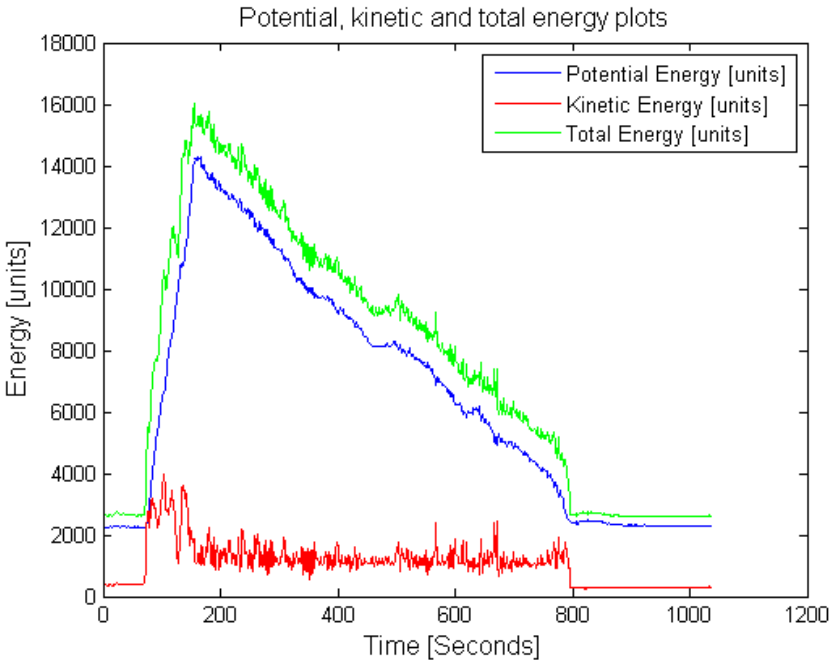


Figure 7.11: Figure showing the potential energy, kinetic energy and total energy of the aircraft for flight 2.

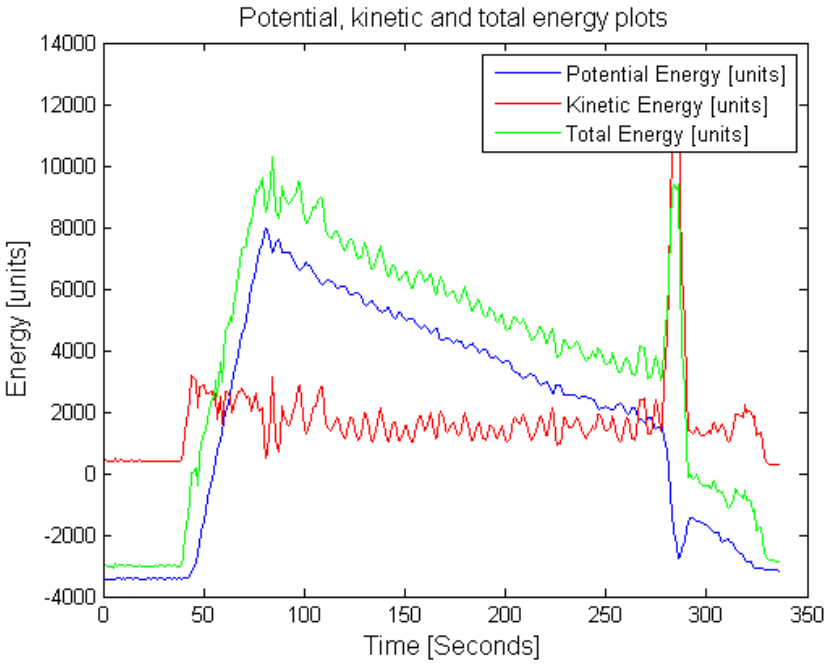


Figure 7.12: Figure showing the potential energy, kinetic energy and total energy of the aircraft for flight 3.

Figures 7.10 - 7.12 show the potential energy, kinetic energy and total energy of the glider during each flight.

Flights one and two were performed during the winter months, as a result, thermal activity was low.

One can see in figure 7.10 that a small thermal was located at around 450 seconds and ending at around 600 seconds; this can be seen by the flat profile of the total energy graph (seen in green). The thermal caught is not strong enough to significantly increase the total energy, and therefore altitude, but is sufficient to sustain flight.

In figure 7.11, one can again see a thermal being located at around 500 seconds; this event has much the same profile as that of figure 7.10, again the resulting lift is just enough to sustain flight.

In figure 7.12, we see the same spike noted in the airspeed subsection above.

There is little thermal activity during this flight as noted by the steady decline in total energy.

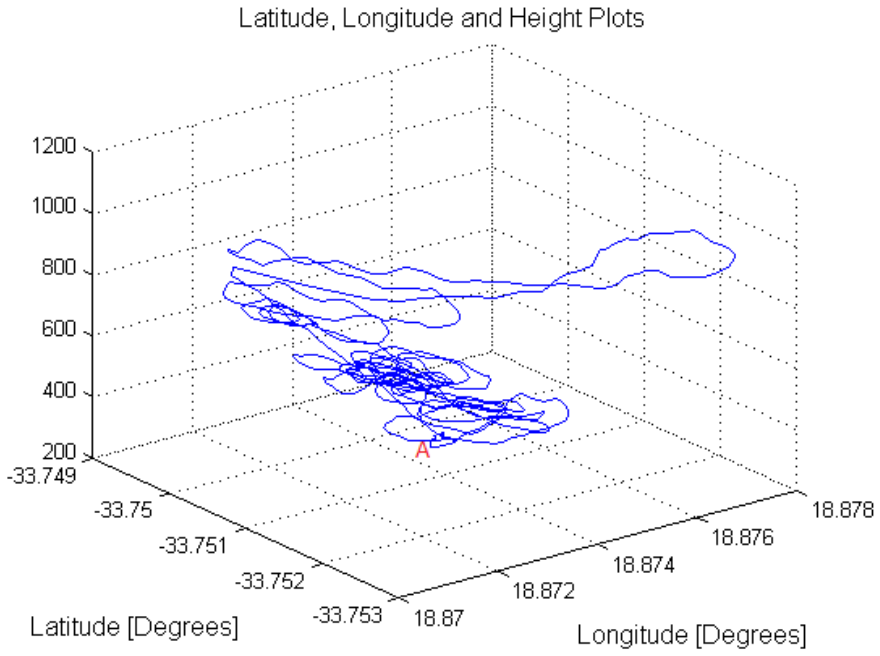


Figure 7.13: 3D Figure showing aircraft position (latitude and longitude) on the x and y axis, and altitude on the z axis for flight 1. Point A denotes the start and endpoint of the flight.

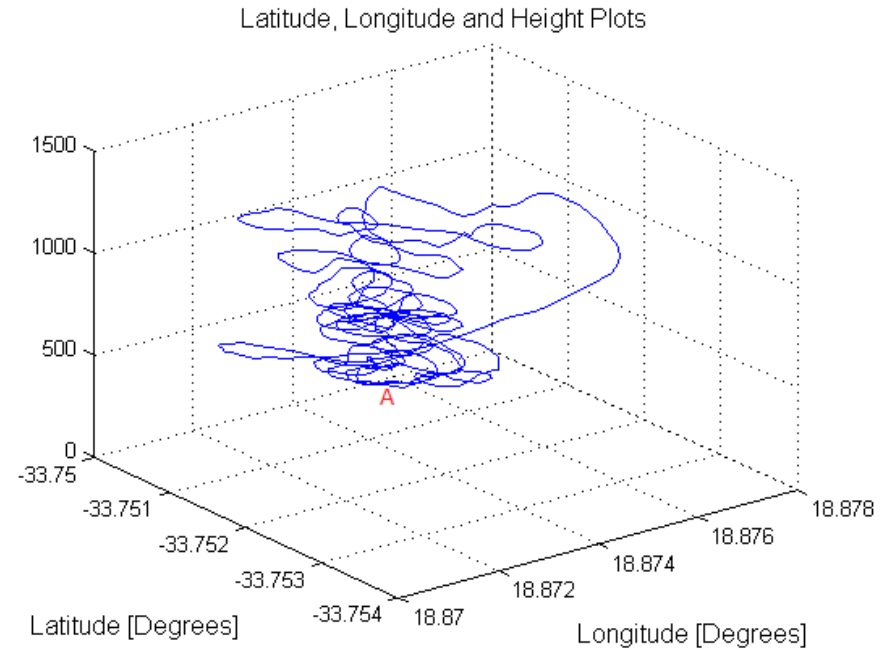


Figure 7.14: 3D Figure showing aircraft position (latitude and longitude) on the x and y axis, and altitude on the z axis for flight 2. Point A denotes the start and endpoint of the flight.

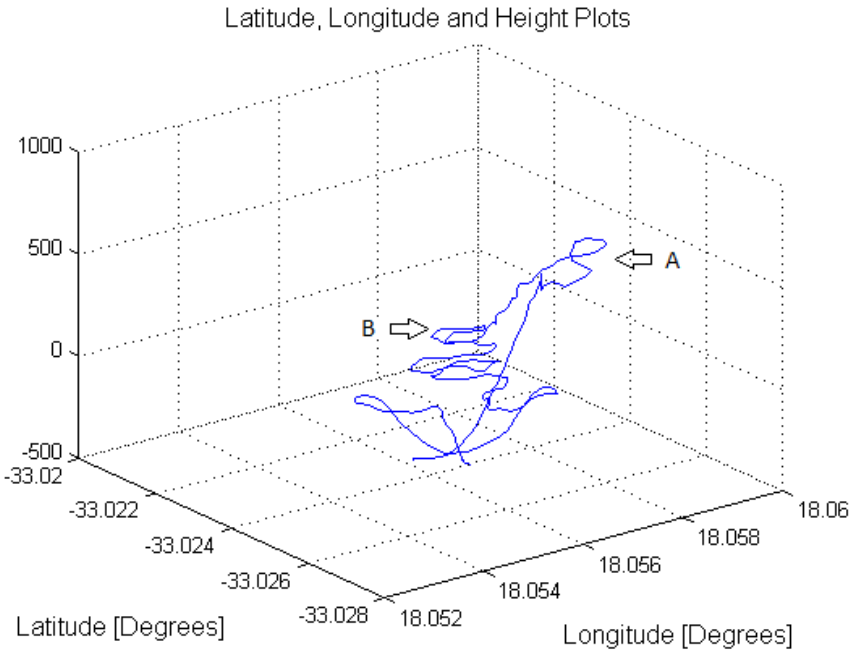


Figure 7.15: 3D Figure showing aircraft position (latitude and longitude) on the x and y axis, and altitude on the z axis for flight 3.

In figures 7.13 to 7.15, we can see the three dimensional flight path of the aircraft for each flight. The point at which the tow line is released is marked as arrow 'A' in figure 7.15, arrow 'B' shows the flight path while searching for a thermal.

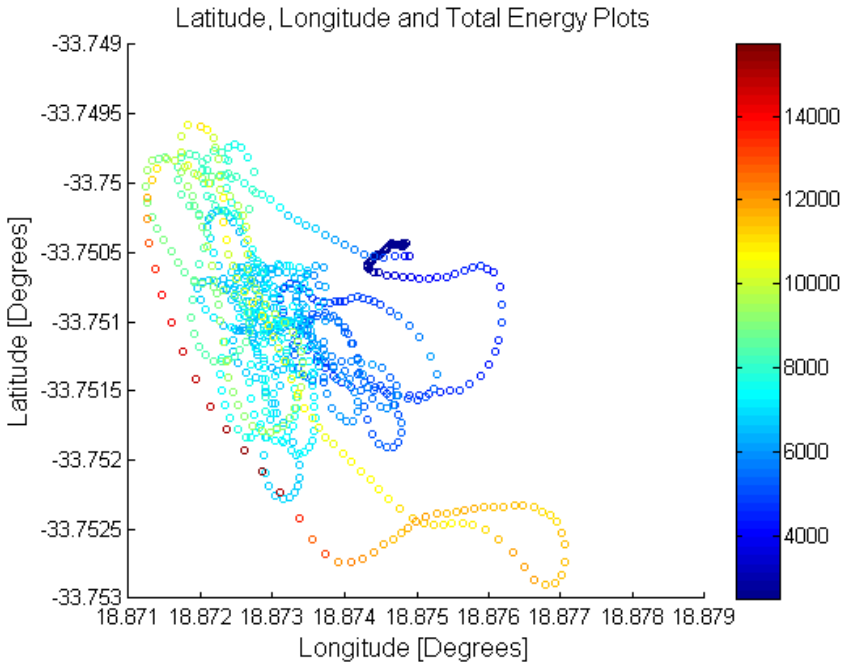


Figure 7.16: Figure showing a scatter graph of aircraft position; marker colour indicates total energy in the system, this figure is for flight 1. Colour bar units are J/m where m is the mass of the aircraft.

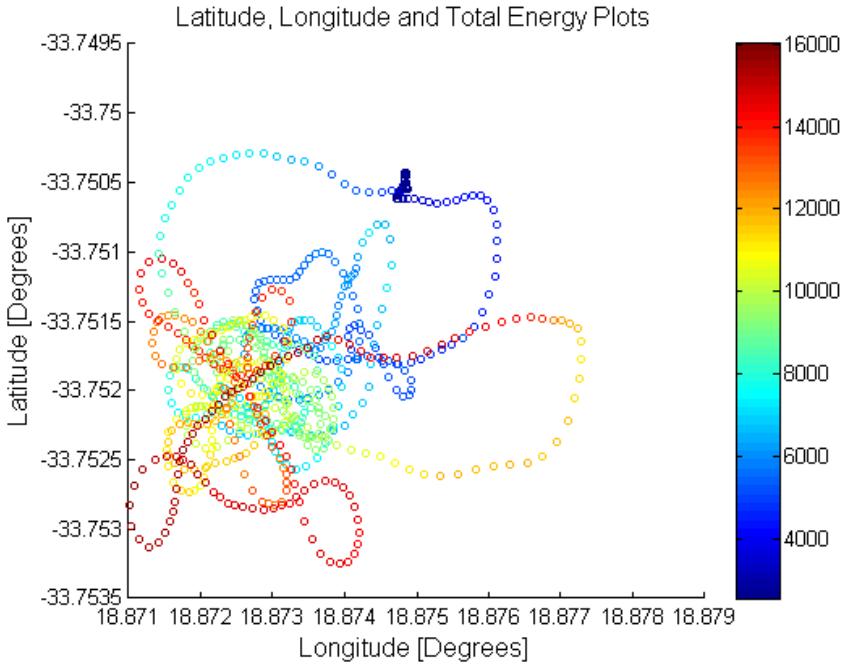


Figure 7.17: Figure showing a scatter graph of aircraft position; marker colour indicates total energy in the system, this figure is for flight 2. Colour bar units are J/m where m is the mass of the aircraft.

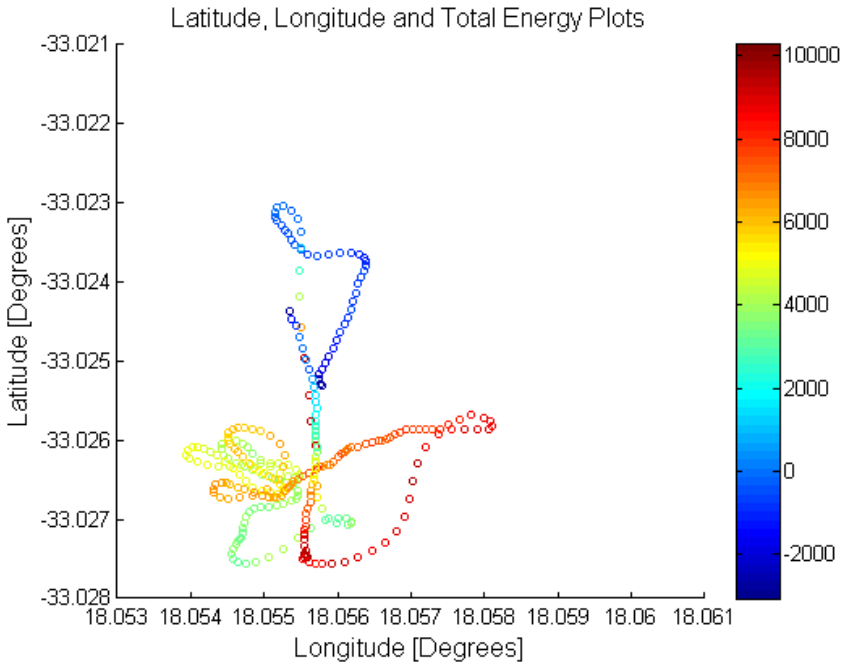


Figure 7.18: Figure showing a scatter graph of aircraft position; marker colour indicates total energy in the system, this figure is for flight 3. Colour bar units are J/m where m is the mass of the aircraft.

Figures 7.16 to 7.18 show the latitude and longitude position of the glider, the colour of the markers represents the total energy in the system.

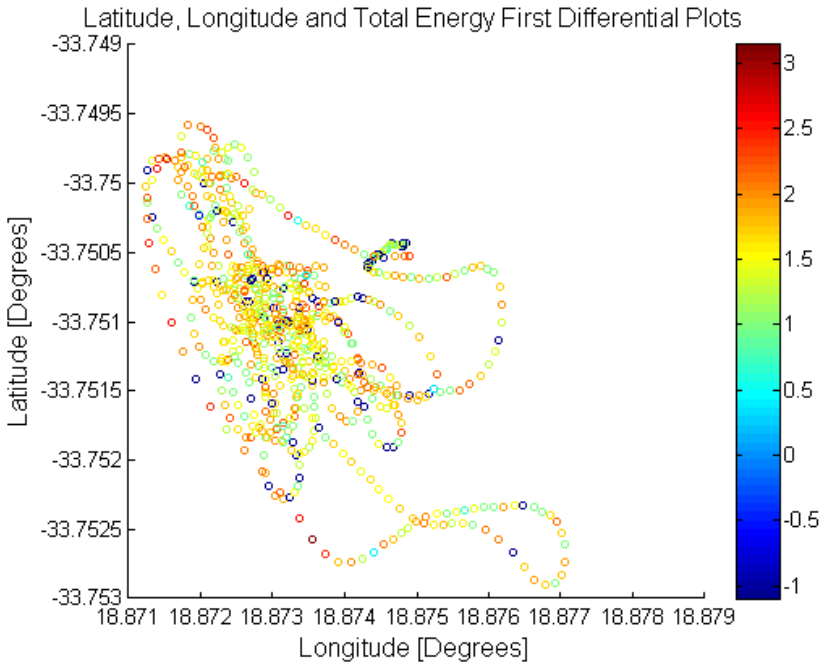


Figure 7.19: Figure showing a scatter graph of aircraft position; marker colour indicates total energy rate in the system, this figure is for flight 1. Colour bar units are log(J/m) where m is the mass of the aircraft.

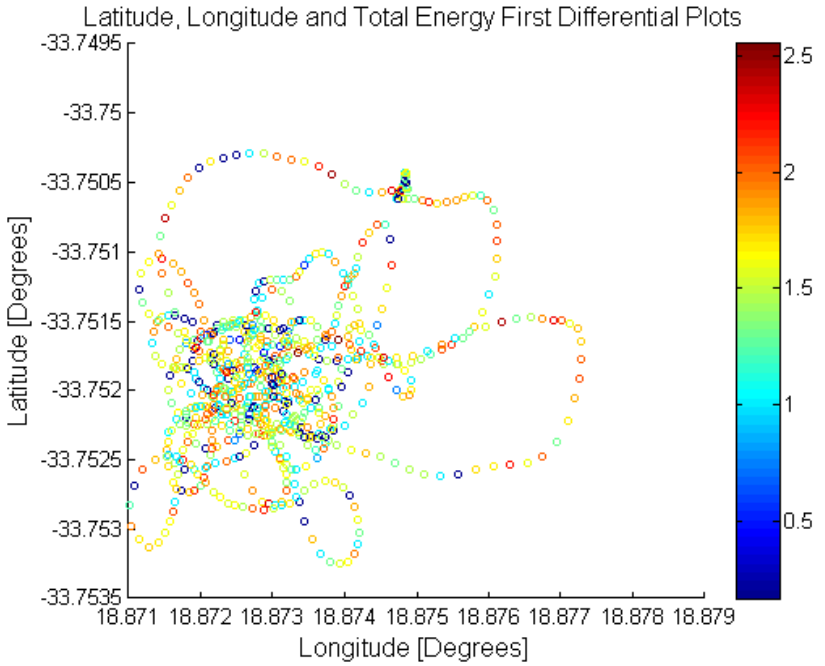


Figure 7.20: Figure showing a scatter graph of aircraft position; marker colour indicates total energy rate in the system, this figure is for flight 2. Colour bar units are log(J/m) where m is the mass of the aircraft.

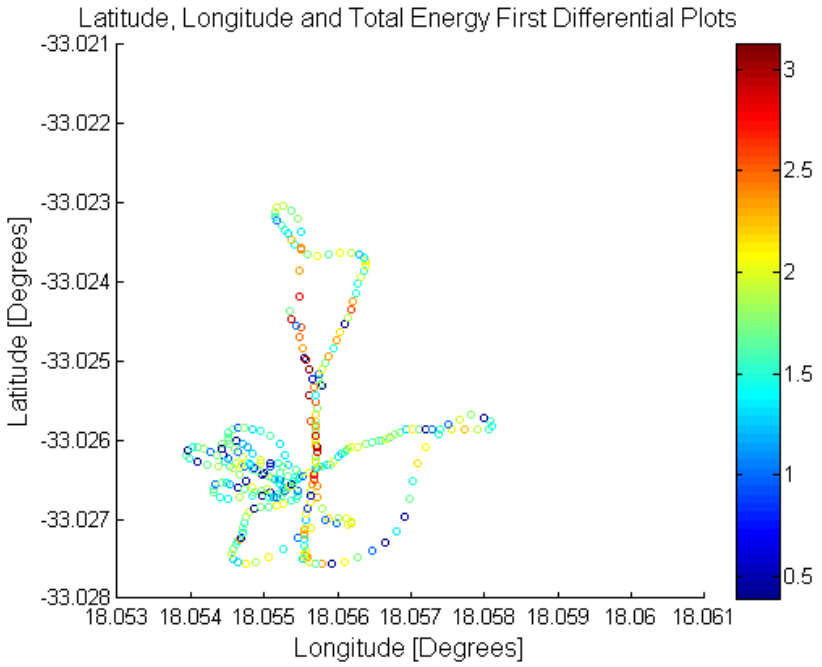


Figure 7.21: Figure showing a scatter graph of aircraft position; marker colour indicates total energy rate in the system, this figure is for flight 3. Colour bar units are log(J/m) where m is the mass of the aircraft.

Figures 7.19 to 7.21 show the position of the glider with the marker colour representing total energy rate. Strong lift or sink can easily be seen using the energy rate. In figure 7.21, the glider tow path can be seen by a number of red and purple markers.

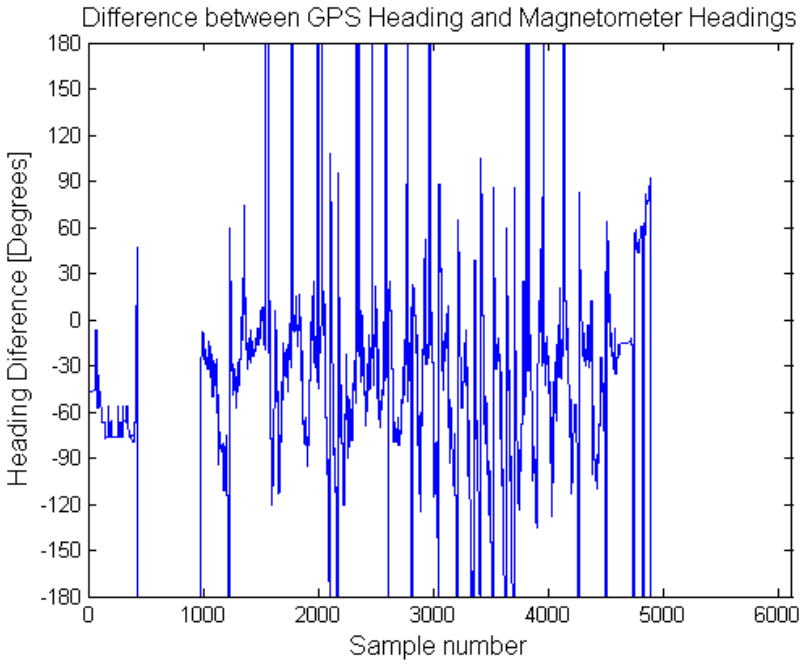


Figure 7.22: Figure showing the difference between the magnetic heading and the aircraft's heading according to the GPS, for flight 1.

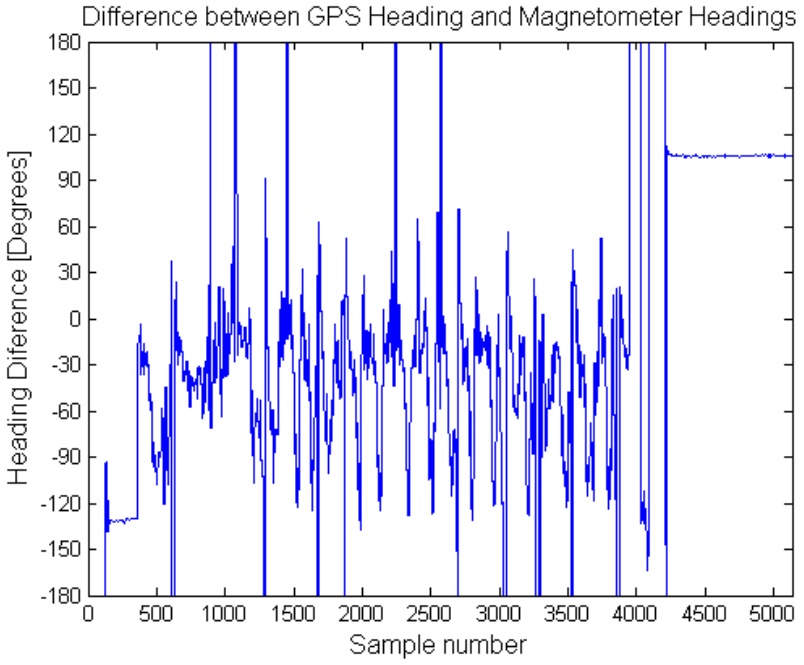


Figure 7.23: Figure showing the difference between the magnetic heading and the aircraft's heading according to the GPS, for flight 2.

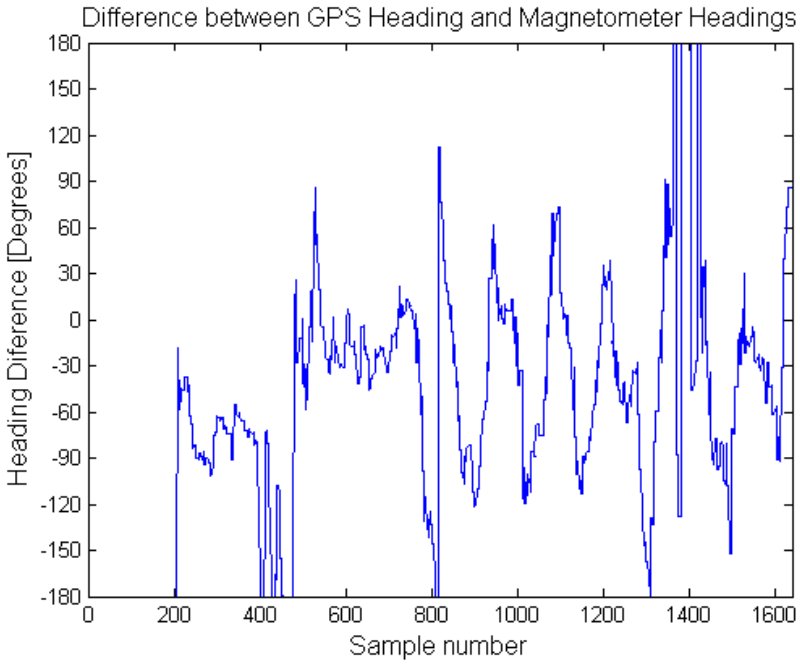


Figure 7.24: Figure showing the difference between the magnetic heading and the aircraft's heading according to the GPS, for flight 3.

The above three figures show the difference between magnetic heading and GPS heading, this allows the side-slip of the aircraft to be determined.

## 7.3 RIDGE SOARING

Ridge soaring was undertaken to test the system in a different environment. This process identified several issues that would not normally have been a factor when thermal soaring on a flat field.

These flights were performed on a farm named Hoogekraal on the outskirts of Cape Town. The conditions of these flights can be seen below in table 7.3.

Table 7.3: Table detailing the ambient weather and geographic details for the two ridge soaring flights.

| Flight Number | Location | Temperature | Wind speed | Comments |
|---|---|---|---|---|
| 1 | Hoogekraal | 36 °C | 45 km/h | Grass mountainside |
| 2 | Hoogekraal | 34 °C | 50 km/h | Grass mountainside |

From observing figures 7.25 and 7.26, one can see that the airspeed fluctuates far more as compared to the previous thermal soaring flights; This is due to the high wind speed at the flying site.

Measuring kinetic energy became more challenging when the wind speed was higher; as the aircraft turned into wind, the headwind added to the airspeed of the aircraft thus making it seem as though the aircraft was moving at a higher speed relative to the ground. This proved to be a problem as it make detecting lift challenging due to the constantly changing headwind.

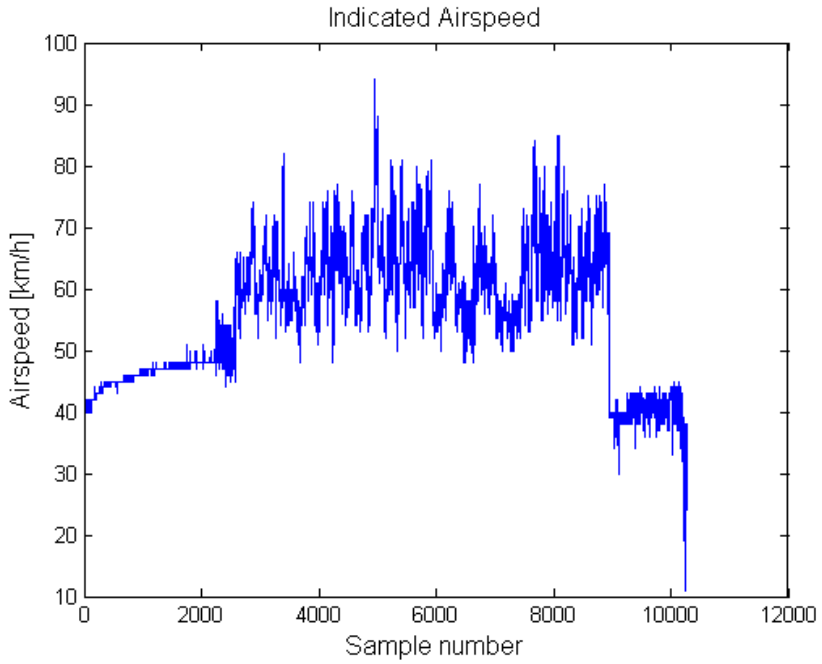


Figure 7.25: Figure showing the indicated airspeed of flight 1.

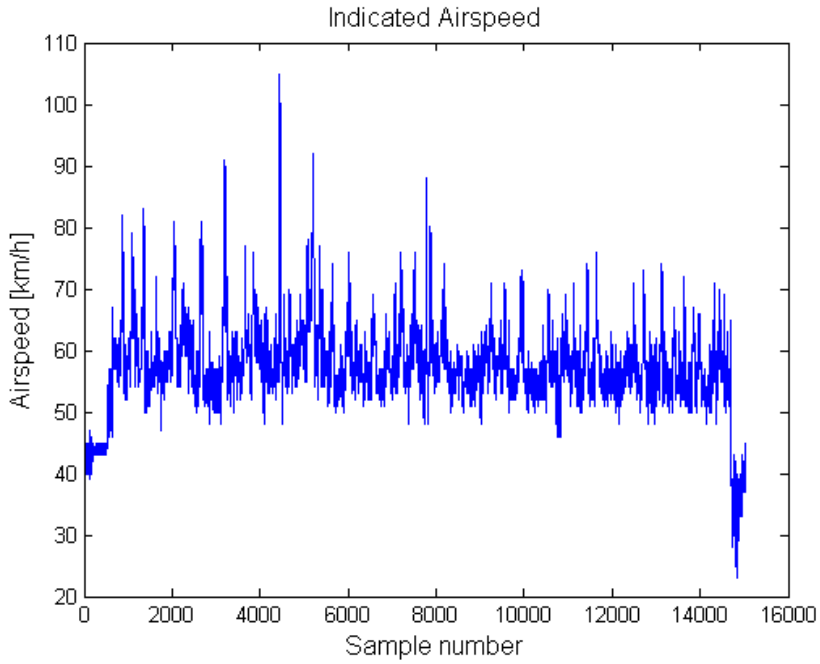


Figure 7.26: Figure showing the indicated airspeed of flight 2.

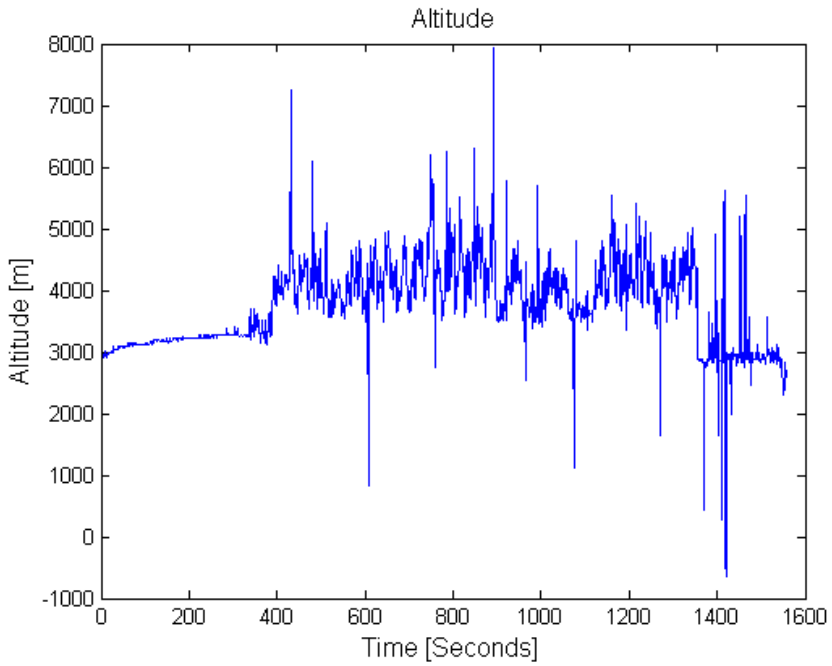


Figure 7.27: Figure showing the aircraft altitude of flight 1.

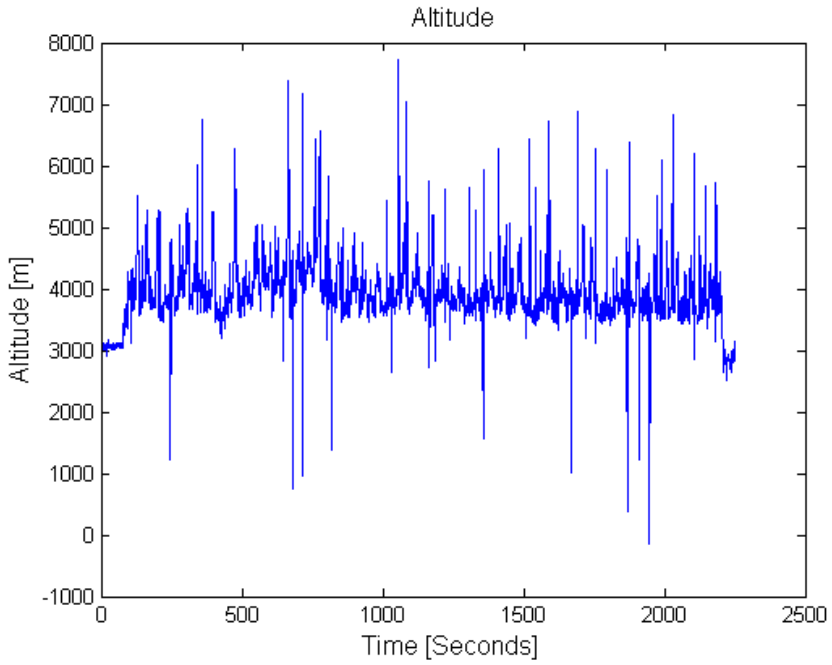


Figure 7.28: Figure showing the aircraft altitude of flight 2.

The altitude measurement also became challenging, as fuselage pressurisation became more of an issue. This can be seen in figures 7.27 and 7.28.

Turbulent air appears to also cause additional noise in the altitude measurement.

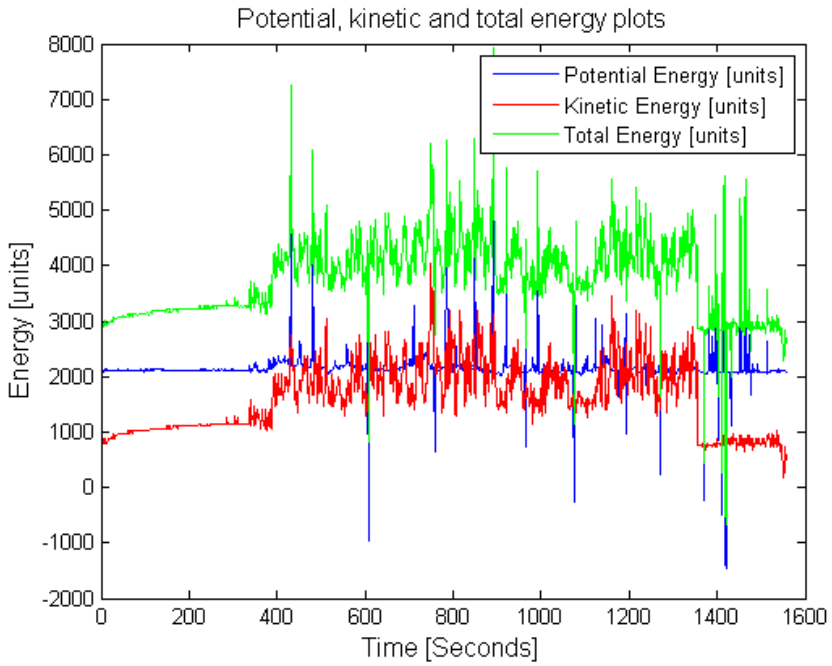


Figure 7.29: Figure showing the potential energy, kinetic energy and total energy of the aircraft for flight 1.

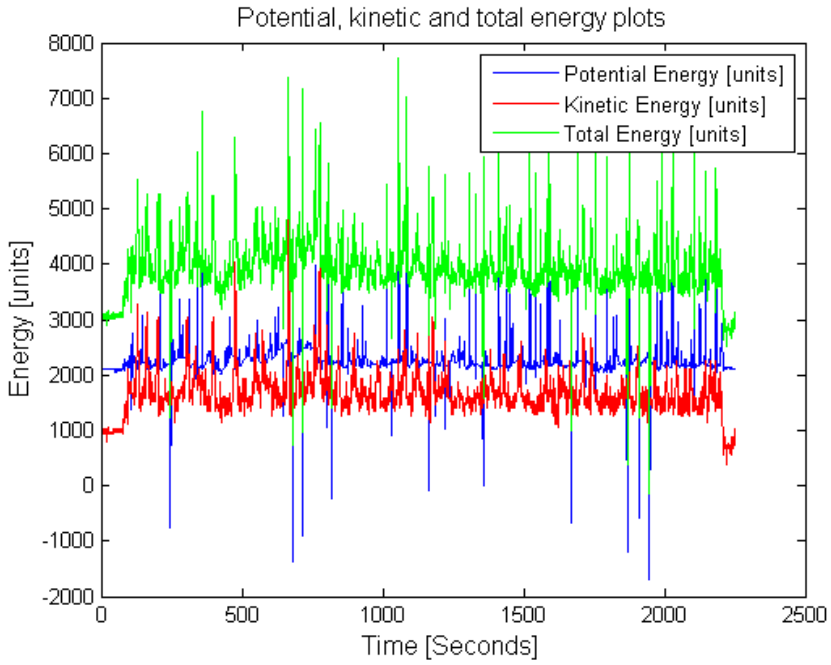


Figure 7.30: Figure showing the potential energy, kinetic energy and total energy of the aircraft for flight 2.

Due to the high noise content of the airspeed and altitude readings as a result of the strong wind, the total energy measured is also noisy, this is exacerbated as kinetic energy is the square of airspeed.

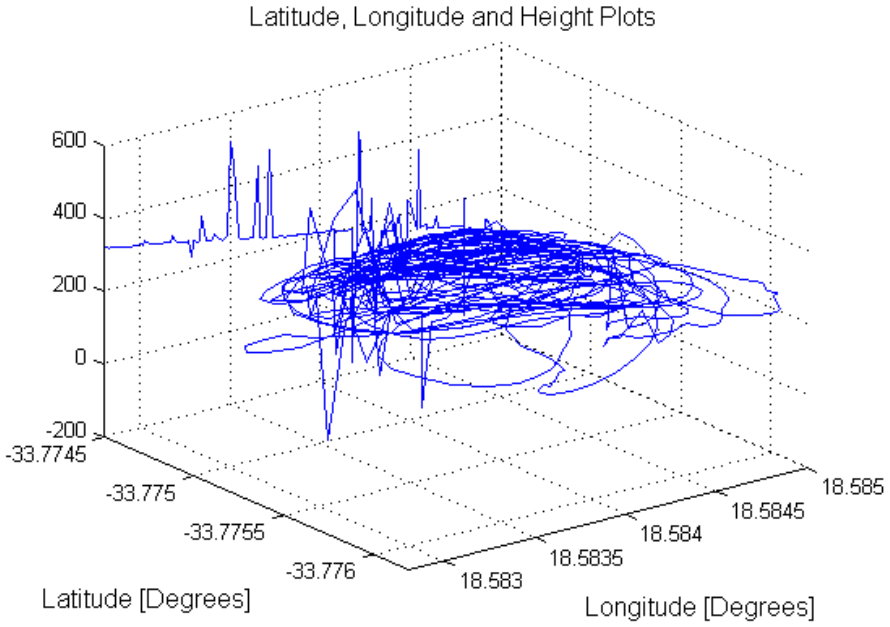


Figure 7.31: 3D Figure showing aircraft position (latitude and longitude) on the x and y axis, and altitude on the z axis for flight 1.

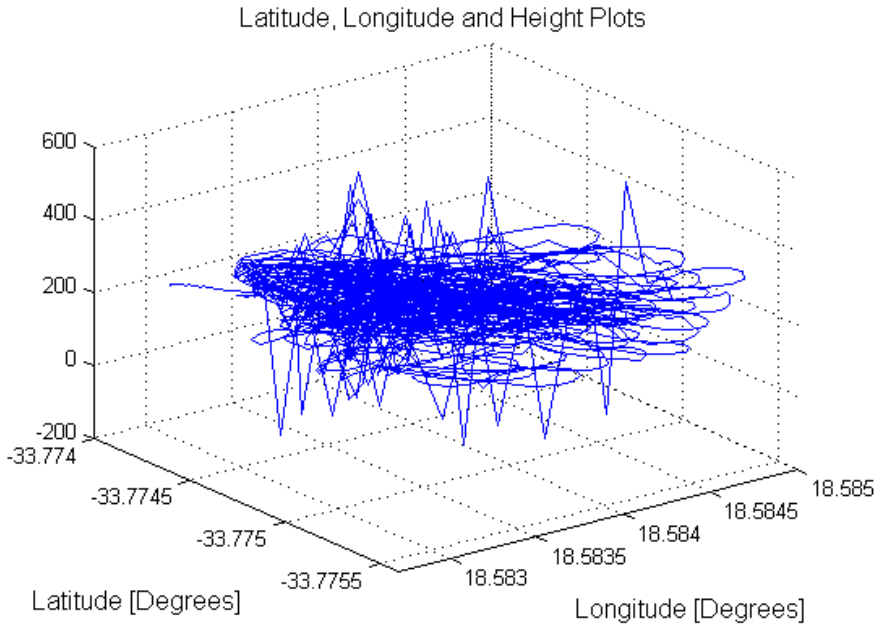


Figure 7.32: 3D Figure showing aircraft position (latitude and longitude) on the x and y axis, and altitude on the z axis for flight 2.

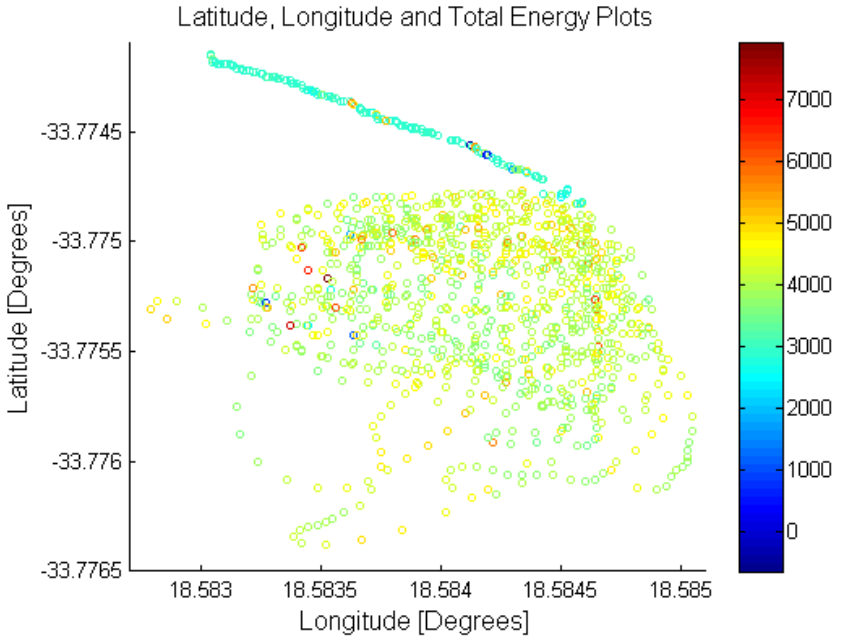


Figure 7.33: Figure showing a scatter graph of aircraft position; marker colour indicates total energy in the system, this figure is for flight 1. Colour bar units are J/m where m is the mass of the aircraft.

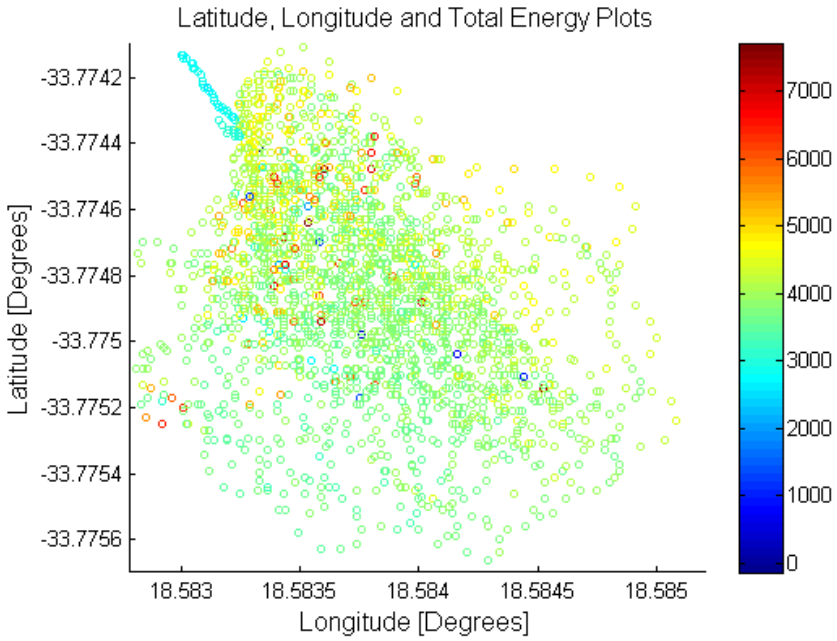


Figure 7.34: Figure showing a scatter graph of aircraft position; marker colour indicates total energy in the system, this figure is for flight 2. Colour bar units are J/m where m is the mass of the aircraft.

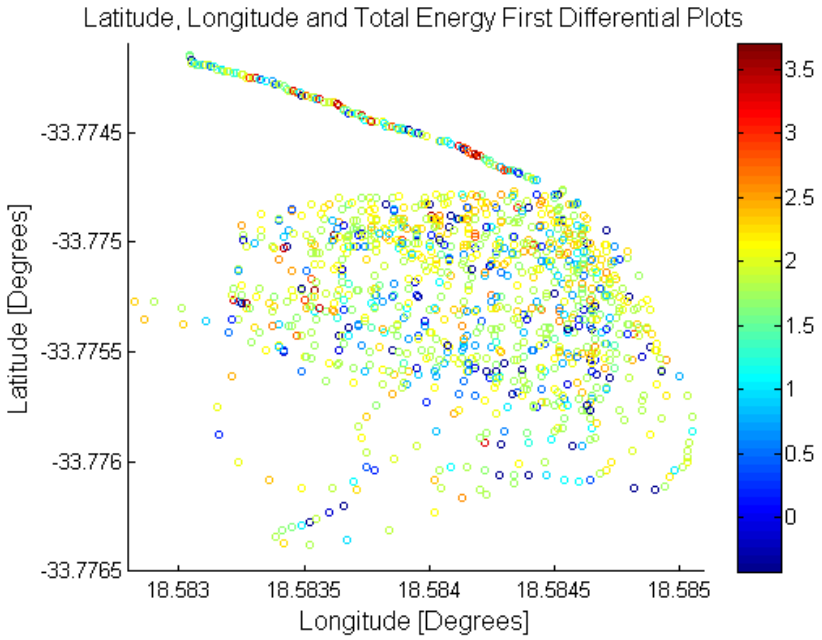


Figure 7.35: Figure showing a scatter graph of aircraft position; marker colour indicates total energy rate in the system, this figure is for flight 1. Colour bar units are log(J/m) where m is the mass of the aircraft.

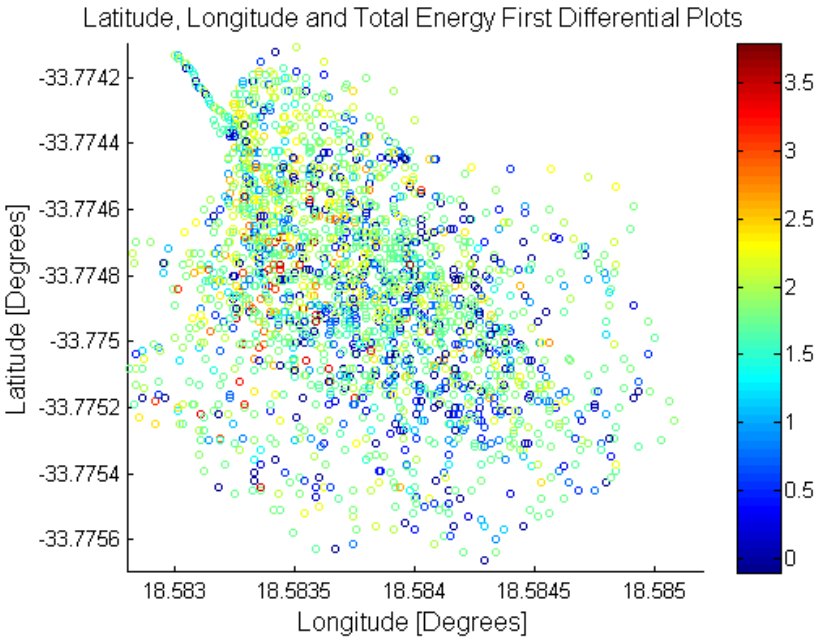


Figure 7.36: Figure showing a scatter graph of aircraft position; marker colour indicates total energy rate in the system, this figure is for flight 2. Colour bar units are log(J/m) where m is the mass of the aircraft.

From figures 7.35 and 7.36, one can see that ridge soaring in the test location is confined to a fairly small area. This is noted by the overlapping flight paths. Scatter plots were used due to the overlapping flight paths, in addition, high energy rate locations are easily identified due to the close proximity and clustering of high energy rate markers.

Figures 7.37 and 7.38 show the difference between magnetic heading and GPS heading for flights one and two respectively; this can also be thought of as the side-slip of the aircraft. These two graphs clearly show that the aircraft is being affected by the strong wind and turbulence.

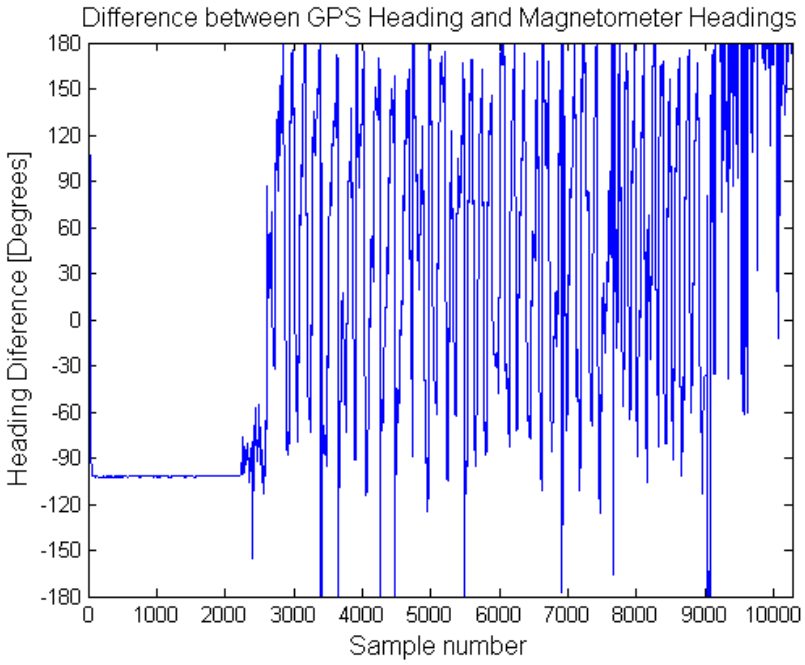


Figure 7.37: Figure showing the difference between the magnetic heading and the aircraft's heading according to the GPS, for flight 1.

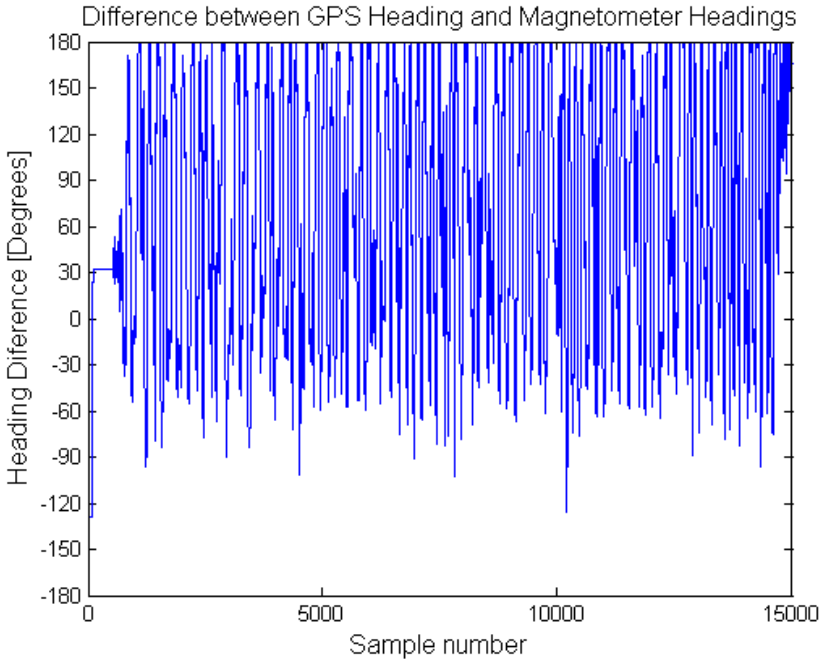


Figure 7.38: Figure showing the difference between the magnetic heading and the aircraft's heading according to the GPS, for flight 2.

CHAPTER 8

# CONCLUSIONS

In this project, a microcontroller based system was developed to determine certain flight parameters of a glider. During the course of the development cycle, a number of different hardware designs were developed and tested.

Two gliders were built for this project: the first was a specialised composite glider and the second was a production glider.

Sensor calibration was done using a wind tunnel to calibrate the airspeed measurement process. A dedicated test apparatus was developed so that the pitot tube could be located on an actual glider wing during the wind tunnel testing phase.

A realtime telemetry system was developed and interfaced with a custom ground station with good results.

Flight testing was done in the field over a period of about six months to test the system in its operating environment; this flight testing was done over different seasons and at different locations. The system was additionally flight tested using ridge soaring techniques; this was done to gather additional data.

The hardware and firmware developed during the course of this project performed well. More work could be done, however, to consolidate all of the component systems into a single system; this would allow smaller aircraft to carry the system in addition to improving the overall robustness.

In conclusion, the system had an acceptable level of performance for this project. Issues were encountered with sensor performance, glider design and flight testing but these issues could however be significantly improved by implementing the changes suggested in the following chapter. Much work can still be done to take this project from an instrumentation system to a full flight controller capable of sustained long endurance soaring.

CHAPTER 9

# FUTURE WORK

A number of improvements can be made to the system developed. These include:

- Move away from 5 V components towards 3.3 V components. The reason for this is that the standard operating voltage of commercial radio control systems is in the region of 5 V; this requires additional batteries to be carried to have sufficient voltage overhead for the linear regulators. One could utilise more complicated regulators to step up the supply voltage but that adds additional complexity.

- Condense all of the subsystems onto a single printed circuit board. Presently there are four separate boards which together form the complete system. Each of these boards plug into one another using header pins; while this type of system is modular and thus is easily reconfigurable, it is physically larger than a condensed board and also has more points of failure, namely, the board inter-connectors. The modular approach was specifically chosen for this project so as not be constrained by hardware more than necessary; this allowed different sensors to be added without requiring a hardware re-design.

- It is highly recommended that the system be ported to a 32-bit microcontroller or embedded PC; this would allow far more complex calculations to be made in realtime. The 8-bit AVR used in this project performed the task, however, the author believes that if one wanted to take this project further, it would become a serious limitation and will reduce the potential of the system

- The next step in this project would be to integrate the system with an autopilot. One could develop one's own autopilot if there was a specific need, but due to the number commercially available systems on the market and the number of open source projects such as the Ardu-Pilot project, it would appear that time is better spent using what is available. This would allow more time to be spent on the soaring controller.

- From a software point of view, the following work is proposed: in order to improve the resolution and accuracy of the system it is proposed that additional data fusion methods be added to the system. The proposed system would fuse barometric altitude, GPS altitude and information from the inertial system so as to improve altitude measurement accuracy; this in turn will allow a better total energy rate to be estimated as better information is

known about the aircraft's vertical velocity and vertical acceleration. This fusion could help alleviate some of the noise present in the airspeed measurement caused by strong winds.

- Further work is proposed to implement and possibly improve on the thermal localisation methods developed by Allen [32], Edwards [31], and Hazard [34]. These methods would allow the system to locate and track thermals in realtime.

- Sensor noise proved to be a significant hurdle, and this necessitated hardware redesigns. Better and more accurate sensors would have made the implementation of the system far easier but due to budget constraints, this was not possible. A dedicated enclosure is recommended to house the system, this should shield the sensors from air turbulence associated with strong wind conditions. The use of a dedicated static air pressure port is strongly encouraged to mitigate the effects of fuselage pressurisation. This should improve barometric pressure measurement and therefore improve altitude measurement accuracy. Further work could also be done to optimise the location the pitot tube.

- The requirement of having to have a tow pilot and tow plane to tow the glider to altitude caused delays due both to scheduling and to tow plane maintenance issues. A better approach would be to use an electric motor onboard to self-launch the aircraft; this would require a method of estimating the energy added to the system as a result of running said motor. However, the time taken to develop and implement this system would easily be less than the time lost due to logistical issues. A winch launch could also be implemented as it would be the simplest method of launching a large glider.

- Due to the very nature of this type of project, the weather plays a significant role in the overall outcome. This project was no exception and was delayed while waiting for better weather conditions. While good results were obtained, testing during the summer months would have improved the results obtained.

# LIST OF REFERENCES


[1] G. Baldwin, R. Mahony, J. Trumpf, T. Hamel, and T. Cheviron, "Complementary filter design on the Special Euclidean group SE(3)." European Control Conference, Kos, Greece, 2007.

[2] Smithsonian National Air and Space Museum, "The Wright Brothers & the invention of the aerial age." Internet: http://airandspace.si.edu/wrightbrothers/. [Accessed 09/02/2013].

[3] Encyclopedia Britannica, "Sir George Cayley, 6th Baronet." Internet: http://www.britannica.com/EBchecked/topic/100795/Sir-George-Cayley-6th-Baronet. [Accessed 04/02/2013].

[4] F. E. Jones, "The air density equation and the transfer of the mass unit," *Journal of Research of the National Bureau of Standards*, vol. 83, p. 419, July 1977.

[5] S. Stovall, "Basic inertial navigation," *Naval Air Warfare Center Weapons Division*, 1997.

[6] Freescale Semiconductor, "Application note: An3461." Rev 2, 06/2007.

[7] Freescale Semiconductor, "Application note: An3447." Rev 0, 03/2007.

[8] X. Xiong, Y. Wu, and W. Jone, "Material fatigue and reliability of mems accelerometers," in *Defect and Fault Tolerance of VLSI Systems, 2008. DFTVS'08. IEEE International Symposium on*, pp. 314–322, IEEE, 2008.

[9] M. J. Caruso, "Applications of magnetoresistive sensors in navigational systems," tech. rep., Honeywell Inc., Plymouth, MN, February 1998.

[10] M. Cook, *Flight Dynamics Principals - A linear systems approach to aircraft stability and control*. Elsevier Ltd, 2 ed., 2007.

[11] M. Euston, P. Coote, R. Mahony, J. Kim, and T. Hamel, "A complementary filter for attitude estimation of a fixed-wing uav," in *Intelligent Robots and Systems, 2008. IROS 2008. IEEE/RSJ International Conference*, pp. 340–345, IEEE, 2008.

[12] D. Choukroun, I. Bar-Itzhack, and Y. Oshman, "Novel quaternion Kalman filter," *Aerospace and Electronic Systems, IEEE Transactions on*, vol. 42, no. 1, pp. 174–190, 2006.

[13] W. Premerlani, "Direction cosine matrix imu: Theory." Internet: www.gentlenav.googlecode.com/files/DCMDraft2.pdf, May 2009. [Accessed: 09/02/2013].

[14] W. Tang, G. Howell, and Y. Tsai, "Barometric altimeter short-term accuracy analysis," *Aerospace and Electronic Systems Magazine, IEEE*, vol. 20, no. 12, pp. 24–26, 2005.

[15] C. Antal, O. Granichin, and S. Levi, "Adaptive autonomous soaring of multiple uavs using simultaneous perturbation stochastic approximation," in *Decision and Control (CDC), 2010 49th IEEE Conference on*, pp. 3656–3661, IEEE, 2010.

[16] J. Kim and S. Sukkarieh, "A baro-altimeter augmented ins/gps navigation system for an uninhabited aerial vehicle," in *Int. Symp. on Satellite Navigation Technologys*, 2003.

[17] Cloud Cap Technologies, "Piccolo flight management system." Internet: http://www.cloudcaptech.com/Sales%20and%20Marketing%20Documents/Piccolo%20Flight%20Management%20System.pdf. [Accessed 12/05/2013].

[18] K. Sprague, V. Gavrilets, D. Dugail, B. Mettler, E. Feron, and I. Martinos, "Design and applications of an avionics system for a miniature acrobatic helicopter," in *Digital Avionics Systems, 2001. DASC. 20th Conference*, vol. 1, pp. 3C5–1, IEEE, 2001.

[19] O. Ariff and T. Go, "Dynamic soaring of small-scale uavs using differential geometry," in *7th IBCAST conference Aerospace Sciences Meeting and Exhibition 8-11 January 2010, Islamabad, Pakistan*.

[20] M. Boslough, "Autonomous dynamic soaring platform for distributed mobile sensor arrays," *Sandia National Laboratories, Sandia National Laboratories, Tech. Rep. SAND2002-1896*, 2002.

[21] J. Grenestedt and J. Spletzer, "Towards perpetual flight of a gliding unmanned aerial vehicle in the jet stream," in *Decision and Control (CDC), 2010 49th IEEE Conference on*, pp. 6343–6349, IEEE, 2010.

[22] M. J. Allen, "Autonomous soaring for improved endurance of a small uninhabited air vehicle," in *43rd AIAA Aerospace Sciences Meeting and Exhibit*, (Reno, NV), 2005.

[23] J. Grenestedt, C. Montella, and J. Spletzer, "Dynamic soaring in hurricanes." International Conference on Unmanned Aircraft Systems (ICUAS), 2012.

[24] J. Langelaan, "Long distance/duration trajectory optimization for small uavs," in *Proceedings of the 2007 AIAA Guidance, Navigation and Control Conference and Exhibit*, 2007.

[25] Experimental Aircraft Association, "Fossett breaks glider altitude record." Internet: http://www.eaa.org/news/2006/2006-08-31_fossett.asp, August 2006. [Accessed 23/01/2013].

[26] J. Wharington and I. Herszberg, "Control of a high endurance unmanned air vehicle," in *Proceedings of the 21st ICAS Congress*, 1998.

[27] Z. Ákos, M. Nagy, S. Leven, and T. Vicsek, "Thermal soaring flight of birds and unmanned aerial vehicles," *Bioinspiration & biomimetics*, vol. 5, no. 4, p. 045003, 2010.

[28] M. J. Allen, "Updraft model for development of autonomous soaring uninhabited air vehicles," in *Forty Fourth AIAA Aerospace Sciences Meeting and Exhibit*, (Reno, Nevada), 2006.

[29] D. J. Edwards, "Implementation details and flight test results of an autonomous soaring controller." AIAA, Guidance, Navigation and Control Conference and Exhibit, Hawaii, 2008.

[30] J. Clarke and W. Chen, "Trajectory generation for autonomous soaring uas," *International Journal of Automation and Computing*, vol. 9, no. 3, pp. 248–256, 2012.

[31] D. J. Edwards, *Autonomous Soaring: The Montague Cross Country Challenge*. PhD thesis, North Carolina State University, 2010.

[32] M. J. Allen, "Guidance and control of an autonomous soaring uav," Tech. Rep. NASA/TM-2007-214611, NASA Dryden Flight Research Center, Edwards, California, 2007.

[33] D. J. Edwards, "Performance testing of rnr's sbxc using a piccolo autopilot." Internet: http://soaring.goosetechnologies.com, March 2008. [Accessed 10 January 2013].

[34] M. Hazard, "Unscented kalman filtering filter for thermal parameter identification," in *48th AIAA Aerospace Sciences Meeting Including the New Horizons Forum and Aerospaces Exposition*, 2010.

[35] D. Lee and K. Andersson, "Hybrid control of long-endurance aerial robotic vehicles for wireless sensor networks," *International Journal of Advanced Robotic Systems*, vol. 8, no. 2, p. 101, 2011.

[36] W. Kagabo, *Optimal trajectory planning for a UAV glider using atmospheric thermals*. PhD thesis, Rochester Institute of Technology, 2010.

[37] M. W. Hazard, "Unscented kalman filtering for real-time atmospheric thermal tracking," Master's thesis, North Carolina State University, 2010.

[38] RnR Products, "Sbxc cross country." Internet: http://www.rnrproducts.com/airframes /gliders/xbxc.htm. [Accessed 28/01/2013].

[39] Freescale Semiconductor, "Integrated silicon pressure sensor on-chip signal conditioned, temperature compensated and calibrated," MPXV5004 Datasheet, September 2009. [Revision 12].

[40] Freescale Semiconductor, "High temperature accuracy integrated silicon pressure sensor for measuring absolute pressure, on-chip signal conditioned, temperature compensated and calibrated," MPXA6115A Datasheet, June 2012. [Revision 7.2].

[41] Analog Devices, "1 deg c accurate, 13-bit, digital temperature sensor," ADT7301 Datasheet, 2011. [Revision B].

[42] Analog Devices, "Ultracompact, precision 10.0 v/5.0 v/2.5 v/3.0 v voltage references," ADR02 Datasheet, 2012. [Revision R].

[43] Analog Devices, "36 v precision, 2.8 nv/sqrt(hz) rail-to-rail output op amp," AD8675 Datasheet, 2012. [Revision E].

[44] Fairchild Semiconductor Corporation, "Npn epitaxial silicon transistor," MJD31/31C Datasheet, February 2012. [Revision A4].

[45] Bosch Sensortec, "Bmp085 digital pressure sensor," BMP085 Datasheet, July 2008. [Revision 1.0].

[46] Sparkfun Electronics, "9 degrees of freedom - razor imu - ahrs compatible." Internet: https://www.sparkfun.com/products/9623. [Accessed 08/02/2013].

[47] Analog Devices, "Mems motion sensor: dual axis pitch and roll 300deg/s analog gyroscope," LPR530AL Datasheet, 2009. [Revision 2].

[48] ST Microelectronics, "Mems inertial sensor single-axis analog and digital output yaw rate gyroscope," LY530AL Datasheet, September 2008. [Revision 1].

[49] Analog Devices, "3-axis, 2 g/4 g/8 g/16 g digital accelerometer," ADXL345 Datasheet, 2011. [Revision C].

[50] Honeywell, "3-axis digital compass ic," HMC5843 Datasheet, June 2010.

[51] J. Munoz, "Sparkfun electronics evaluation code for the razor imu:." Internet: https://github.com/a1ronzo/SparkFun-9DOF-Razor-IMU-Test-Firmware#readme. [Accessed 08/02/2013].

[52] GlobalTop Technology Inc, "Gms-u1lp gpsmodule," Gms-u1LP Datasheet, 2010. [Revision VOE].

[53] Isoboard, "Properties." Internet: http://www.isoboard.com/literature/applicationGuides/properties_Isoboard_thermal_insolution.pdf, January 2011. [Accessed 09/02/2013].

[54] Texas Instruments, "Lm1117/lm1117i 800ma low-dropout linear regulator," LM1117 Datasheet, May 2004. [Revised July 2012].

[55] Sparkfun Electronics, "Xbee explorer usb." Internet: https://www.sparkfun.com/products/8687. [Accessed 08/02/2013].

APPENDIX A

# TESTING PHOTOGRAPHS

Additional photographs from the field testing phase can be seen below.

Figure A.1: Photograph showing the glider on the right, and tow plane on the left.

Figure A.2: Photograph of the tow plane and glider moments after takeoff.

Figure A.3: Photograph showing the glider about to land, the picture also shows the placement of the Pitot tube as highlighted with a red circle.

APPENDIX B

# SCHEMATICS AND PCB DESIGNS

In this chapter, all of the schematics and printed circuit board designs will be presented.

Three printed circuit board designs were utilised during the course of this project, namely:

1. First Prototype
    - Analog acquisition board
    - Logging board
2. Second prototype
    - Completely integrated logger board

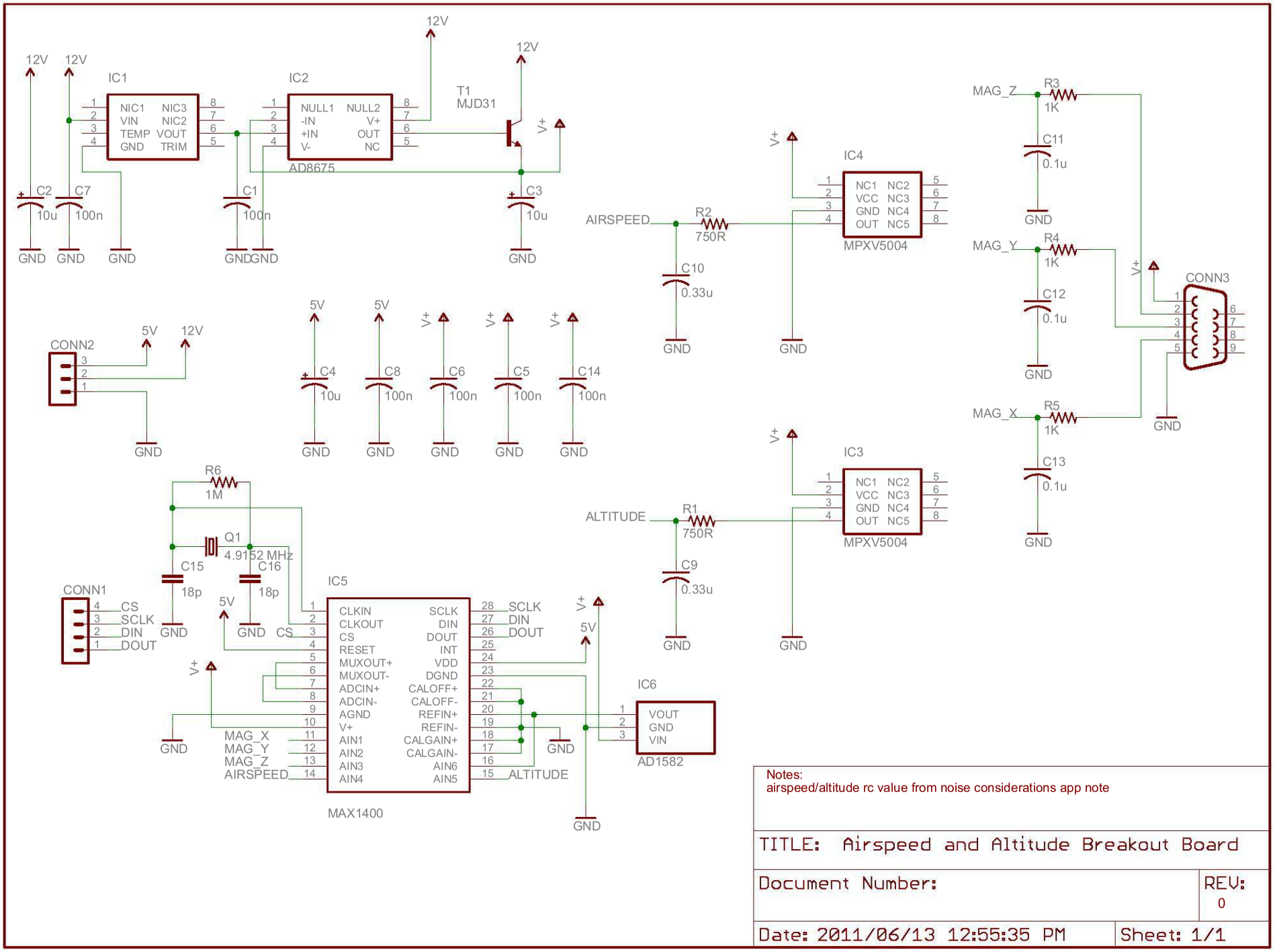
IC1
NIC1 NIC3
VIN NIC2
TEMP VOUT
GND TRIM
IC2
NULL1 NULL2
-IN V+
+IN OUT
V- NC
AD8675
T1
MJD31
12V
V+
C1 100n
C2 10u
C7 100n
C3 10u
GND
IC4
NC1 NC2
VCC NC3
GND NC4
OUT NC5
MPXV5004
AIRSPEED
R2 750R
C10 0.33u
IC3
ALTITUDE
R1 750R
C9 0.33u
MAG_Z
MAG_Y
MAG_X
R3 1K
R4 1K
R5 1K
C11 0.1u
C12 0.1u
C13 0.1u
CONN3
CONN2
5V
C4 10u
C8 100n
C6 100n
C5 100n
C14 100n
R6 1M
Q1 4.9152 MHz
C15 18p
C16 18p
CONN1
CS
SCLK
DIN
DOUT
IC5
CLKIN SCLK
CLKOUT DIN
CS DOUT
RESET INT
MUXOUT+ VDD
MUXOUT- DGND
ADCIN+ CALOFF+
ADCIN- CALOFF-
AGND REFIN+
V+ REFIN-
AIN1 CALGAIN+
AIN2 CALGAIN-
AIN3 AIN6
AIN4 AIN5
MAX1400
IC6
VOUT
GND
VIN
AD1582
Notes:
airspeed/altitude rc value from noise considerations app note
TITLE: Airspeed and Altitude Breakout Board
Document Number:
REV: 0
Date: 2011/06/13 12:55:35 PM
Sheet: 1/1

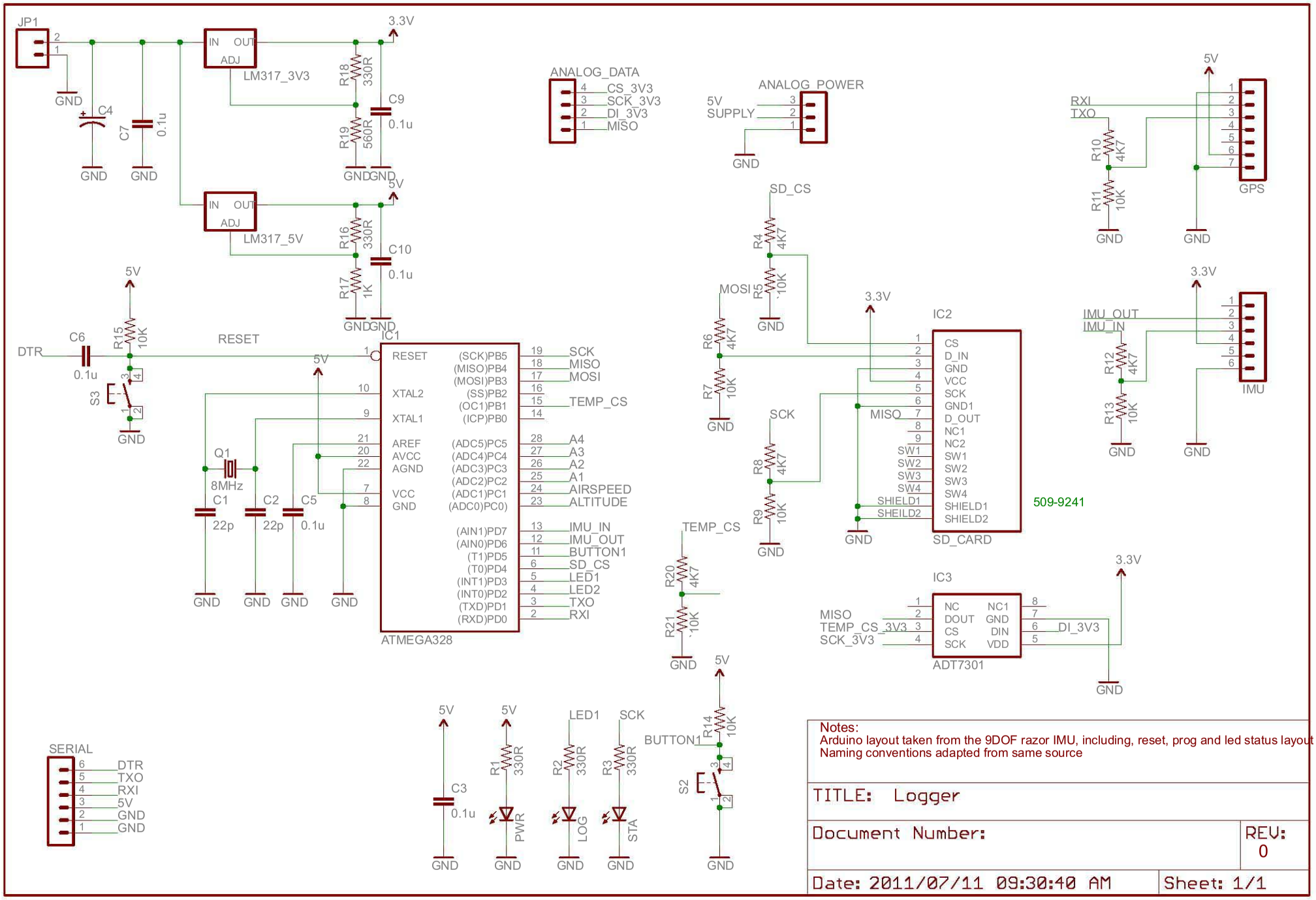


Notes:
Arduino layout taken from the 9DOF razor IMU, including, reset, prog and led status layout
Naming conventions adapted from same source

| | |
|---|---|
| TITLE: Logger | |
| Document Number: | REV: 0 |
| Date: 2011/07/11 09:30:40 AM | Sheet: 1/1 |

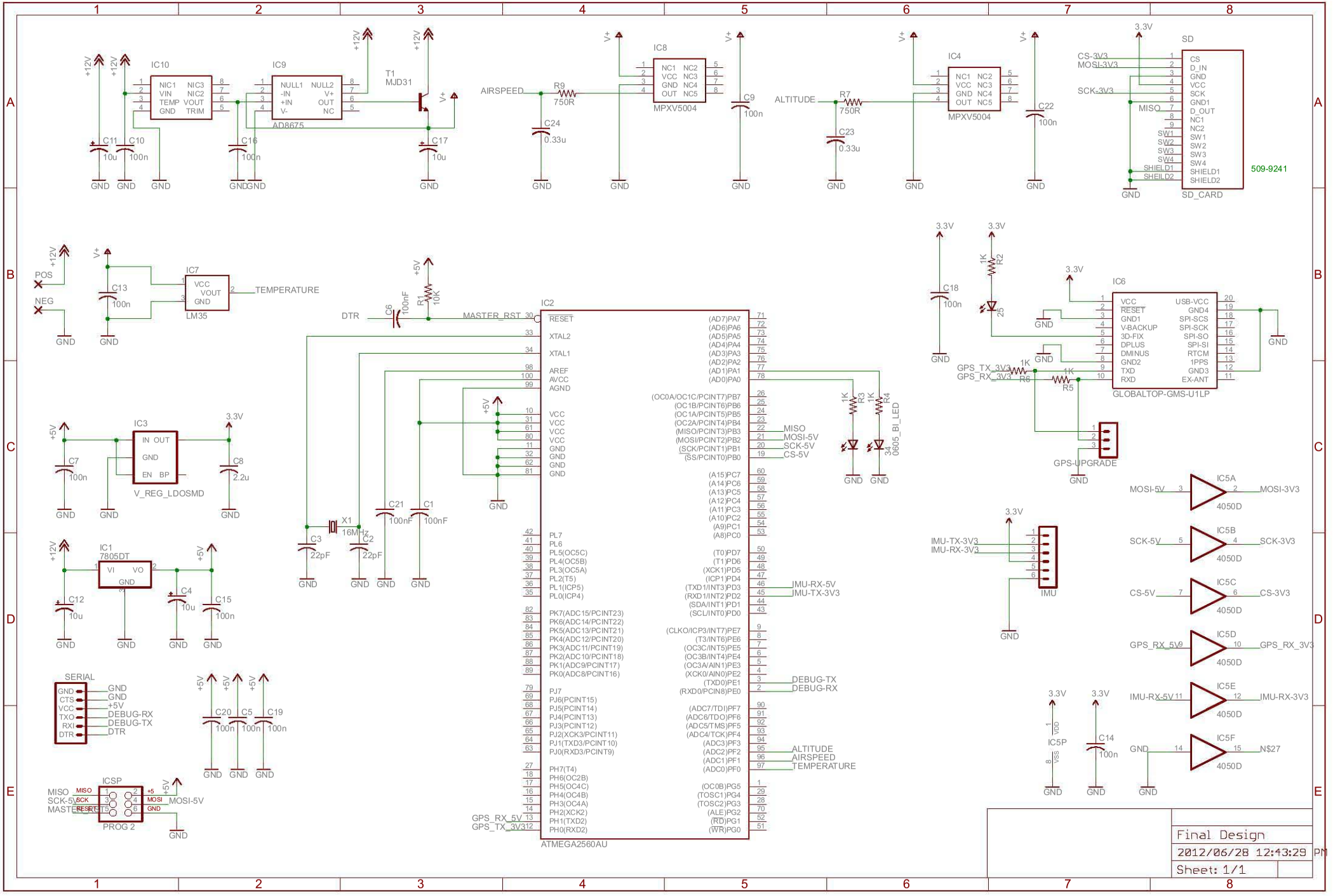
IC10
IC9
AD8675
T1
MJD31
IC8
MPXV5004
AIRSPEED
ALTITUDE
IC4
MPXV5004
SD
SD_CARD
509-9241
IC7
LM35
TEMPERATURE
IC2
ATMEGA2560AU
MASTER_RST
IC3
V_REG_LDOSMD
IC1
7805DT
IC6
GLOBALTOP-GMS-U1LP
GPS-UPGRADE
IMU
IC5A
IC5B
IC5C
IC5D
IC5E
IC5F
4050D
IC5P
SERIAL
ICSP
PROG 2
Final Design
2012/06/28 12:43:29 PM
Sheet: 1/1

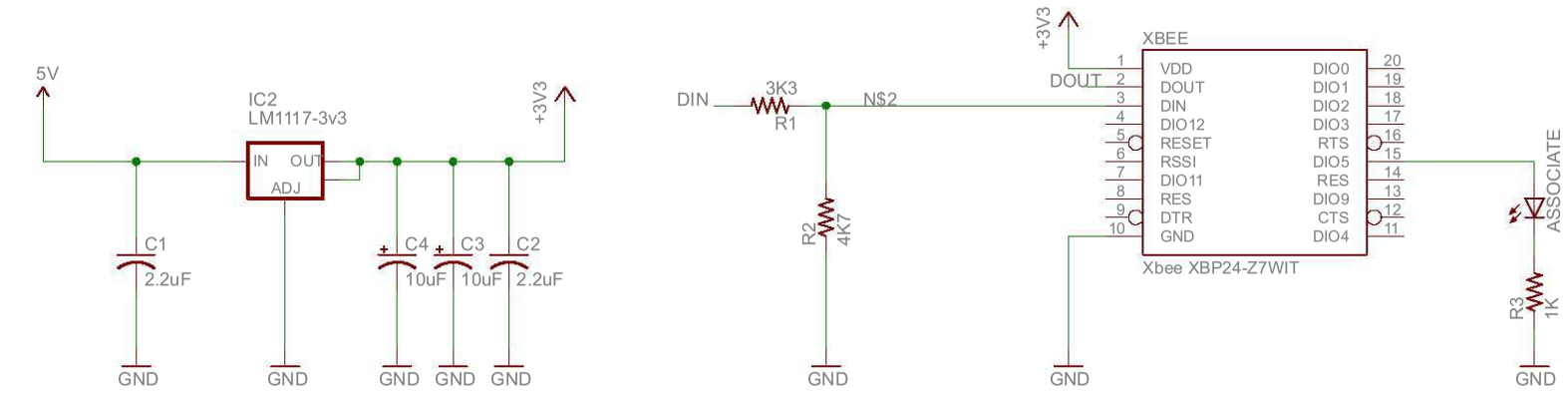


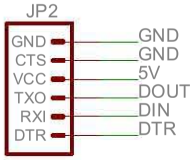


To System

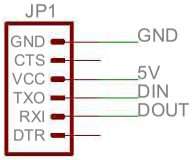


To PC

| | |
|---|---|
| TITLE: Xbee Interface | |
| Document Number: | REV: 0 |
| Date: 10/23/2012 12:39:02 PM | Sheet: 1/1 |

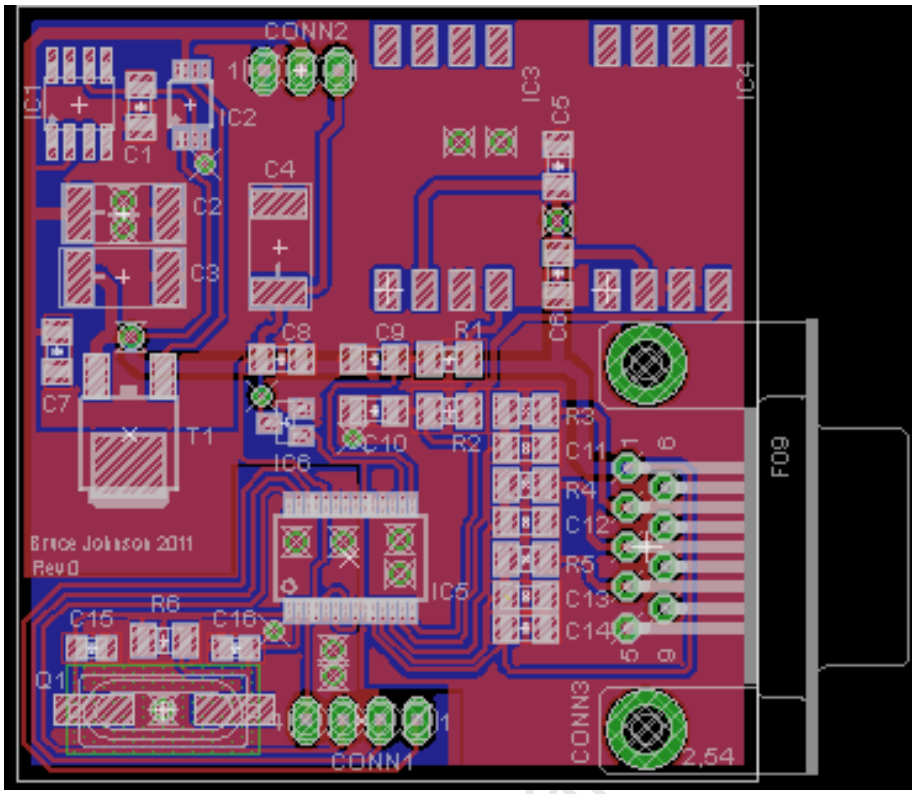


Figure B.1: Analog acquisition printed circuit board layout - Complete view

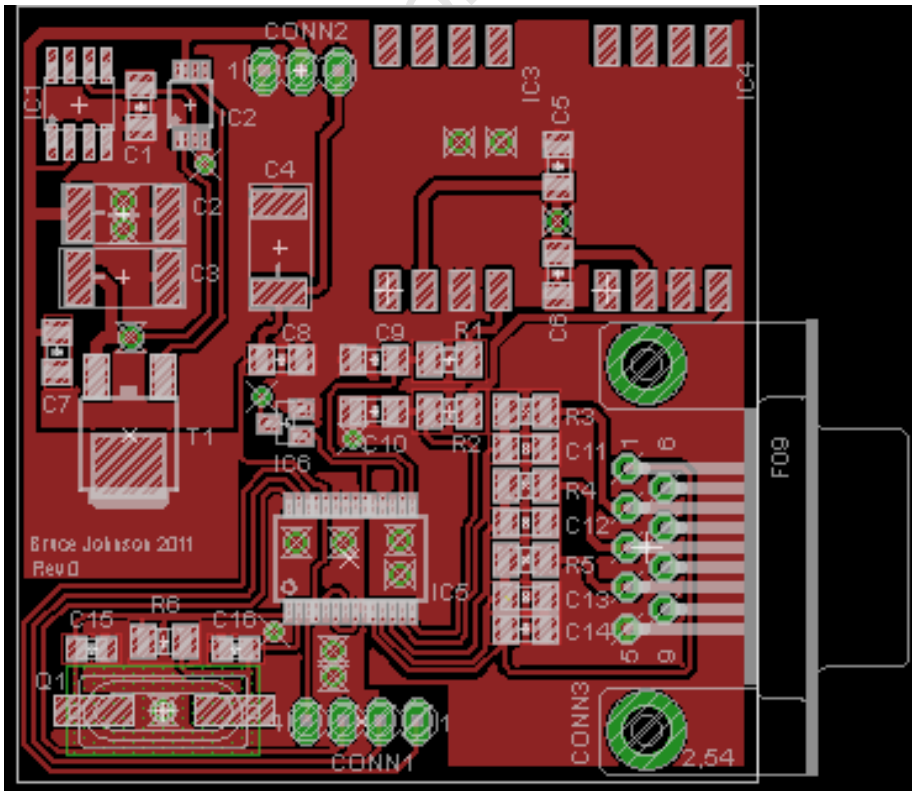


Figure B.2: Analog acquisition printed circuit board layout - Top view

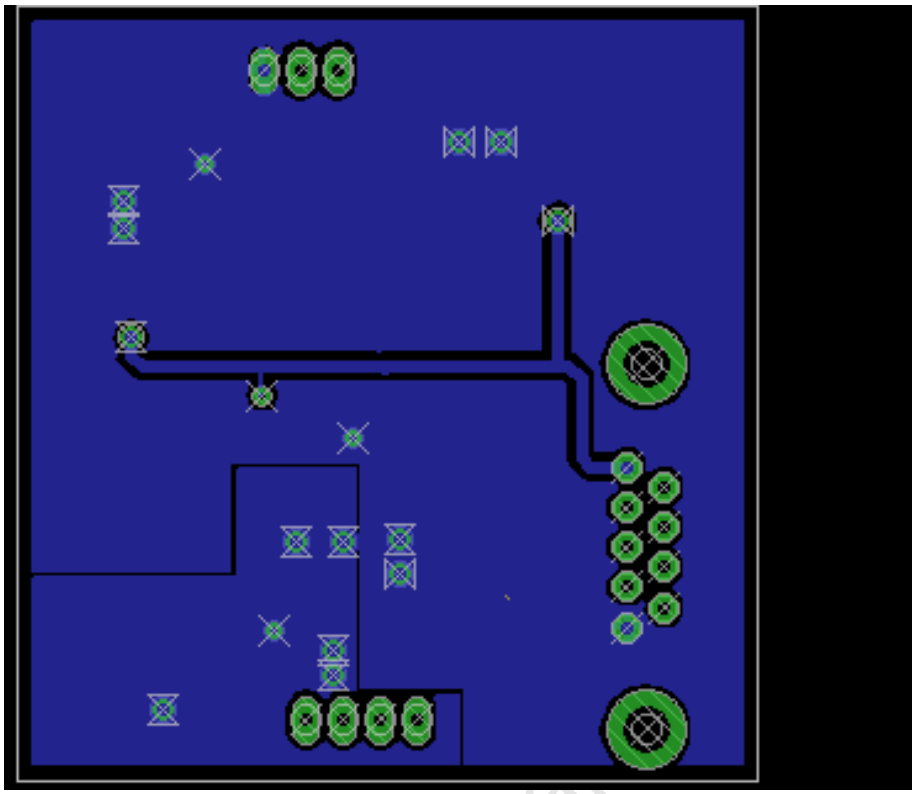

Figure B.3: Analog acquisition printed circuit board layout - Bottom view

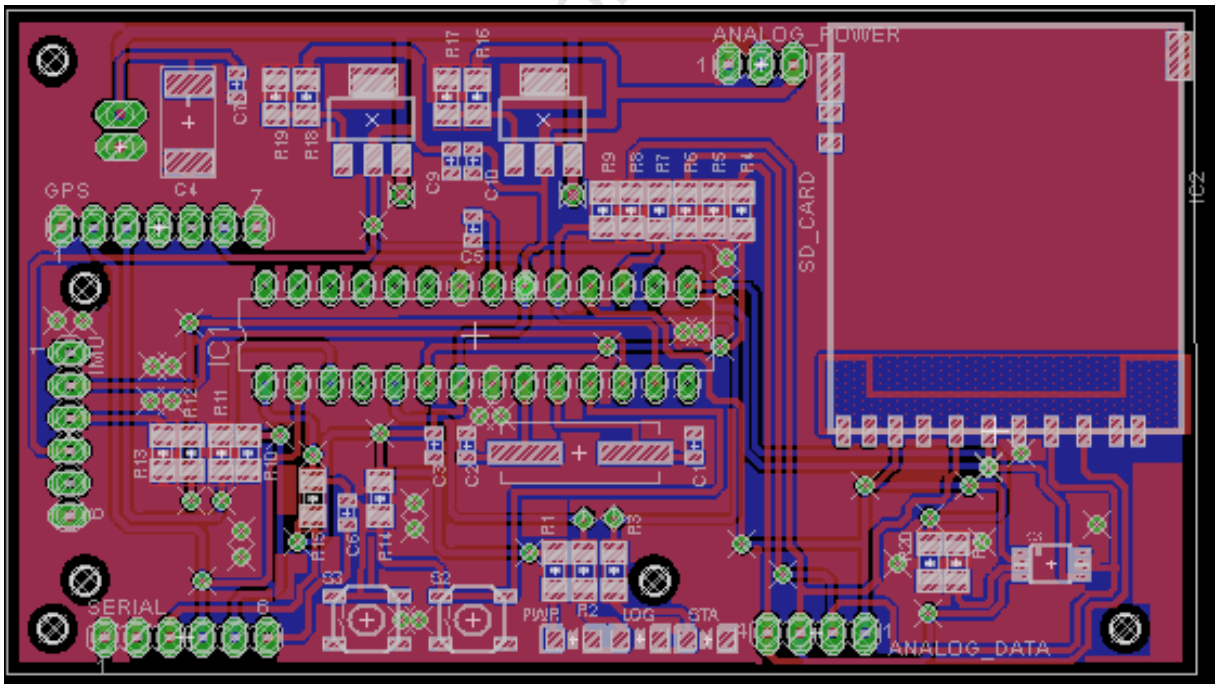


Figure B.4: Logging printed circuit board layout - Complete view

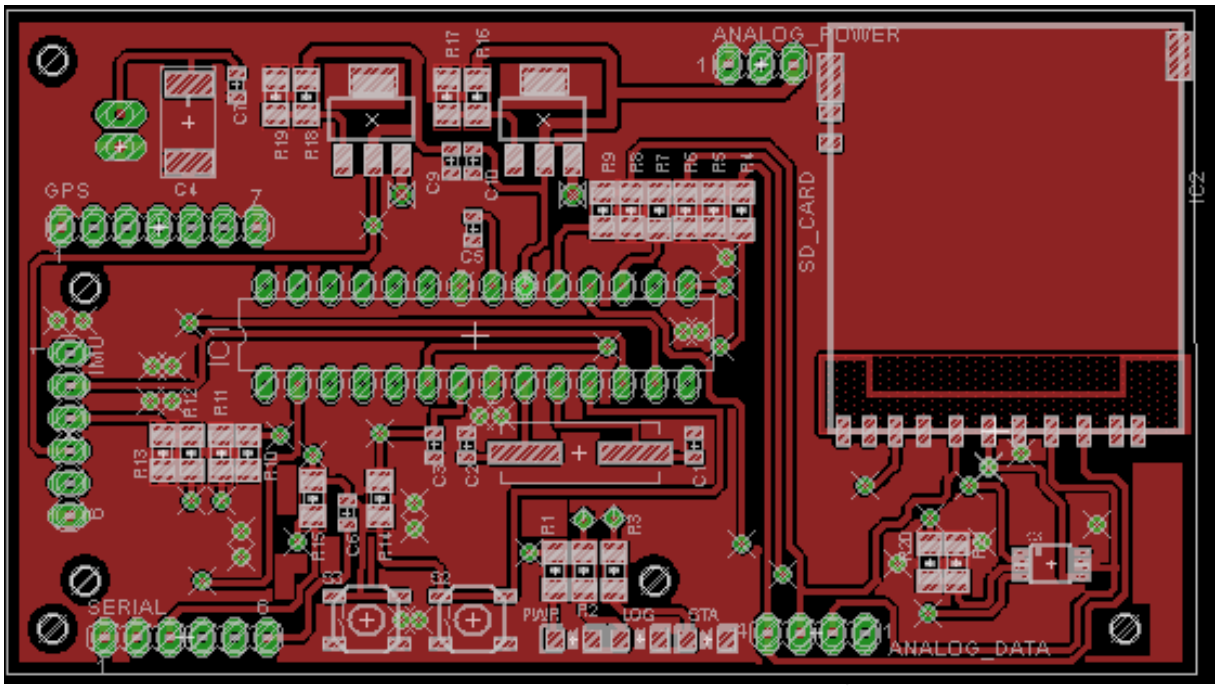


Figure B.5: Logging printed circuit board layout - Top view

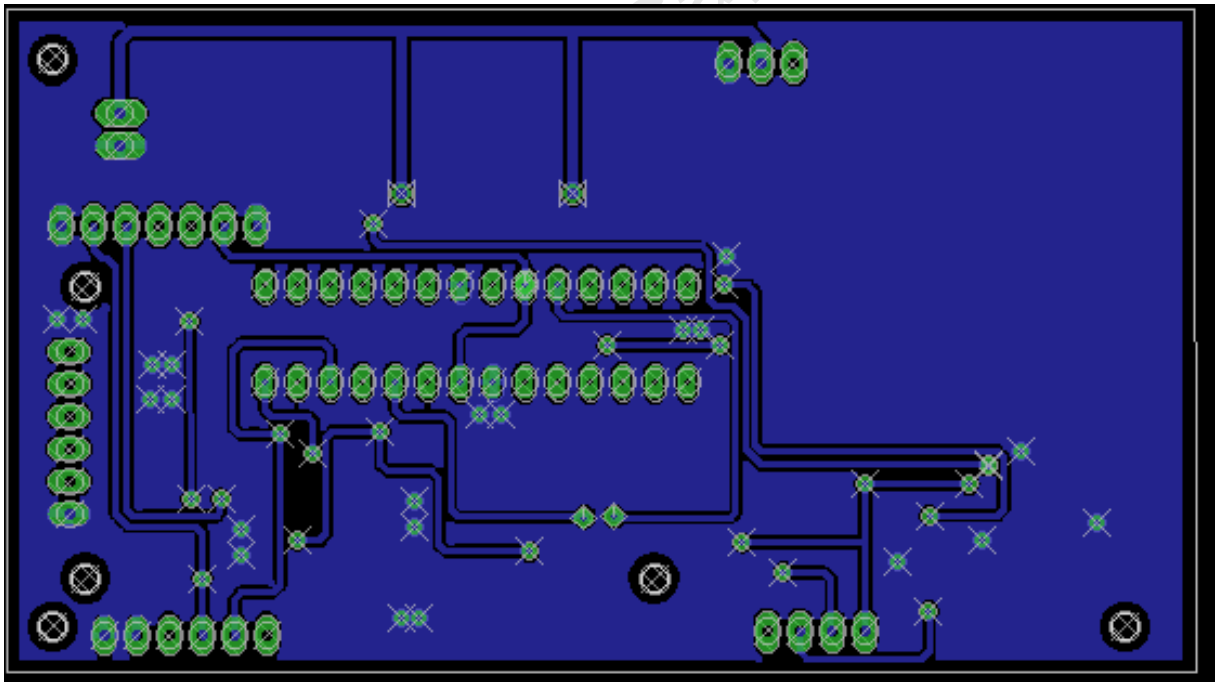

Figure B.6: Logging printed circuit board layout - Bottom view

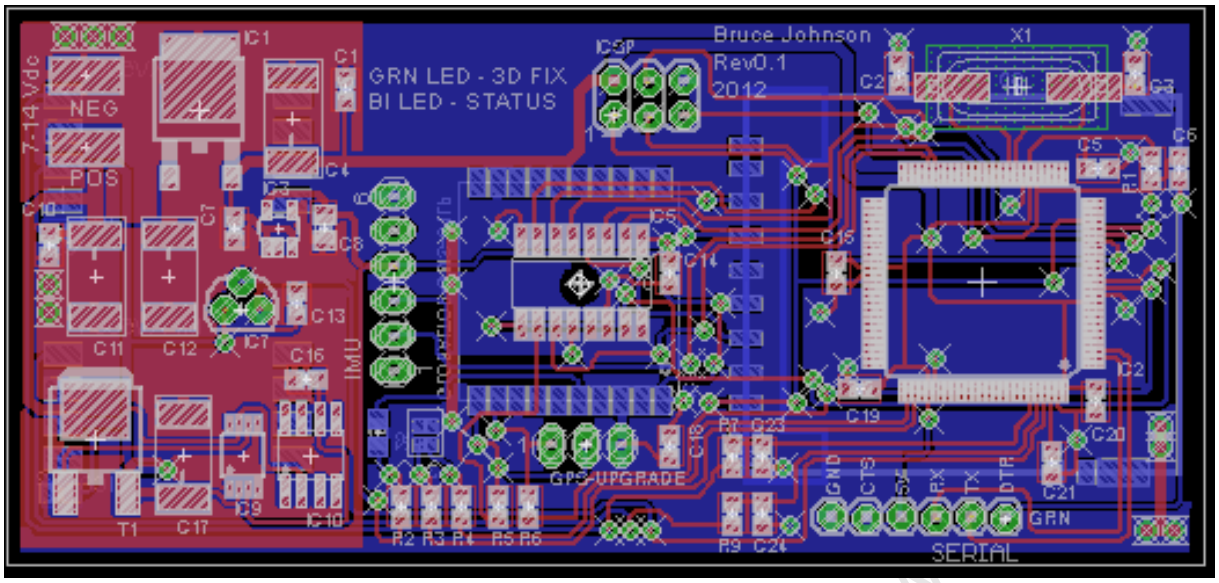


Figure B.7: Completely integrated logger printed circuit board layout - Complete view

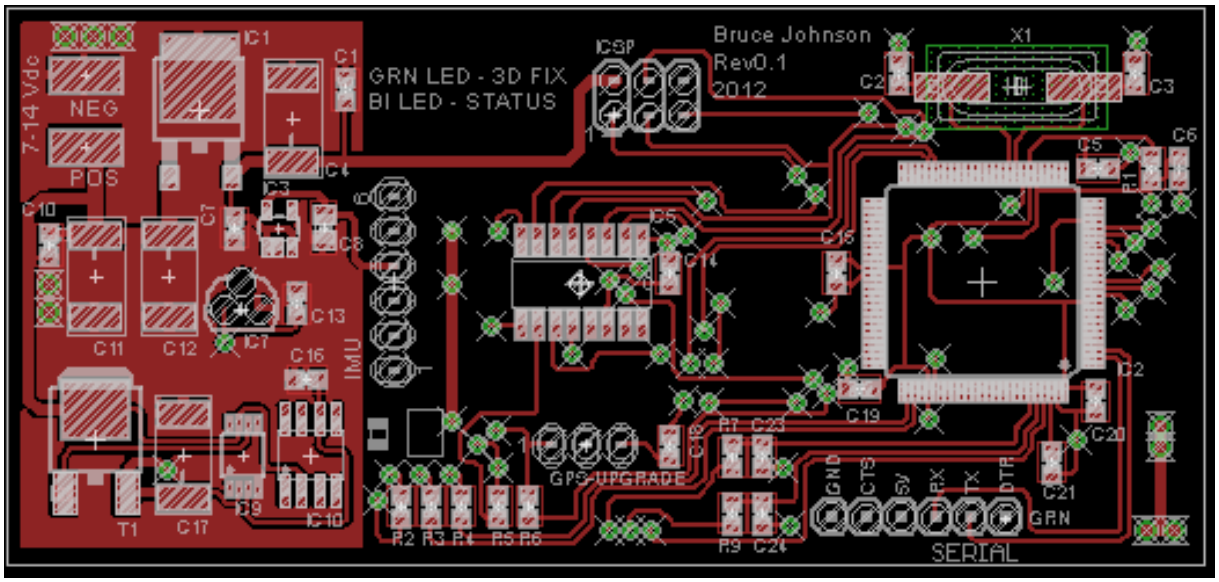


Figure B.8: Completely integrated logger printed circuit board layout - Top view

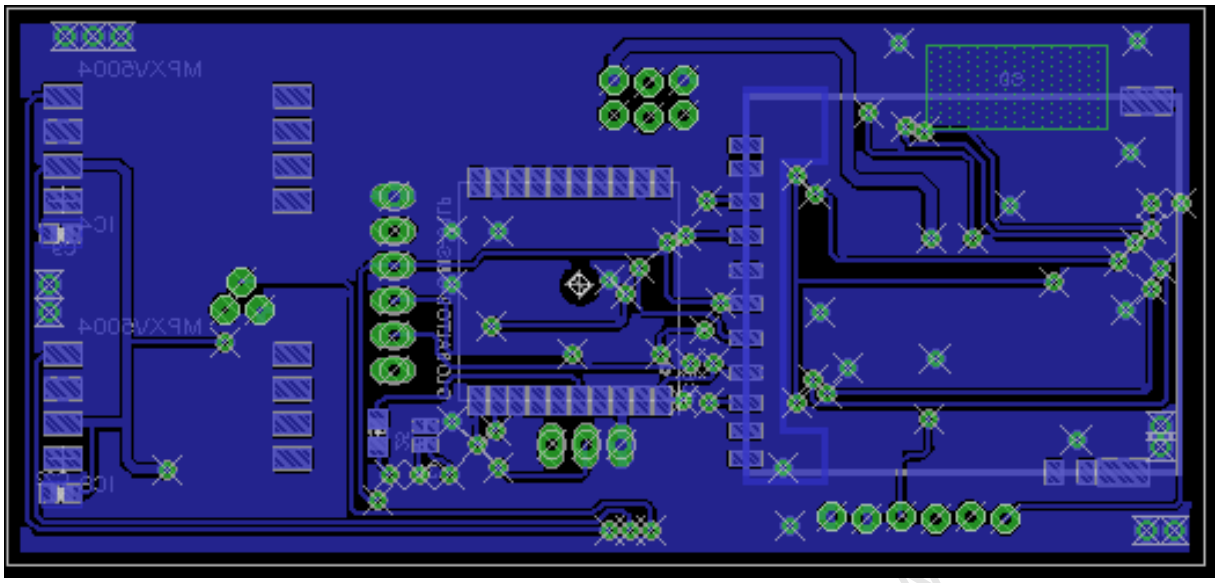

Figure B.9: Completely integrated logger printed circuit board layout - Bottom view

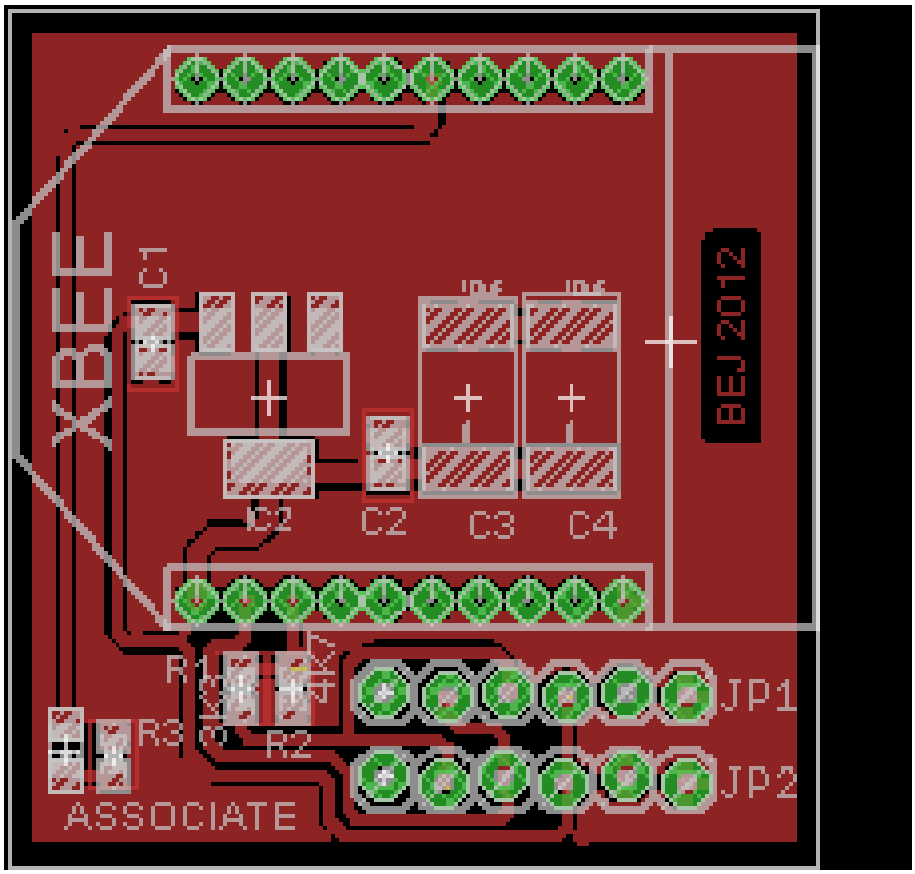


Figure B.10: Telemetry Interface board layout - Complete View

APPENDIX C

# WIND TUNNEL CALIBRATION

The following photographs illustrate the setup used during the airspeed calibration procedure.

Figure C.1: Photograph showing the overall arrangement of the apparatus in the wind tunnel from front.

Figure C.2: Photograph showing the overall arrangement of the apparatus in the wind tunnel from the rear.

Figure C.3: Photograph showing the wing joiner clamp in more detail.

The design for the stand can be seen on the following page.

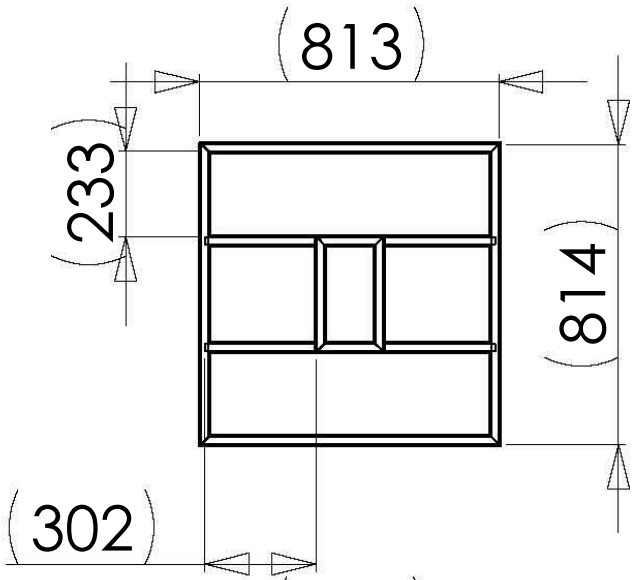


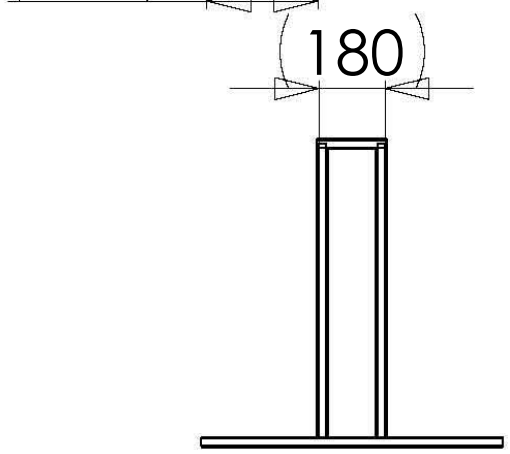


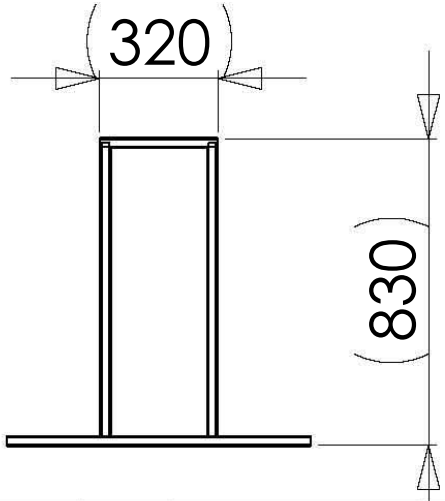


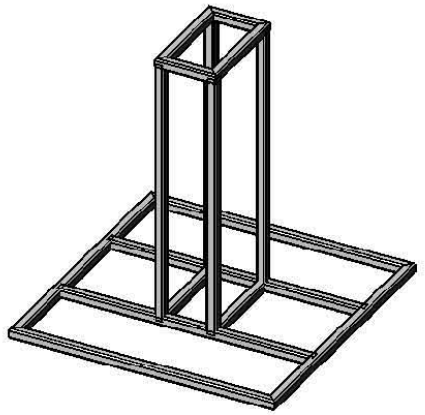

| | | | | | |
|---|---|---|---|---|---|
| | | DIMENSIONS ARE IN MILLIMETERS | | NAME | DATE |
| | | | DRAWN | Bruce Johnson | 06/03/2012 |
| | | | CHECKED | | |
| | | | ENG APPR. | | |
| | | | MFG APPR. | | |
| | | MATERIAL MILD STEEL 30x30x2.5 | Q.A. | | |
| | | | COMMENTS: | | |
| NEXT ASSY | USED ON | FINISH -- | | | |
| APPLICATION | | DO NOT SCALE DRAWING | | | |

# Wind Tunnel Test Stand

| SIZE | DWG. NO. | REV. |
|---|---|---|
| A | | 0 |
| SCALE:1:20 | WEIGHT: | SHEET 1 OF 1 |

APPENDIX D

# ADDITIONAL FILES

Additional files created and used during this dissertation can be found on the supplied CD.

The files included are:

- Firmware
  - Logger Firmware
    - Analog.pde
    - Calculations.pde
    - comms.pde
    - Display.pde
    - GPS.pde
    - init_ports.pde
    - logger.pde
    - SDCard.pde
    - variables.h
  - AHRS Firmware
    - AHRS.pde
    - AHRS_library.pde
    - comms.pde
    - Variables.h
- Software - Read_CSV_file.m
- Printed Circuit Board Designs
  - Airspeed and Altitude Breakout Board.brd
  - Airspeed and Altitude Breakout Board.sch
  - bmp085.brd

  - bmp085.sch
  - Final Design.brd
  - Final Design.sch
  - Logger.brd
  - Logger.sch
  - Xbee Interface.brd
  - Xbee Interface.sch

- Labview Files
  - GrounStation.vi
  - Simple_Filter.vi

Department of Mechanical Engineering
MEC4061F/Z – Laboratory/Research Project
**Risk Assessment Form – 2012**

- **Risk Assessments are not required for simple workshop activities covered by the Safety Declaration. However permission must be obtained from Mr Glen Newins before commencing any activity in the Workshop.**
- **Activities performed in Mechanical Engineering laboratories only need your Supervisor's signature and do not need a Safety Officer's signature. The responsible person for the laboratory space must however be informed of your planned activitybefore commencing the activity.**
- **A new Risk Assessment form needs to be completed for each new activity within your project.**
- **You are required to include this document (signed) in your bound project submission and mount a copy next to any rig / apparatus you are using.**

| | |
|---|---|
| **Your Name** | Bruce Johnson |
| **Your Supervisor** | Robyn Verrinder |
| **Project title and number** | FUSION OF SENSOR INFORMATION TO MEASURE THE TOTAL ENERGY OF AN AIRCRAFT AND PROVIDE INFORMATION ABOUT FLIGHT PERFORMANCE AND LOCAL MICROCLIMATE. |
| **Area Safety Officer** | Dr Christopher von Klemperer |
| **Lab Responsible Person** | Prof C Redelinghuys |

| ***This Section to be completed by the student (Must be typed and the declaration signed)*** | | | |
|---|---|---|---|
| Location(where the activity will take place): | Duncan Mcmillan laboratory | | |
| Describe the activity: | Airspeed calibration in a closed circuit wind tunnel of a wing mounted pitot tube. | | |
| Names of persons involved in this activity: | Bruce Johnson<br>Robyn Verrinder<br>C Redelinghuys | | |
| Describe in detail the risks you (and others) will face during this activity and the potential consequences of your activities.: | High noise levels associated with the high wind speed may cause hearing damage to persons in the immediate vacinity.<br>The high wind speeds associated with the wind tunnel may blow debris; this may cause physical harm to a persons body and/or eyes. This may cause physical injury to a persons body and potential blinding. | | |
| Does your project involve the use of any materials (chemicals, gasses, etc.) which may be hazardous to health, or the environment | No<br>☒ | Yes<br>☐ | |
| Does this activity involve any equipment / device designed or built by you which is to be plugged into mains electricity? | No<br>☒ | Yes<br>☐ | |
| Does your project involve any new equipment / devices designed which contain air or gas at pressure? | No<br>☒ | Yes<br>☐ | |
| What precautions are required to protect against the risks detailed above: | Make sure that any objects or debris are secure so that they cannot be moved by the wind forces associated with the tunnel, if an object/debris cannot be secured, it should be removed and placed away from the tunnel. The object/device placed in the wind tunnel needs to be firmly secured so that it cannot come adrift. Persons involved will use safety glasses and hearing protection. | | |
| Describe the personal protective equipment (PPE) required during this activity – specify in detail: | Safety glasses and ear plugs or ear muffs need to be worn. | | |
| Describe the shutdown procedure in detail: | Bring the pressure provided by the small compressor up to 100 kPa, the red stop button may be pressed once the pressure has reached 100kPa, wait until the main blades have stopped before turning off the small compressor, only once everything has stopped may the pressure be turned down using the control knob on the control panel. | | |
| Describe any relevant emergency procedures, e.g. spillage response etc. | A red stop button is provided on the wind tunnel control panel to shutdown the tunnel. | | |

| *I declare that I am aware of the risks associated with this activity and will take all necessary steps to mitigate these risks.* | **Signature** | **Date** |
|---|---|---|
| | Signed by candidate | 17/04/2012 |

| ***This section to be completed by the Project Supervisor****Tick relevant box below.* | | |
|---|---|---|
| Level of supervision required (Please tick relevant block) | A = work may not take place without supervisor present. | |
| | B = work may not take place without a 2nd party present. | X |
| | C = no specific extra supervision requirements. | |
| *I am satisfied that my student is aware of the risks associated with this activity and grant approval for it to proceed.* | **Signature** | **Date** |
| | | 2012-04-17 |

| ***This section to be completed by the Area Safety Officer for work at SAFL or BISRU or CME.*** |
|---|

| *A satisfactory Risk Assessment has been performed and I grant approval for this activity to proceed.* | **Signature** | **Date** |
|---|---|---|
| | Signed by candidate | 202-04-17 |